EFFECT OF THE TAILPIPE ENTRY GEOMETRY ON A TWO-STROKE ENGINE'S PERFORMANCE PREDICTION

By

Cornelius Gysbert Johannes van Niekerk

Presented in partial fulfilment of the requirements for the degree

MASTER OF ENGINEERING

In the Faculty of Engineering,

University of Pretoria

Pretoria

December 2000

ABSTRACT

Title: **Effect of the Tailpipe Entry Geometry on a Two-Stroke Engine's Performance Prediction**

Author: **CGJ van Niekerk**
Promoters: **Prof JA Visser, Mr DJ de Kock**
Department: **Department Mechanical and Aeronautical Engineering**
Degree: **Master in Engineering (Mechanical)**

It is standard practice in one-dimensional gasdynamic simulations of high performance two-stroke engines to model the exhaust tail pipe entry as an area change using an algorithm similar to the area change of the reverse cone. In the reverse cone the area continually steps down while at the tail pipe entry it changes from stepping down to constant area. At this point a vena contracta can form that effects the flow resistance of the tail pipe.

In an effort to improve the accuracy of the gasdynamic simulations the area change algorithm at the tail pipe entry was replaced with a restriction algorithm that incorporates a coefficient of discharge and allows an increase in entropy on the expansion side. The coefficient of discharge is defined as the actual measured mass flow divided by the mass flow predicted by the restriction algorithm.

An experimental set up was designed and constructed to measure mass flows for a variety of tail pipe entry geometries at a range of pressures covering the pressure ratios encountered in a real engine. From the mass flow results the coefficients of discharge for a range of pressure and area ratios and reverse cone angles could be calculated and arranged into matrix form to define Cd-maps. The Cd-maps were incorporated into the simulation software and tested to ensure that it functioned correctly.

Finally, the simulation results with and without the Cd-maps were compared to measured results and it was shown that incorporating this refinement improves the accuracy of the simulation results on the "over run" part of the power curve. This is the part of the power curve after maximum power and very important in the development of high performance two-stroke engines. These maps can be used for all future simulations on any engine size that uses the same tail pipe geometry.

SAMEVATTING

Titel: **Die Invloed van die Afbloeipyp se Geometrie op die Voorspelling van die Werkverrigting van 'n Tweeslagenjin**

Outeur: **CGJ van Niekerk**
Promotors: **Prof JA Visser, Mnr DJ de Kock**
Departement: **Departement Meganiese en Lugvaartkundige Ingenieurswese**
Graad: **Magister in Ingenieurswese (Meganies)**

Dit is standaard praktyk in die een-dimensionele gasdinamiese simulasies van hoë werkverrigting tweeslag enjins om die ingang van uitlaatstelsel se afbloeipyp as 'n area verandering te modelleer deur dieselfde algoritme te gebruik as wat vir die modellering van die trukaatskegel gebruik word. In werklikheid verskil die twee deurdat die trukaats kegel se deursnit oppervlakte kontinu verklein, terwyl die deursnit oppervlakte van die afbloeipyp se ingang verander van 'n afnemende waarde na 'n konstante waarde. By dié punt kan 'n vloeivernouing ontstaan wat die vloei weerstand kan beïnvloed.

In 'n poging om die akkuraatheid van die gasdinamiese simulasies te verbeter, is die varieërende oppervlak-algoritme by die afbloeipyp se inlaat vervang met 'n weerstandsalgoritme wat 'n vloeiweerstandskoeëfisiënt insluit en wat toelaat vir 'n verhoging in entropie na die weerstand. Die vloeiweerstandskoeëfisiënt word gedefiniëer as die verhouding tussen die gemete massavloei en die voorspelde massavloei soos voorspel deur die weerstandsalgoritme.

'n Eksperimentele opstelling is ontwerp en gebou om massavloeie by 'n reeks afbloeipyp ingangsgeometrië te meet by 'n reeks drukke wat die drukverhoudings, soos wat in werklike enjins voorkom, te meet. Uit die massavloei resultate kan die vloeiweerstandskoeëfisiënt vir 'n reeks druk- en oppervlakverhoudings en trukaatskegel ingeslote hoeke, bereken word en in 'n matriks gerangskik word om vloeiweerstandskoeëfisiënt-kontoerkaarte te vorm. Die kontoerkaarte is in die sagteware geïnkorporeer en getoets.

Ten slotte is die simulasie resultate met en sonder die kontoerkaarte met gemete resultate vergelyk en dit is gevind dat die verfyning die akkuraatheid van die simulasie verbeter by die gedeelte van die drywingskromme na maksimum drywing. Hierdie gedeelte van die drywingskromme is baie belangrik by hoë werkverigting tweeslag enjins. Die kontoerkaarte maak nou deel uit van die simulasie sagteware en is van toepassing op alle enjins wat die tipe uitlaatstelsel gebruik.

ACKNOWLEDGEMENTS

Boart Longyear Seco for the use of their rock drill test facility.

Mr Gavin Pemberton of Boart Longyear Seco for his help with the tests.

Vickers OMC for the loan of the pressure transducers, thermocouples and Budenburg calibrator.

Desire van Niekerk, my loving wife, for the gentle but persistent pressure to complete the work and for the moral support.

TABLE OF CONTENTS

CHAPTER 5: SIMULATION STUDY

CHAPTER 6: SUMMARY, CONCLUSION AND RECOMMENDATIONS

APPENDICES

LIST OF TABLES

Table Number

LIST OF FIGURES

Figure Number

NOMENCLATURE

List of Symbols

A	Area
Ar	Area Ratio
a	Sonic Velocity
Cd	Coefficient of Discharge
Cp	Specific Heat at Constant Pressure
c	Particle Velocity
d	Diameter
F	Function
h	Enthalpy
l	Length
M	Mach Number
$\dot{m}$	Mass Flow Rate
P	Pressure
Pr	Pressure Ratio
R	Gas Constant
T	Temperature
δE	Change in Internal Energy
δm	Change in Mass
δQ	Heat Transferred
δW	Work
γ	Ratio of Specific Heats
θ	Included Angle of the Reverse Cone
ρ	Density

Subscripts

0	Reference Conditions
1	Values for Pipe 1
2	Values for Pipe 2
i	Incident
m	Mesh
r	Reflected
t	Throat
teff	Effective Value in Throat

Definitions

$$G5 = \frac{2}{\gamma - 1}$$

$$G6 = \frac{\gamma + 1}{\gamma - 1}$$

$$G7 = \frac{2\gamma}{\gamma - 1}$$

$$X = \left(\frac{P}{P_0}\right)^{\frac{1}{G7}}$$

Abbreviation

FCT	Flux Corrected Transport
GPB	Gordon P Blair
HLLE	Harten-Lax-Van Leer-Einfelt
LW	Lax-Wendroff
MoC	Method of Characteristics
EngMod2T	Acronym for The two-stroke engine simulation software

EFFECT OF THE TAILPIPE ENTRY GEOMETRY ON A TWO-STROKE ENGINE'S PERFORMANCE PREDICTION

By

Cornelius Gysbert Johannes van Niekerk

Presented in partial fulfilment of the requirements for the degree

MASTER OF ENGINEERING

In the Faculty of Engineering,

University of Pretoria

Pretoria

December 2000

ABSTRACT

Title: **Effect of the Tailpipe Entry Geometry on a Two-Stroke Engine's Performance Prediction**

Author: **CGJ van Niekerk**
Promoters: **Prof JA Visser, Mr DJ de Kock**
Department: **Department Mechanical and Aeronautical Engineering**
Degree: **Master in Engineering (Mechanical)**

It is standard practice in one-dimensional gasdynamic simulations of high performance two-stroke engines to model the exhaust tail pipe entry as an area change using an algorithm similar to the area change of the reverse cone. In the reverse cone the area continually steps down while at the tail pipe entry it changes from stepping down to constant area. At this point a vena contracta can form that effects the flow resistance of the tail pipe.

In an effort to improve the accuracy of the gasdynamic simulations the area change algorithm at the tail pipe entry was replaced with a restriction algorithm that incorporates a coefficient of discharge and allows an increase in entropy on the expansion side. The coefficient of discharge is defined as the actual measured mass flow divided by the mass flow predicted by the restriction algorithm.

An experimental set up was designed and constructed to measure mass flows for a variety of tail pipe entry geometries at a range of pressures covering the pressure ratios encountered in a real engine. From the mass flow results the coefficients of discharge for a range of pressure and area ratios and reverse cone angles could be calculated and arranged into matrix form to define Cd-maps. The Cd-maps were incorporated into the simulation software and tested to ensure that it functioned correctly.

Finally, the simulation results with and without the Cd-maps were compared to measured results and it was shown that incorporating this refinement improves the accuracy of the simulation results on the "over run" part of the power curve. This is the part of the power curve after maximum power and very important in the development of high performance two-stroke engines. These maps can be used for all future simulations on any engine size that uses the same tail pipe geometry.

SAMEVATTING

Titel: **Die Invloed van die Afbloeipyp se Geometrie op die Voorspelling van die Werkverrigting van ‘n Tweeslagenjin**

Outeur: **CGJ van Niekerk**
Promotors: **Prof JA Visser, Mnr DJ de Kock**
Departement: **Departement Meganiese en Lugvaartkundige Ingenieurswese**
Graad: **Magister in Ingenieurswese (Meganies)**

Dit is standaard praktyk in die een-dimensionele gasdinamiese simulasies van hoë werkverrigting tweeslag enjins om die ingang van uitlaatstelsel se afbloeipyp as ‘n area verandering te modelleer deur dieselfde algoritme te gebruik as wat vir die modellering van die trukaatskegel gebruik word. In werklikheid verskil die twee deurdat die trukaats kegel se deursnit oppervlakte kontinu verklein, terwyl die deursnit oppervlakte van die afbloeipyp se ingang verander van ‘n afnemende waarde na ‘n konstante waarde. By dié punt kan ‘n vloeivernouing ontstaan wat die vloei weerstand kan beïnvloed.

In ‘n poging om die akkuraatheid van die gasdinamiese simulasies te verbeter, is die varieërende oppervlak-algoritme by die afbloeipyp se inlaat vervang met ‘n weerstandsalgoritme wat ‘n vloeiweerstandskoeëfisiënt insluit en wat toelaat vir ‘n verhoging in entropie na die weerstand. Die vloeiweerstandskoeëfisiënt word gedefiniëer as die verhouding tussen die gemete massavloei en die voorspelde massavloei soos voorspel deur die weerstandsalgoritme.

‘n Eksperimentele opstelling is ontwerp en gebou om massavloeie by ‘n reeks afbloeipyp ingangsgeometrië te meet by ‘n reeks drukke wat die drukverhoudings, soos wat in werklike enjins voorkom, te meet. Uit die massavloei resultate kan die vloeiweerstandskoeëfisiënt vir ‘n reeks druk- en oppervlakverhoudings en trukaatskegel ingeslote hoeke, bereken word en in ‘n matriks gerangskik word om vloeiweerstandskoeëfisiënt-kontoerkaarte te vorm. Die kontoerkaarte is in die sagteware geïnkorporeer en getoets.

Ten slotte is die simulasie resultate met en sonder die kontoerkaarte met gemete resultate vergelyk en dit is gevind dat die verfyning die akkuraatheid van die simulasie verbeter by die gedeelte van die drywingskromme na maksimum drywing. Hierdie gedeelte van die drywingskromme is baie belangrik by hoë werkverigting tweeslag enjins. Die kontoerkaarte maak nou deel uit van die simulasie sagteware en is van toepassing op alle enjins wat die tipe uitlaatstelsel gebruik.

ACKNOWLEDGEMENTS

Boart Longyear Seco for the use of their rock drill test facility.

Mr Gavin Pemberton of Boart Longyear Seco for his help with the tests.

Vickers OMC for the loan of the pressure transducers, thermocouples and Budenburg calibrator.

Desire van Niekerk, my loving wife, for the gentle but persistent pressure to complete the work and for the moral support.

TABLE OF CONTENTS

CHAPTER 5: SIMULATION STUDY

CHAPTER 6: SUMMARY, CONCLUSION AND RECOMMENDATIONS

APPENDICES

LIST OF TABLES

Table Number

LIST OF FIGURES

Figure Number

NOMENCLATURE

List of Symbols

A	Area
Ar	Area Ratio
a	Sonic Velocity
Cd	Coefficient of Discharge
Cp	Specific Heat at Constant Pressure
c	Particle Velocity
d	Diameter
F	Function
h	Enthalpy
l	Length
M	Mach Number
$\dot{m}$	Mass Flow Rate
P	Pressure
Pr	Pressure Ratio
R	Gas Constant
T	Temperature
δE	Change in Internal Energy
δm	Change in Mass
δQ	Heat Transferred
δW	Work
γ	Ratio of Specific Heats
θ	Included Angle of the Reverse Cone
ρ	Density

Subscripts

0	Reference Conditions
1	Values for Pipe 1
2	Values for Pipe 2
i	Incident
m	Mesh
r	Reflected
t	Throat
teff	Effective Value in Throat

Definitions

$$G5 = \frac{2}{\gamma - 1}$$

$$G6 = \frac{\gamma + 1}{\gamma - 1}$$

$$G7 = \frac{2\gamma}{\gamma - 1}$$

$$X = \left(\frac{P}{P_0} \right)^{\frac{1}{G7}}$$

Abbreviation

FCT	Flux Corrected Transport
GPB	Gordon P Blair
HLLE	Harten-Lax-Van Leer-Einfelt
LW	Lax-Wendroff
MoC	Method of Characteristics
EngMod2T	Acronym for The two-stroke engine simulation software

CHAPTER 1

INTRODUCTION

1.1 BACKGROUND

The performance of a naturally aspirated two-stroke internal combustion engine depends to a large extent on the wave action in the intake and exhaust system. Before the advent of computers these ducts were designed using empirical formulas and finalised through a large amount of testing using the “cut and try” method. Since computers became readily available during the 1960’s, simulation methods were developed to shorten the “cut and try” cycles and to save on development costs. The results were very good when applied to industrial engines but lacked accuracy when applied to very high performance competition engines. During the last 20 years various new numerical methods for the solution of the unsteady compressible flow in the ducts were developed and the accuracy improved steadily. Better boundary condition formulations, scavenging models and combustion models also improved the accuracy.

One area that has not received attention is the modelling methodology of the tail pipe entry geometry (Figure 1.1) and flow characteristics on the performance prediction of a two-stroke engine.

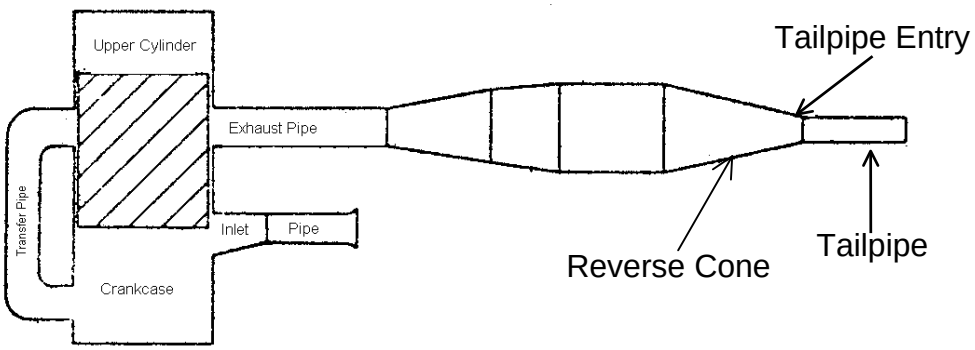

Figure 1.1: Schematic of Two-Stroke Engine

It is standard practice to model the tailpipe entry using the same formulation as used for the reverse cone. By using a more sophisticated model combined with a measured coefficient of discharge it is hoped that the accuracy of the simulation can be improved. The engine simulation software, EngMod2T, will be used for the evaluation. (Refer to Appendix I for a more detailed description of EngMod2T) This software was written to simulate the performance characteristics of a high specific output two-stroke spark ignition internal combustion engine. It simulates the pipe and duct flows using one-dimensional gasdynamics and follows the current trend by modelling the tailpipe entrance as an area change. By modelling it as an orifice with an experimentally determined discharge coefficient it is hoped to improve the accuracy of the simulation software.

During the past 8 years some factory racing motorcycles started using restrictions or venturies at the tailpipe inlet. Other than for one brief reference (Irving, 1969:189) no explanation or motivation for using it could be found. This study also aims to clarify this point.

1.2 CURRENT LEVEL OF KNOWLEDGE

The mathematics for one-dimensional gasdynamics was developed in the late 1940's and 1950's. By setting up the differential equations and solving them graphically using the method of characteristics, early researchers could determine the pressure pulse history for one or maybe two cycles of an engine. This was obviously very cumbersome and slow. The graphical method was adapted to a mesh method that could be computerised (Benson, Garg & Woollatt, 1964). During the next 25 years this method was refined and used for various types of engines. It was used extensively by a research group at the Queens University of Belfast for the simulation of high performance two stroke engines. They added combustion and scavenging models and developed a reedvalve induction model. The early version of EngMod2T was based on this work.

As the specific output of engines continued to rise the need for more accurate and faster methods became necessary. During the 1980's various methods were developed and evaluated. These methods include the well-known two-step Lax-Wendrof method with flux correction and the HLLE (Harten-Lax-van Leer - Einfeldt) upwind difference scheme.

These proved to be successful but still had certain shortfalls for the specific application of high performance two-stroke engines. It proved difficult to solve for contact discontinuities, especially ones that included not just temperature discontinuities but were a combination of temperature and gas composition discontinuities.

In 1991 Blair published a new method, the GPB-method (Blair, 1991) that solved these discontinuities. Blair and co-workers continued to develop this method and also developed improved boundary condition solutions. The method can accommodate parallel or taper pipes, stepped pipes, pipes with restrictions and pipe junctions. It solves the gas dynamic equation for varying gas composition, temperature and density. It can handle state and gas composition discontinuities. The solution calculates heat transfer and the effect of friction and is fully non-homentropic. The current version of EngMod2T (version 2.2) is based on this work. It also models the flow into the tailpipe as a smooth transition from the reverse cone to the tailpipe with no contraction or losses.

1.3 MOTIVATION

From the preceding paragraphs it follows that most of the phenomena involved in the gasdynamic modelling has received attention. One area that has not received attention is the entry to the tailpipe.

1.4 SCOPE

This work starts off with a literature survey of firstly the background and history of one-dimensional gasdynamics followed by a description of the GPB method. Next, a closer look is taken at the modelling methodology of the tailpipe entry geometry. The literature survey finishes with a look at discharge coefficients and how to use them in a simulation method.

In chapter 3 the mathematical model for a restriction in a pipe, as used in the GPB method, is discussed. The equations are developed to a format that allows them to be solved by the Newton-Raphson method for simultaneous non-linear equations. The software developed from this and its incorporation and testing into EngMod2T is described.

In the following chapter, chapter 4, data necessary to determine the discharge coefficients for the various combinations of tailpipe entry restrictions are determined experimentally on a flow bench. This is followed by a description of the method and software developed to determine the discharge coefficients and the final processed results in graphical form.

This is followed in chapter 5 with a simulation study to determine the influence of the tailpipe coefficient of discharge on the performance predicted by EngMod2T. The results are compared with experimental data.

The summary, conclusions and recommendations are given in chapter 6.

CHAPTER 2

LITERATURE REVIEW

2.1 PREAMBLE

This chapter is divided into four main categories. The first gives a brief description of the history and current state of the use of 1-Dimensional Gasdynamics to solve the unsteady compressible flow in the pipes and ducts of internal combustion engines.

The second part describes the GPB method of solving the 1-Dimensional Gasdynamics equations; it's comparison to other modern methods and the reasons for its choice above the others.

The third part describes the current methodology used in modelling the tailpipe entry geometry and flow. It also points out where the approach used in this study differs from the conventional way.

Finally, the determination of discharge coefficients and its influence on the accuracy of the simulations are discussed. An alternative way of defining the coefficient of discharge is explained.

2.2 GENERAL 1-DIMENSIONAL METHODS - HISTORY

In the analysis of sound waves it is possible to use two approaches. If, in the derivation of the wave equation the assumption is made the wave amplitudes are small the second order terms can be neglected and the resulting equation is the well-known small wave equation. (Annand & Roe, 1974:31) These small amplitude sound waves are linear waves, meaning that during superposition their amplitudes are summed. They are the well-known acoustic waves. Acoustic waves do not change shape as they travel through a gas.

If the amplitude is not small the second order terms cannot be neglected resulting in non-linear wave equations. Earnshaw (1910) developed these non-linear equations for sound waves. He showed that the pressure and velocity of the superposition wave is related to that of the individual waves by a seventh power law. These large amplitude sound waves are known as finite waves and they do change shape as they travel through a gas.

The finite wave equations are hyperbolic differential equations and cannot be solved analytically. Riemann, in 1858 (Winterbone & Pearson, 2000) proposed the Method of Characteristics (MoC) for solving them. This is a graphical method and very cumbersome and slow. Early researchers into the application of wave methods to the manifolds of internal combustion engines compared the results obtained with acoustic waves to those with finite waves to determine which one is correct for the application. Bannister and Mucklow (1948) studied the wave action following the sudden release of compressed gas from a cylinder. Wallace and Stuart-Mitchell (1953) included the effect of ports. Wallace and Nassif (1954) included the engine cylinder. Mucklow and Wilson (1955) studied the effect of friction and heat transfer while Wallace and Boxer (1956) investigated wave action in diffusers. By this time

there was no more doubt that the finite wave theory was the correct one to apply to manifolds of internal combustion engines. The theoretical derivation of the equations was summarized by Bannister (1958) and this publication is still used as a reference to date.

Benson, Garg and Woollatt (1964) developed a computerised version of the MoC using a mesh method. This involved dividing the pipes and ducts into equal length meshes and through interpolation the values of the left and right moving characteristics could be determined at each mesh boundary as a function of time. This landmark paper established the MoC as the method of choice for solving the gasdynamics in engine manifolds and ducts for the next 20 years. During this time a large number of papers were published using the MoC as a base.

Of particular interest to this study are the papers published by a research group at the Queen's University of Belfast (QUB). Under the leadership of Professor Gordon P Blair they concentrated on the analysis and simulation of two-stroke engines. They started by applying the MoC to a straight exhaust pipe (Blair & Goulburn, 1967) followed by a pipe with tapered sections (Blair & Johnson, 1968). Next they analysed the flow in the induction system, (Blair & Arbuckle, 1970), and developed a more sophisticated treatment of boundary conditions (Blair & Cahoon, 1972). At this stage they could analyse the open cycle of a two-stroke engine. By including the calculation of the gas purity in each mesh (Blair & Ashe, 1976) and a rate of heat release combustion model (Blair, 1976) the power output of a two-stroke engine could be predicted. As a further refinement a reed valve model was developed and included in the simulation software (Hinds & Blair, 1978; Blair, Hinds & Fleck, 1979; Fleck, Blair & Houston, 1987 and Fleck, Cartwright & Thornhill, 1997).

The original version of EngMod2T was based on the work by this group at QUB and a small sample program published by Blair (1990).

The MoC has several major drawbacks. Firstly, most of the time it was used in a homentropic form. Solving the equations in the non-homentropic formulation requires particle pathline tracking (Benson et al. 1964) resulting in very long execution times. The homentropic solution ignores contact discontinuities (large jumps in temperature and gas composition that occurs for instance when fresh charge short circuits out the exhaust port during the scavenging phase and comes into "contact" with the hot exhaust gas) resulting in inaccurate prediction of the wave action (Blair &Blair, 1987; McGinnity, Douglas & Blair, 1990 and Douglas, McGinnity & Blair, 1991).

Secondly, the MoC assumes constant values for the specific heats and gas constant for each mesh in a pipe. Poloni, Winterbone and Nichols (1988) investigated this assumption and showed that it can lead to inaccuracies.

Thirdly, the wave equations as solved by the MoC are in the non-conservative form meaning that mass artificially lost or created between the ends of a pipe (Winterbone & Pearson, 2000:8, Van Howe & Sierens, 1991). This becomes particularly severe when there are large entropy variations or changes of cross section in the pipe, as is typical for a two-stroke engine.

In an effort to overcome these defects finite difference methods were developed. It is possible to write the solution algorithms based on the equations in the conservative

form, which removes the generation or loss of properties (Winterbone & Pearson, 2000:8; Laney, 1998). These methods have the drawback in that numerical overshoots and spurious oscillations occur at contact discontinuities. A number of methods were and are being developed to solve this problem. Solutions include flux limiters, flux corrections, flux splitting and non-linear filters (Laney, 1998). Arguably the two best-known methods are the Two Step Lax-Wendroff method with flux corrected transport (LW+FCT) and the Harten-Lax-Van Leer-Einfelt (HLLE) upwind difference scheme (Chen, Veshagh & Wallace, 1992).

During the last 15 years these methods have gradually replaced the MoC as the preferred method for solving manifold flows. They are much more efficient than the non-homentropic MoC but including varying gas composition slows them down by between 80% and 600% (Kirkpatrick, Blair, Fleck & McMullen, 1994). The flux limiters also cause a small amount of numerical smearing.

2.3 THE GPB- METHOD

In an effort to resolve these problems Professor Gordon P Blair of the Queen's University of Belfast developed a new method to solve the 1-dimensional gasdynamic equations for flow in pipes (Blair, 1991; Blair, 1993). It follows the work of Bannister and Mucklow (1948) and Wallace and Nassif (1954) by solving Earnshaw's (1910) equation directly for the wave motion. It is known as the GPB-method.

The GPB-method solves the non-linear wave equation over what is called "finite spaces". It first determines the motion and pressure of the left and right moving waves and their superposition in each control volume. From this and using conservation of mass, energy and momentum the particle velocity, temperature, density, purity and gas values for each control volume can be determined for that time step.

Over the last 10 years the GPB-method has undergone a large amount of testing, verification and development at QUB. Blair (1993) shows good correlation between measured and simulated engine data. Kirkpatrick, Blair, Fleck and McMullen (1994) compared the GPB-method with the LW+FCT-method, the HLLE-method and both the homentropic MoC and the non-homentropic MoC. Simulating pipe flows with constant gas values the GPB-method, the LW+FCT-method and the HLLE-method gives similar results and run times (about 20% of the nonh-MoC). Including varying gas values slows the LW+FCT-method and HLLE-method dramatically. It has no effect on the GPB-method, as the varying gas values are included in its formulation in any case. Blair, Kirkpatrick and Fleck (1995) showed the importance of taking the gas composition and temperature effect on the gas values into consideration. Ignoring it resulted in incorrectly predicted wave phasing, amplitude and shape. Blair, Kirkpatrick, Mackey and Fleck (1995) developed the algorithms for area discontinuities and Mackey, Blair and Fleck (1996) developed a noise emission algorithm.

The GPB-method simulates the effect of a gradual area change as a series of short parallel pipes connected by area discontinuities, expansion or contraction discontinuities depending on the direction of flow (Blair & Magee, 1993). These short pipes have a length equal to the mesh length (Figure 2.1). For each of these pipes

the pressure loss through friction, the heat loss or gain through heat transfer, the heat generation from the friction and the mass, energy and momentum transported across the two boundaries are calculated.

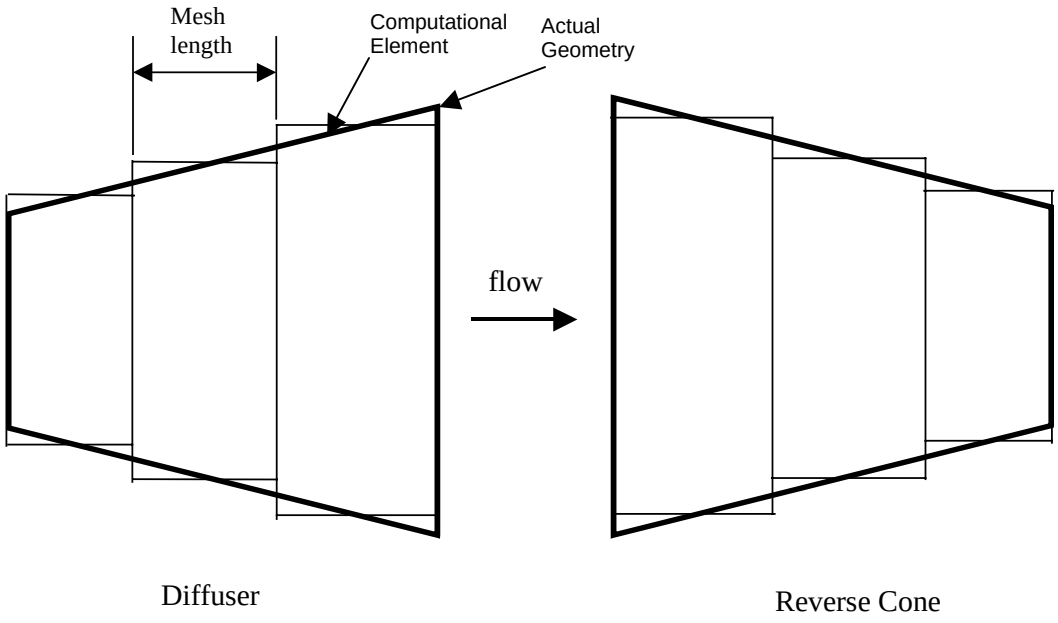

Figure 2.1: Modelling taper pipes as a series of parallel pipes.

2.4 TAILPIPE ENTRY GEOMETRIC AND FLOW MODELLING

It is standard practice to model the flow into tailpipe entry using the same algorithm as for the area change in the reverse cone. In the GPB-method the area contraction algorithm is used (Blair & Magee, 1993) and in the finite difference methods the area change is incorporated in the source terms of the equations. Figure 2.2 shows a schematic drawing of the current methodology in the GPB-method.

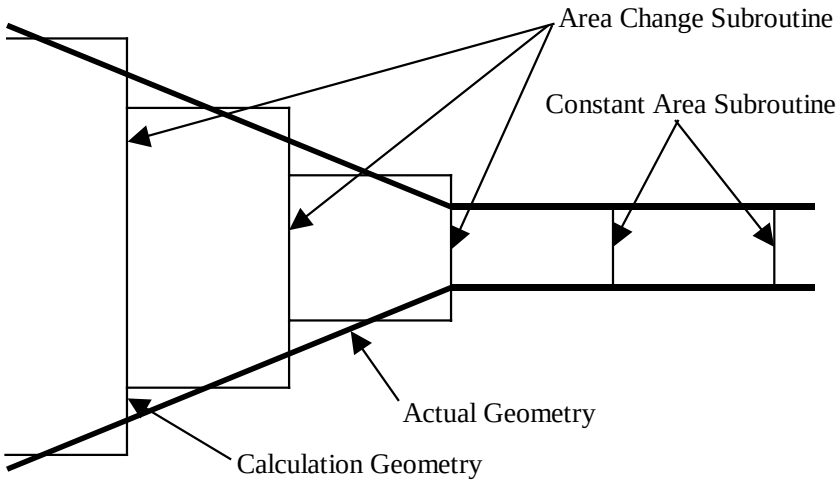

Figure 2.2: Current modelling of tailpipe entry flow.

The area change algorithm in neither the GPB-method nor the finite difference methods makes any provision for a flow contraction or flow breakaway at the tailpipe

entry. Both assume a smooth transition from the reverse cone to the tailpipe. Blair, Kirkpatrick, Mackey and Fleck (1995) developed the algorithms for area discontinuities and particularly a contraction-expansion restriction that incorporates a coefficient of discharge. In this study the effect of replacing the area contraction algorithm at the tailpipe entry with this restriction algorithm combined with experimentally determined coefficients of discharge are investigated. The proposed calculation layout is shown in Figure 2.3.

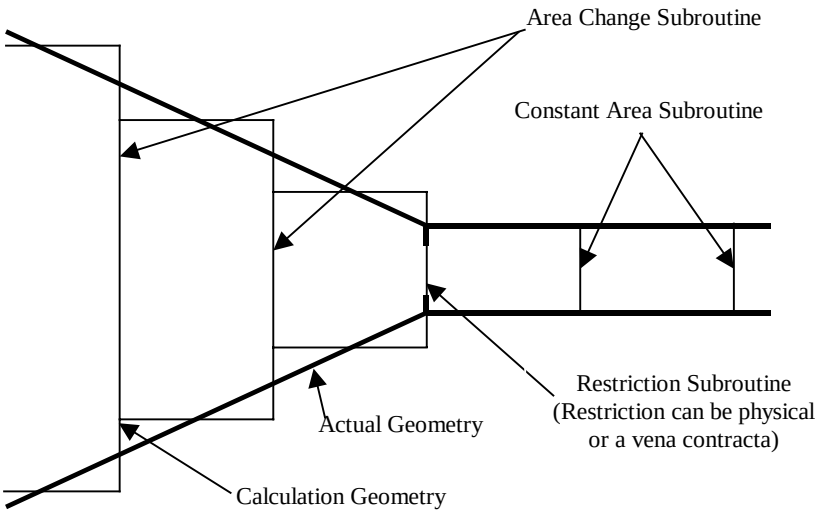

Figure 2.3: Proposed modelling of tailpipe entry flow.

Corberán, Royo, Pérez and Santiago (1994) simulated the performance of a 1993 HONDA RS125R Grand Prix motorcycle that uses a venturi at the tailpipe entry. They do not state how the entry was modelled but do emphasise that they found that its inclusion in the model had a small but important effect on the results. They found a better match between the measured and simulated results by including the effect of the venturi.

2.5 DISCHARGE COEFFICIENTS

An inherent part of a non-isentropic analysis of the cylinder to duct boundary, or a duct to atmosphere boundary, or a duct-to-duct boundary, includes the physical geometry of the aperture. This describes the geometry of the port, valve plus port or the orifice and the area of the duct or ducts adjacent to the boundary. As all real flows contract in area as they pass through the eye of the aperture, it is normal practice to describe this behaviour by a discharge coefficient.

The discharge coefficient is traditionally measured in a steady flow experiment and applied to an unsteady flow simulation in a quasi-steady fashion (Benson, 1959). An attempt was also made to determine the coefficient of discharge using theoretical means (Benson & Pool, 1965a; Benson & Pool, 1965b; Decker, 1978).

Recently Blair, Lau, Cartwright, Raghanathan and Mackey (1995) pointed out that the traditional definition of discharge coefficient is the measured mass flow divided by

the isentropically calculated mass flow through the area of the aperture. They defined this coefficient of discharge as the “theoretical coefficient of discharge”. During a simulation it is more correct to use a discharge coefficient defined as the measured mass flow divided by the calculated mass flow where the calculation was conducted using the same theoretical model for that specific geometry as used in the simulation software. They defined this as the “actual coefficient of discharge”. Blair and Drouin (1996) showed that using the actual coefficient of discharge greatly enhances the accuracy of the simulations. This approach is used in EngMod2T and uses the discharge coefficients for the ports, reed valves and pipe ends as determined by Fleck and Cartwright (1996).

2.6 CLOSING

A brief investigation into the various methods used in one-dimensional gasdynamics was conducted and some of their advantages and disadvantages were discussed. This was followed by a more in depth look at the GPB-method that is used in the simulation software. The current practice of modelling the tailpipe entry as just another gradual area change was investigated and a new methodology was proposed. Finally a more realistic definition of the Coefficient of Discharge was discussed.

CHAPTER 3

THERMODYNAMIC AND COMPUTER MODEL OF RESTRICTION

3.1 PREAMBLE

In this chapter a set of thermodynamic equations describing the 1-dimensional flow through a restriction is developed. These are then written in a suitable format for inclusion into the computer program. The subroutine that solves these equations are then developed and tested.

3.2 THERMODYNAMIC MODEL OF RESTRICTION

The theoretical model as described was developed by Blair (1996). The formulation used is from Blair, Kirkpatrick, Mackey and Fleck (1995). The sudden area change model presented is more complex but more accurate than the traditional method of considering a restriction as firstly a contraction in one mesh followed by an expansion in the next mesh, Blair and Magee (1993). Refer to Figure 3.1 for a schematic of the geometry. By using the Newton-Raphson method the geometry can be solved as one boundary condition. It can also be applied to sudden contractions or expansions in pipes by considering the throat area to be the effective area, the vena-contracta. Two flow regimes may exist, namely subsonic and sonic flow, and these are presented separately in the following sections.

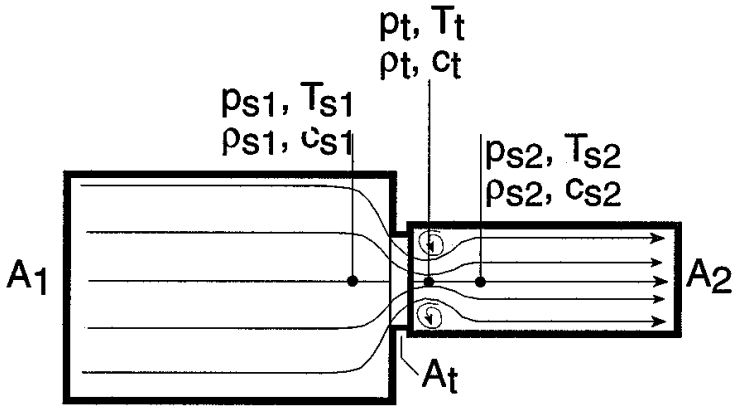

Figure 3.1: Particle flow regimes at a restricted area change

The following five equations has to be solved:

Mass flow (continuity) from pipe 1 to throat

$$\dot{m}_1 = \dot{m}_t \tag{3.1}$$

Mass flow (continuity) from throat to pipe 2

$$\dot{m}_t = \dot{m}_2 \tag{3.2}$$

Conservation of energy (first law of thermodynamics) from pipe1 to throat

$$\delta Q + \delta m_1 (h_1 + \frac{c_1^2}{2}) = \delta E + \delta m_t (h_t + \frac{c_t^2}{2}) + \delta W \tag{3.3}$$

Conservation of energy (first law of thermodynamics) from throat to pipe 2

$$\delta Q + \delta m_t (h_t + \frac{c_t^2}{2}) = \delta E + \delta m_2 (h_2 + \frac{c_2^2}{2}) + \delta W \tag{3.4}$$

Conservation of momentum from throat to pipe 2

$$A_2 (P_t - P_2) + \dot{m}(c_t - c_2) = 0 \tag{3.5}$$

These five equations has to be transformed into a suitable format to be solved inside the application of the GPB-method.

3.2.1 Subsonic Flow

For subsonic flow the following assumptions are made:

- The contracting flow from pipe 1 to the throat is isentropic
- The expanding flow from the throat to pipe 2 is adiabatic but not isentropic, due to the “dead” zone between the jet surface and the wall.

A temperature/entropy diagram for the subsonic flow process is shown in Figure 3.2. In Figure 3.1 the expanding flow from the throat to the downstream superposition point 2 is seen to leave turbulent vortices in the corners of that section. That the streamlines of the flow give rise to particle flow separation implies a gain of entropy from the throat to area at point 2. This is summarised on the temperature/entropy diagram in Figure 3.2, where the gain in entropy for the flow rising from pressure P_t to P_2 is clearly visible.

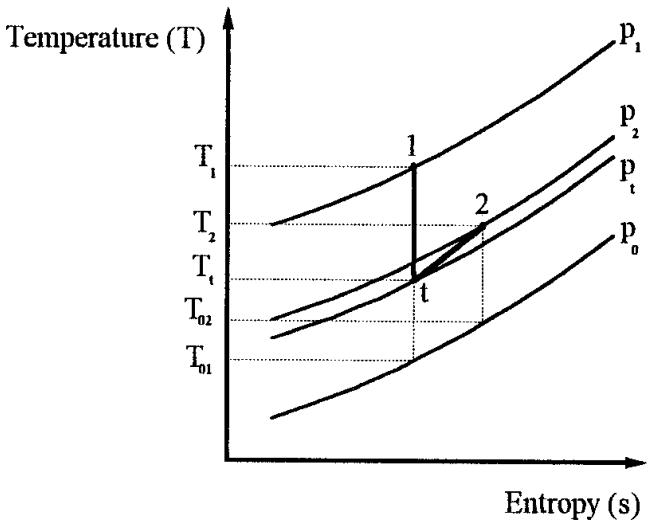

Figure 3.2: Temperature / Entropy diagram for subsonic flow

A further assumption is made in that it is assumed that the gas constant and the specific heats are those of the gas at the upstream point. This lead to the following reference state conditions:

Density:

$$\rho_{01} = \rho_{0t} = \frac{P_0}{RT_{01}} \tag{3.6}$$

$$\rho_{02} = \frac{P_0}{RT_{02}} \tag{3.7}$$

Acoustic velocity:

$$a_{01} = a_{0t} = \sqrt{\gamma RT_{01}} \tag{3.8}$$

$$a_{02} = \sqrt{\gamma RT_{02}} \tag{3.9}$$

The continuity equation from pipe 1 to the throat may be stated as (Eq 3.1):

$$\rho_1 A_1 c_1 = \rho_t A_{teff} c_t \tag{3.10}$$

Where A_{teff} is the effective throat area, related to the geometric throat area A_t, by:

$$A_{teff} = C_d A_t \tag{3.11}$$

From the gas-dynamic equations (Blair, 1996) it follows that

$$\rho = \rho_0 X^{G5} \tag{3.12}$$

and by substituting in equation (3.10)

$$\rho_{01} A_1 X_1^{G5} c_1 = \rho_{0t} A_{teff} X_t^{G5} c_t \tag{3.13}$$

as the contraction process is assumed isentropic, using equation (3.6)

$$A_1 X_1^{G5} c_1 - A_{teff} X_t^{G5} c_t = 0 \tag{3.14}$$

The continuity equation from the throat to pipe 2 is (Eq 3.2)

$$\rho_t A_{teff} c_t = \rho_2 A_2 c_2 \tag{3.15}$$

Using equation (3.12)

$$\rho_{0t} A_{teff} X_t^{G5} c_t = \rho_{02} A_2 X_2^{G5} c_2 \tag{3.16}$$

and as

$$\rho_{0t} = \rho_{01}$$

and from (3.6) and (3.9)

$$\rho_{01} = \frac{\gamma P_0}{a_{01}^2} \tag{3.17}$$

and from (3.7) and (3.9)

$$\rho_{02} = \frac{\gamma P_0}{a_{02}^2} \tag{3.18}$$

substituting equations (3.17) and (3.18) into (3.16)

$$a_{02}^2 A_{teff} X_t^{G5} c_t = a_{01}^2 A_2 X_2^{G5} c_2 \tag{3.19}$$

The first law of thermodynamics from pipe 1 to the throat may be stated (Eq 3.3):

$$\delta Q + \delta m_1 (h_1 + \frac{c_1^2}{2}) = \delta E + \delta m_t (h_t + \frac{c_t^2}{2}) + \delta W \tag{3.20}$$

Assuming flow to be quasi-steady and steady state, the mass flow increments must satisfy the continuity equation and thus equation (3.20) reduces to:

$$h_1 + \frac{c_1^2}{2} = h_t + \frac{c_t^2}{2} \tag{3.21}$$

By definition

$$h = C_p T \tag{3.22}$$

and

$$C_p = \frac{\gamma R}{\gamma - 1} \tag{3.23}$$

and by substituting in equation (3.21)

$$\frac{2\gamma}{\gamma - 1} RT_1 + c_1^2 = \frac{2\gamma}{\gamma - 1} RT_t + c_t^2 \tag{3.24}$$

Since $$a = \sqrt{\gamma RT} = a_0 X \tag{3.25}$$

And $$G5 = \frac{2}{\gamma - 1} \tag{3.26}$$

it follows that:

$$G5 a_{01}^2 X_1^{\ 2} + c_1^2 - G5 a_{01}^2 X_t^{\ 2} - c_t^2 = 0 \tag{3.27}$$

Using the same assumptions the first law of thermodynamics from throat to pipe 2 may be stated as (Eq 3.4):

$$h_t + \frac{c_t^2}{2} = h_2 + \frac{c_2^2}{2} \tag{3.28}$$

which becomes using the same logic:

$$G5 a_{01}^2 X_t^{\ 2} + c_t^2 - G5 a_{02}^2 X_2^{\ 2} - c_2^2 = 0 \tag{3.29}$$

The momentum equation from throat to pipe 2 may be stated as (Eq 3.5):

$$A_2(P_t - P_2) + \dot{m}(c_t - c_2) = 0 \tag{3.30}$$

by substituting $\dot{m} = \rho_1 A_1 c_1$ dividing by P_0 and writing in terms of pressure amplitude:

$$A_2(X_t^{\ G7} - X_2^{\ G7}) + \frac{\rho_1}{P_0} A_1 c_1 (c_t - c_2) = 0 \tag{3.31}$$

By using equation (3.12) this becomes:

$$A_2(X_t^{\ G7} - X_2^{\ G7}) + \frac{\rho_{01}}{P_0} A_1 X_1^{\ G5} c_1 (c_t - c_2) = 0 \tag{3.32}$$

By using $a_0 = \sqrt{\frac{\gamma P_0}{\rho_0}}$ and substituting it in equation (3.32):

$$a_{01}^2 A_2(X_t^{\ G7} - X_2^{\ G7}) + \gamma A_1 X_1^{\ G5} c_1 (c_t - c_2) = 0 \tag{3.33}$$

Equations (3.14), (3.19), (3.27), (3.29) and (3.33) are the fundamental equations governing the flow scenario as illustrated in Figure 3.1. By using the pressure ratios as defined in the GPB method and the definitions of particle speed:

$$X_1 = X_{r1} + X_{i1} - 1$$

$$X_2 = X_{r2} + X_{i2} - 1$$

$$c_1 = G5 a_{01}(X_{i1} - X_{r1})$$

$$c_2 = G5 a_{02}(X_{r2} - X_{i2}) \tag{3.34}$$

and substituting them into these five equations, this results in the following equations where $F(i)$=0:

$$F(1) = 0 = A_1(X_{r1} + X_{i1} - 1)^{G5} a_{01} G5(X_{i1} - X_{r1}) - A_{teff} X_t^{G5} c_t \quad (3.35)$$

$$F(2) = 0 = a_{02}^2 A_{teff} X_t^{G5} c_t - a_{01}^2 (X_{r2} + X_{i2} - 1)^{G5} a_{02} A_2 G5(X_{r2} - X_{i2}) \quad (3.36)$$

$$F(3) = 0 = G5 a_{01}^2 (X_{r1} + X_{i1} - 1)^2 + (G5 a_{01}(X_{i1} - X_{r1}))^2 - G5 a_{01}^2 X_t^2 - c_t^2 \quad (3.37)$$

$$F(4) = 0 = G5 a_{01}^2 X_t^2 + c_t^2 - G5 a_{02}^2 (X_{r2} + X_{i2} - 1)^2 - (G5 a_{02}(X_{r2} - X_{i2}))^2 \quad (3.38)$$

$$F(5) = 0 = a_{01}^2 A_2 (X_t^{G7} - (X_{r2} + X_{i2} - 1)^{G7}) + \gamma A_1 (X_{r1} + X_{i1} - 1)^{G5} \times G5 a_{01}(X_{i1} - X_{r1})(c_t - G5 a_{02}(X_{r2} - X_{i2})) \quad (3.39)$$

Equations (3.35) to (3.39) contain five unknowns, namely X_{r1}, X_{r2}, X_t, c_t and a_{02}. By using the Newton-Raphson method for multiple non-linear polynomials these values are determined. A listing of the subroutine is included in Appendix B.

3.2.2 Sonic Flow

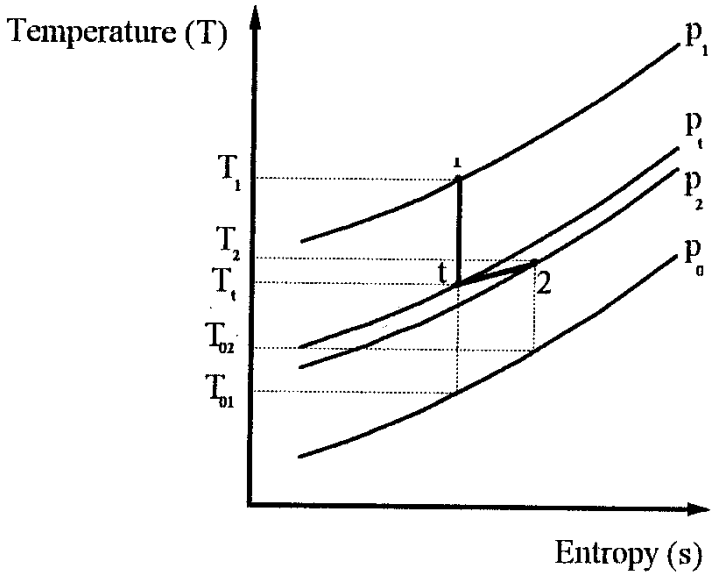

Figure 3.3: Temperature / Entropy diagram for sonic flow

The temperature / entropy diagram for the sonic flow process is shown in Figure 3.3. For sonic flow the Mach number in the throat is unity. This implies that:

$$M_t = \frac{c_t}{a_{01} X_t} = 1 \quad (3.40)$$

and thus:

$$c_t = a_{01} X_t \tag{3.41}$$

Substituting this result into equation (3.14), the continuity equation from pipe 1 to the throat is:

$$A_1 X_1^{G5} c_1 - A_{teff} a_{01} X_t^{G6} = 0 \tag{3.42}$$

And similarly, equation (3.19) becomes:

$$A_{teff} a_{02}^2 X_t^{G6} - A_2 a_{01} X_2^{G5} c_2 = 0 \tag{3.43}$$

The first law of thermodynamics from pipe 1 to the throat, equation (3.27) becomes:

$$G5 a_{01}^2 X_1^2 + c_1^2 - G6 a_{01}^2 X_t^2 = 0 \tag{3.44}$$

and similarly, equation (3.29) becomes:

$$G6 a_{01}^2 X_t^2 - G5 a_{02}^2 X_2^2 - c_2^2 = 0 \tag{3.45}$$

Equations (3.42) to (3.45) are the fundamental equations governing the flow scenario for sonic flow as illustrated in Figure 3.1.

By substituting the values as defined by equation (3.34) the four equations are in the required format to be incorporated in the software. This results in the following equations where $F(i)$=0.0:

$$F(1) = 0 = A_1 (X_{r1} + X_{i1} - 1)^{G5} G5 (X_{r1} - X_{i1}) - A_{teff} X_t^{G6} \tag{3.46}$$

$$F(2) = 0 = a_{02} A_{teff} X_t^{G6} - a_{01} A_2 (X_{r2} + X_{i2} - 1)^{G5} G5 (X_{r2} - X_{i2}) \tag{3.47}$$

$$F(3) = 0 = G5 (X_{i1} + X_{r1} - 1)^2 + (G5 (X_{i1} - X_{r1}))^2 - G6 X_t^2 \tag{3.48}$$

$$F(4) = 0 = G6 a_{01}^2 X_t^2 - G5 a_{02}^2 (X_{r2} + X_{i2} - 1)^2 - (G5 a_{02} (X_{r2} - X_{i2}))^2 \tag{3.49}$$

Equations (3.46) to (3.49) contain four unknowns, namely X_{r1}, X_{r2}, X_t and a_{02}. By using the Newton-Raphson method for multiple non-linear simultaneous equations, these values are determined. A listing of the subroutine is included in Appendix B.

3.3 COMPUTER MODEL OF AREA DISCONTINUITY WITH RESTRICTION

The subroutine, RESTRICT.FOR, was written to solve the two sets of non-linear simultaneous equations, five for subsonic flow and four for sonic flow. (Refer to Appendix B for a listing of the subroutines). It is written in FORTRAN 77. It uses the same methodology as the other boundary condition subroutines in EngMod2T. A flow diagram for the subroutine is shown in Figure 3.4.

3.3.1 Description of RESTRICT

The subroutine starts of by setting the initial values. Using starting values close to the final result is required to allow the Newton-Raphson method to converge to the answer. If it is the first time that the routine is called, it sets the initial values to default values based on the start up values in the exhaust pipe. Otherwise it uses the output results from the previous call to the subroutine from that specific restriction as the new starting values.

This is followed by the subsonic loop. It calls the subroutine SUBSONIC which calculates the values of each function $F(i)$ and the numerical partial derivatives of each function with respect to each unknown variable. This is done numerically and stored in the Jacobian matrix $A(i, j)$ and returned to subroutine RESTRICT. Subroutine LUDCMP is called which firstly checks that matrix A is not singular after which it does LU decomposition of A and determines the determinant D of matrix A. This is returned to RESTRICT which calls subroutine LUBKSB that does the back substitution of matrix A and stores the results in F and returns to RESTRICT. The new values for the unknown variables are calculated and the flow is checked for sonic condition. If the flow is subsonic the values are checked for convergence.

If the convergence criteria are met, these values are returned to the main program. If not, the new values are used as the new initial conditions and the iteration is repeated.

If sonic flow was reached the process jumps out of the subsonic loop to the sonic loop where new initial conditions are set (the particle velocity in the throat is set to the sonic value) and subroutine SONIC is called which calculates the function $F(i)$ and the Jacobian matrix $A(i, j)$ for sonic conditions. After this the calculation proceeds the same way as for the subsonic case.

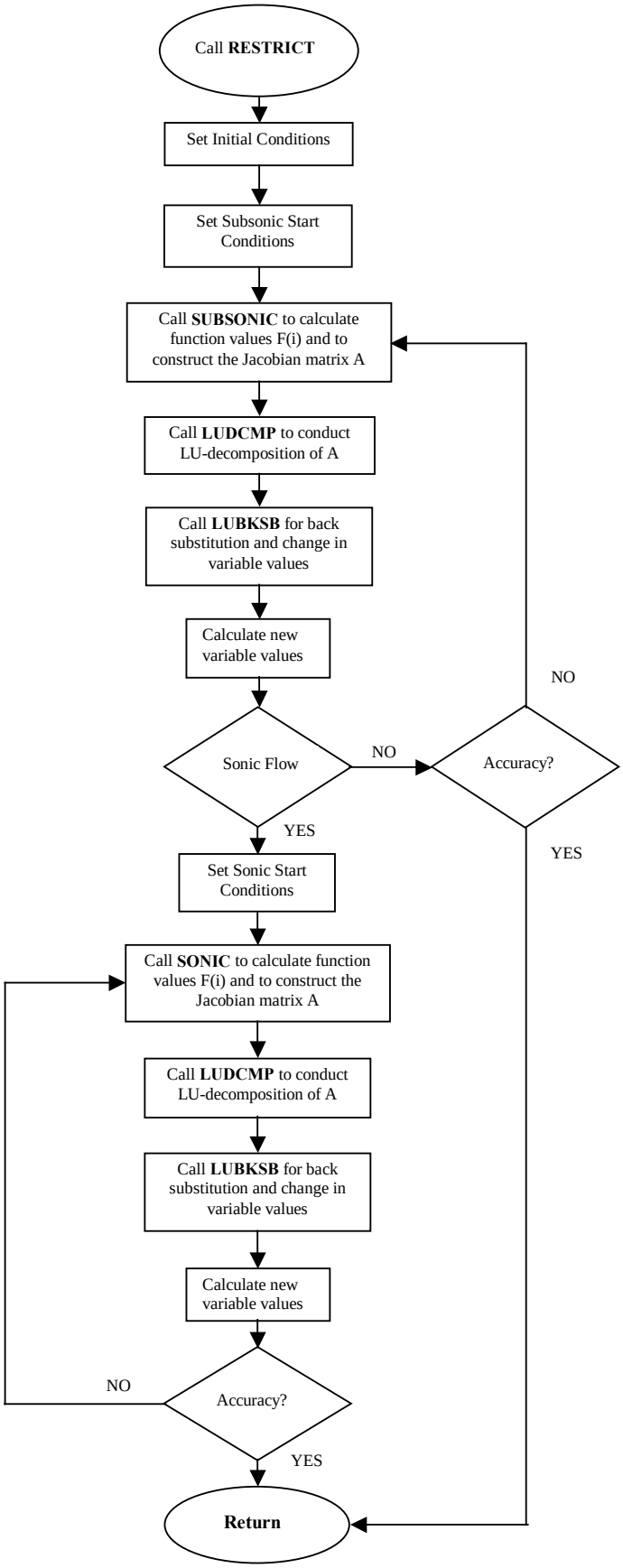

Figure 3.4: Flow Diagram of Subroutine RESTRICT

3.3.2 Testing of RESTRICT

Before RESTRICT could be incorporated into EngMod2T it was necessary to test the subroutine to ensure that it gave the correct results. It had to give the same results as the stepped pipe subroutines for a contraction $(A_1 > A_2)$ and for an expansion $(A_1 < A_2)$ with no restriction. (For $A_{teff} = A_2$ or $A_{teff} = A_1$ respectively with the relevant coefficients of discharge) For the purpose of these tests the test results given in Blair (1996) are used to compare the results of the stepped pipes with a restriction. By using RESTRICT, CONTRACT, and EXPAND as programs with the initial values given in Table 3.1, it gives the results that are summarised in Table 3.2. CONTRACT and EXPAND are the stepped pipe subroutines for contraction and expansion in pipe area as used in EngMod2T. To ensure consistency with the theory used in the pipe subroutine of EngMod2T the results of no area change ($A_1 = A_2 = A_{teff}$, Cd = 1.0) should return the same values as the pipe subroutine for no area change, TEMPDISC, would have.

Table 3.1: The initial values used to compare RESTRICT with CONTRACT, EXPAND and TEMPDISC.

Test No	d_1	d_2	d_t	C_d	Ar	Pi_1	Pi_2
1	25	50	25	1.0	4.0	1.2	1.0
2	25	50	25	0.85	4.0	1.2	1.0
3	50	25	25	1.0	0.25	1.2	1.0
4	50	25	25	0.7	0.25	1.2	1.0
5	50	25	15	0.85	0.25	1.2	1.0
6	25	50	15	0.85	4.0	1.2	1.0
7	25	25	25	1.0	1.0	1.2	1.0
8	25	25	25	0.85	1.0	1.2	1.0

Table 3.2: Results of the comparison of RESTRICT with CONTRACT, EXPAND and TEMPDISC.

	Expand Contract, Tempdisc or Results by Blair (1996)			Restrict	
Test No	**Pr_1**	**Pr_2**	**Theory**	**Pr_1**	**Pr_2**
1	0.8850	1.0785	Expand	0.88501	1.07851
2	0.8931	1.0768	Blair	0.89307	1.07683
3	1.1227	1.3118	Contract	1.12270	1.31180
4	1.1239	1.3075	Blair	1.12389	1.30752
5	1.1436	1.2351	Blair	1.14363	1.23508
6	0.9967	1.0537	Blair	0.99669	1.05368
7	1.0000	1.2000	Tempdisc	1.00000	1.20000
8	1.0002	1.1998	Tempdisc	1.00022	1.19981

The test results as summarised in Table 3.2 indicates that it is acceptable to include subroutine RESTRICT into the program EngMod2T. The results of the three subroutines give identical results to RESTRICT. This is as expected as the same theoretical approach is used as well as the same numerical solution scheme.

3.4 CLOSING

The thermodynamic equations for 1-dimensional compressible flow through a restriction as given by Blair (1996) was developed into a suitable format for programming and subroutine RESTRICT was developed and tested. It gave acceptable test results and was included into the program EngMod2T.

CHAPTER 4

DETERMINATION OF DISCHARGE COEFFICIENTS

4.1 PRE-AMBLE

The chapter starts off by describing the experimental apparatus used to determine the flow through the different tailpipe entry configurations. This is followed by the development of the equations and software necessary to determine the coefficient of discharge from the experimental results. Next, the results from the tests are presented.

4.2 DESCRIPTION OF EXPERIMENTAL APPARATUS

The experimental apparatus for the measurement of the coefficients of discharge is shown in Figure 4.1. It was developed for these tests. The required range of pressure and mass flow ratios were determined by conducting a series of simulations with the tail pipe pressure ratio and mass flow as outputs. A sample of the results is shown in Appendix D. Originally the plan was to use the SuperFlow flow bench model SF110 that is available in the engineering laboratory at the University of Pretoria.

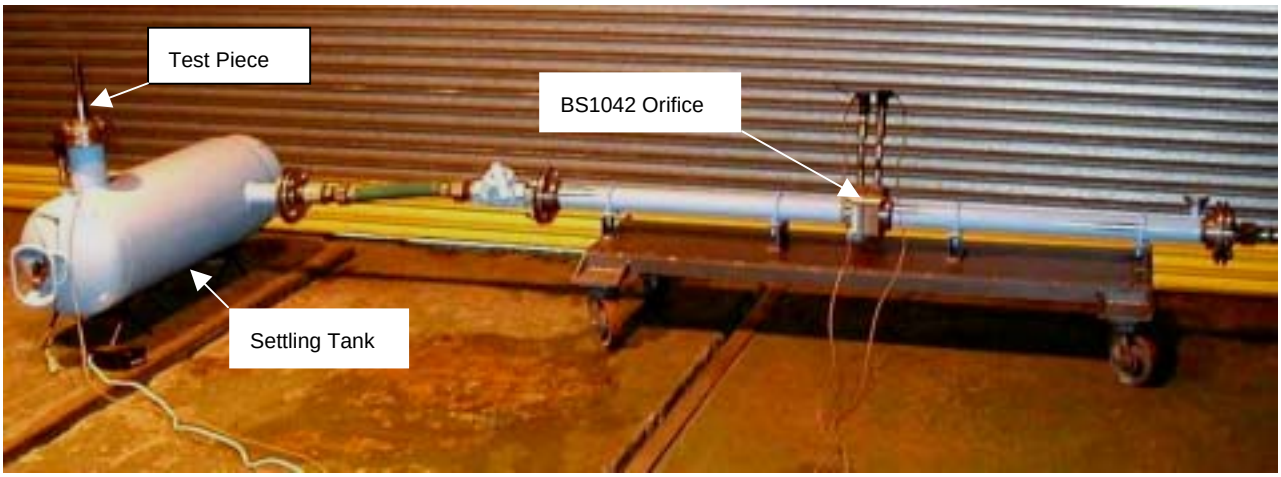

Figure 4.1: Experimental Apparatus

This flow bench is a small model and does not have a sufficient flow capacity to execute the tests at the required pressure ratios and mass flow values.

The compressor at the company Boart Longyear Seco was used to obtain the required mass flows and pressure ratios. This is a large industrial compressor capable of a sustained flow of 100kg/s at a pressure of 800kPa. The outlet of the compressor is connected to a pressure regulator and air drier. This regulator is used to control the pressure in the settling tank. (Refer to Figure 4.2 for a schematic layout of the test apparatus.)

From the drier the air passes through the flow measurement section containing an orifice, changeable in diameter to measure more accurately differing flow rates, with corner pressure tappings designed to conform to British Standard BS1042 (Anon)

and ending in the settling tank. The settling tank has pressure and temperature sensors. On top of the settling tank is a pipe at the end of which the test pieces are mounted. The outlet of the test piece is to atmosphere, of which the temperature and pressure are recorded.

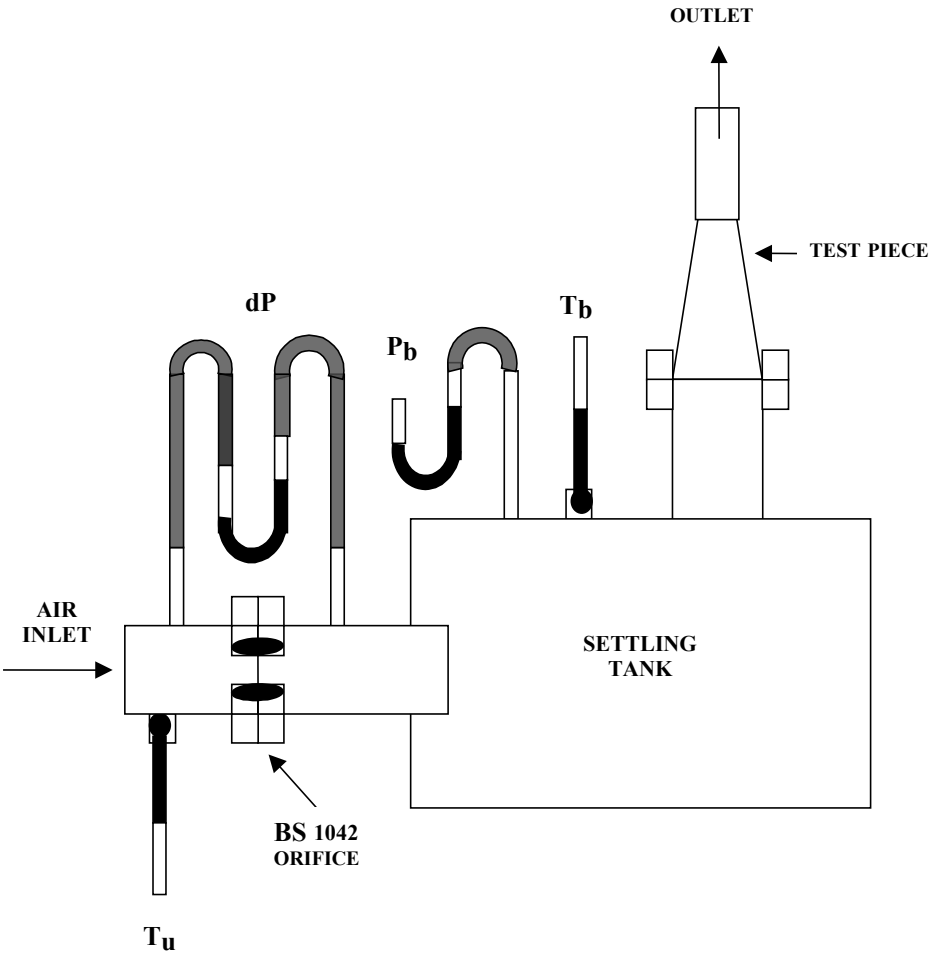

Figure 4.2: Schematic Drawing of Experimental Layout

A detailed description of the various sensors used and their calibration factors are included in Appendix C. Included as well are the detail drawings and the design limits of the flow-measuring device according to British Standard BS1042.

4.3 DEVELOPMENT OF SOFTWARE TO CALCULATE THE COEFFICIENT OF DISCHARGE

The coefficient of discharge used in the subroutine RESTRICT is the actual coefficient of discharge as described in by Blair et al (1995). Briefly, this means that if the orifice and ducts are modelled using the GPB method and the equations as derived in chapter 3, the calculated coefficient of discharge will, if used in the simulation with the same boundary conditions, predict the same mass flow as the measured mass flow.

To achieve this a program, FLOWPROG, was written using the pipe flow and the pipe boundary condition subroutines of EngMod2T combined with subroutine RESTRICT as developed in chapter 3. FLOWPROG simulates the actual flow bench, flow bench test pieces and boundary conditions. It uses the settling tank pressure and temperature as the inflow conditions to the test piece and the atmospheric temperature and pressure for the outflow boundary conditions. FLOWPROG uses as input the following parameters:

i. Test piece geometry

ii. Test Pressure (Refer to Figure 4.2)

iii. Test Temperature

iv. Atmospheric temperature and pressure

v. Corrected measured mass flow.

The program starts off by assuming a coefficient of discharge of 1.0 and calculates the mass flow. It then decreases the coefficient of discharge and recalculates the mass flow. This process is repeated until the measured and predicted mass flows are within 1% of each other.

4.4 EXPERIMENTAL DETERMINATION OF COEFFICIENT OF DISCHARGE.

It is not possible to test the restriction in isolation because of the physical constraints. The restriction is by its very nature the result of the flow through the joining of the reverse cone and tailpipe of the exhaust system. However, testing the tailpipe/reverse cone combination on the flow bench adds the complication to the test that the inflow discharge coefficient at the test piece inlet diameter is a partial unknown. The effect of the friction factor (and thus the effect of the length of the test piece) is also unclear at this stage. It is therefore necessary to evaluate these effects first to ensure that their influence on the final test results are minimised before the actual testing to determine the coefficients of discharge commences.

4.4.1 Influence of test piece length and inlet diameter on results

In order to minimise the effect of the flow losses at the inlet of the reverse cone it is advantages to use a sufficiently large diameter to reduce the entry speed of the air. This has however the adverse result of lengthening the reverse cone as the included angle is one of the controlling parameters of the restriction that is being studied.

In order to study this effect, four test cases were modelled and tested using FLOWPROG. The test piece dimensions and the test results at a range of test pressures are shown in Table 4.1. The coefficient of discharge at the test piece entry from the settling tank (which conforms to the definition by Blair and Drouin (1996) of an open ended plain pipe) and is described by the following polynomial function:

$$1.0<Pr<1.4 \quad Cd = -23.543+60.686Pr-51.04Pr^2+14.387Pr^3 \qquad (4.1a)$$

1.4<Pr Cd = 0.838 (4.1b)

For the purpose of this investigation the coefficient of discharge at the tailpipe entry was fixed to a value of 1.0. The inlet pressure was varied from 120 kPa to 180 kPa in steps of 20 kPa and an atmospheric pressure of 100 kPa was used. At each pressure the mass flow was calculated using both the coefficient of discharge calculated from equation 4.1 and a value of 1.0. By comparing the results an indication of the sensitivity of the calculated mass flow to test piece entry diameter could be determined. The results are summarised in Table 4.1 and the dimensions refer to Figure 4.3.

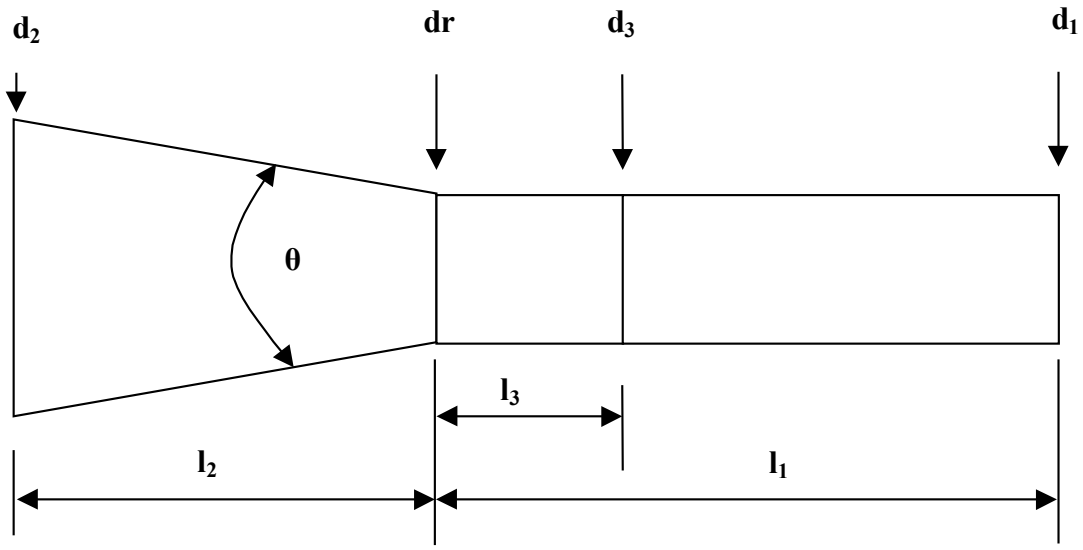

Figure 4.3: Schematic layout of test piece

Table 4.1: Simulation test results for plain inlet with 25° included angle

TEST PIECE DIMENSIONS						MASS FLOW AT THE FOLLOWING PRESSURE RATIOS AND Cd VALUES							
					Pr	1.2		1.4		1.6		1.8	
					Cd	Eq 4.1	1.0	Eq 4.1	1.0	Eq 4.1	1.0	Eq 4.1	1.0
No	d_1	d_t	d_2	l_1	l_2								
1	21.5	21.5	55	100	75	0.0660	0.0667	0.0937	0.0945	0.1150	0.1158	0.1328	0.1337
2	21.5	21.5	66	100	100	0.0663	0.0667	0.0941	0.0945	0.1154	0.1158	0.1332	0.1337
3	21.5	21.5	82	100	125	0.0666	0.0667	0.0944	0.0946	0.1157	0.1159	0.1336	0.1337
4	21.5	21.5	99	100	150	0.0666	0.0667	0.0945	0.0946	0.1158	0.1159	0.1336	0.1337

The results show that the sensitivity of the tests on the test piece inlet conditions (coefficient of discharge and diameter) decreases as the diameter increases. However, the difference in mass flow for the 55mm diameter entrance using a Cd value of 1.0 versus the calculated Cd value using equation 4.1 is only 1.2 percent. Thus, even if the calculated Cd value incorporates an error, the effect on the results will be at maximum 1.2 percent, assuming the incorrect value will fall between 1.0 and the correct value. Based on this fact, a test piece starting diameter of 63mm was selected as this is a freely available hydraulic pipe diameter and therefor a convenient size. The length for these sizes of test pieces has no effect.

4.4.2 Description of the test pieces

In order to create a coefficient of discharge map or to develop some mathematical relationship between the geometry, pressure ratio and coefficient of discharge for the conventional type of tail pipe entry four test pieces were constructed having the same entry diameters and the same size tail pipes. The only value that was varied was the included angle (and resulting from that, the cone length) in steps of 10 degrees starting from 10 degrees and ending at 40 degrees. In tuned pipes the included angle varies typically from 15 degrees to 30 degrees depending on the application of the engine. The first four test pieces cover this spread of values. (Test pieces no 1 to 4)

The dimensions of the test pieces are shown in Table 4.2. The dimensions are as per Figure 4.3.

To investigate the size effect of the tailpipe a further two test pieces were constructed but with a bigger diameter and a smaller diameter tail pipe than used with the first four test pieces. The included angle was kept to 30 degrees. (Test pieces no 5 and no 6)

The next series of test pieces were variations of the type where the end of the reverse cone is smaller than the tail pipe. Two test pieces were constructed with the reverse cone end stepping up directly from its diameter to the tail pipe diameter. This is the layout used by the Aprillia Racing Team. (Test pieces no 7 and 8) This type of tail pipe geometry is known as the **Restrictor** type of tailpipe.

The final two test pieces were a further development on this theme. Instead of stepping up directly from the reverse cone end diameter to the tail pipe diameter, a gradual increase to the tail pipe diameter is used. This results in a venturi at the tail pipe entrance and is the layout as used by the Honda Racing Team. This is also the layout that prompted this research project. (Test pieces no 9 and no 10) This type of tail pipe geometry is known as the **Venturi** type of tailpipe.

Table 4.2: Test Piece Dimensions

No	d_1	d_2	d_3	dr	l_1	l_2	l_3	θ
1	21.8	63.2	21.8	21.8	100	236	0	10
2	21.8	63.2	21.8	21.8	100	117	0	20
3	21.8	63.2	21.8	21.8	100	77	0	30
4	21.8	63.2	21.8	21.8	100	57	0	40
5	20.5	63.2	20.5	20.5	100	79	0	30
6	23.5	63.2	23.5	23.5	100	75	0	30
7	22.0	63.2	22.0	20.5	100	79	0	30
8	23.5	63.2	23.5	20.5	100	79	0	30
9	22.0	63.2	22.0	20.5	80	79	20	30
10	23.5	63.2	23.5	20.5	80	79	20	30

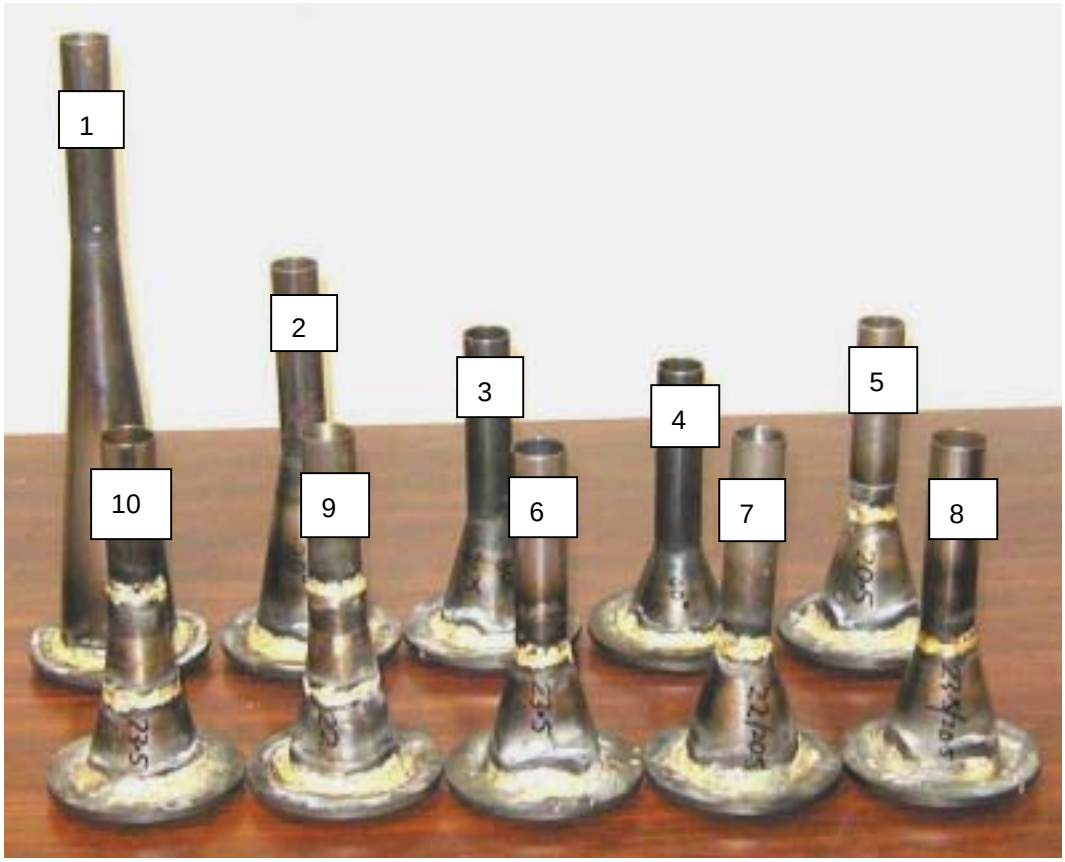

Figure 4.4: Photo of test pieces

4.4.3 Experimental Procedure

The test sequence is as follows:

i) The test apparatus is connected in the manner of Figure 4.2.

ii) The pressure transducers are calibrated using a Budenburg tester. This is done with the transducer connected to the computer with the same connecting cables as used in the actual tests.

iii) With the pressure transducers in place and the test piece connected the regulator is opened and adjusted to obtain the required pressure in the settling tank.

iv) Once the pressure values have stabilised the pressures and temperatures are recorded.

v) The orifice pressures are used to calculate the pressure differential over the orifice to ensure that the orifice size falls inside the prescribed requirements of BS1042. If not, the size must be changed and the results recorded again.

vi) If the pressure differential conforms to BS1042 the regulator is adjusted to obtain the next settling tank pressure and points iii to v are repeated.

vii) Once the results for required range of pressures for the test piece have been recorded the next test piece is installed and the process is repeated starting at point iii.

4.4.4 Experimental Results

The mass flow for each test piece for the range of test pressure ratios are calculated from the test results. The calculations are done according to BS1042 for the orifice and uses the following inputs:

i) Upstream pressure

ii) Downstream pressure

iii) Upstream temperature

iv) Orifice and tube diameters

v) Atmospheric pressure.

A program was written using the methodology as described in BS1042: Part 1.4 to speed up the calculation process. Firstly the measured pressures are averaged over a sample period of 15 seconds to eliminate the effect of a small problem with noise, then corrected using the calibration curves obtained from the Budenburg tester and than further corrected according to the Wika calibration curve. The results are then used in the BS1042 program to calculate the mass flow. The results are summarised in Appendix E.

4.5 PROCESSED RESULTS

4.5.1 Discussion of Processing Methodology

The mass flow and pressure results from the tests were used as input values into program FLOWPROG and the coefficient of discharge for each test piece at the tested range of pressure ratios was determined. The effect of an additional variable was also included, the mesh length as used by the GPB method.

The mesh length is an inverse function of the engine speed and is usually chosen to be the distance travelled by the pressure wave in one degree of crank rotation [46]. This has the effect of shortening the mesh length as the engine speed increases. With this decrease in length, the length of the final mesh in the reverse cone decreases and thus it's cross sectional area (The cross sectional area of a mesh is the mesh volume divided by the mesh length, Figure 2.1).

The cross sectional area of the final mesh in the reverse cone divided by the smallest area of the restriction (which for a conventional layout is the tailpipe cross sectional area) is defined as the mesh area ratio, Ar_m.

An additional effect of this is that the calculated pressure in the final mesh will also change as the calculated mesh pressure is the average pressure in the mesh. The restriction pressure ratio, P_r, is defined as the pressure in the final reverse cone mesh divided by the pressure in the first tailpipe mesh.

As an alternative it would also be possible to use the pressure in the throat of the restriction in the place of the pressure in the tailpipe. This has the disadvantage that the Cd-values for subsonic and sonic flows will be two separate curves because the pressure/flow relationship in the throat is different for subsonic and sonic flow conditions (Equation 3.35). Using the pressure ratio as defined circumvents this problem and leads to an easily implemented solution.

A coefficient of discharge for a fixed orifice can usually be described by a polynomial function that is a function of pressure only. In this case the area ratio is not fixed and instead of a function, it will be a surface (Known as a Cd-map) that is a function of both the pressure ratio and the area ratio. Typically mesh lengths varies between 8mm and 20mm for engine simulations (Blair, 1999). To cover this spread of mesh lengths the mesh lengths in FLOWPROG was varied by varying the mesh area ratio in steps starting from a ratio that resulted in a mesh length of about 5mm to a ratio that resulted in a mesh length of about 25mm.

The complete set of results is included as Appendix F. As an example, the Cd-map for the 30 degree included angle cone (test piece 3) for an area ratio of 1.2 is shown here, Figure 4.5. What is clear from the figure is that the coefficient of discharge is a strong function of the pressure ratio but it varies to a much lesser extent with the area ratio.

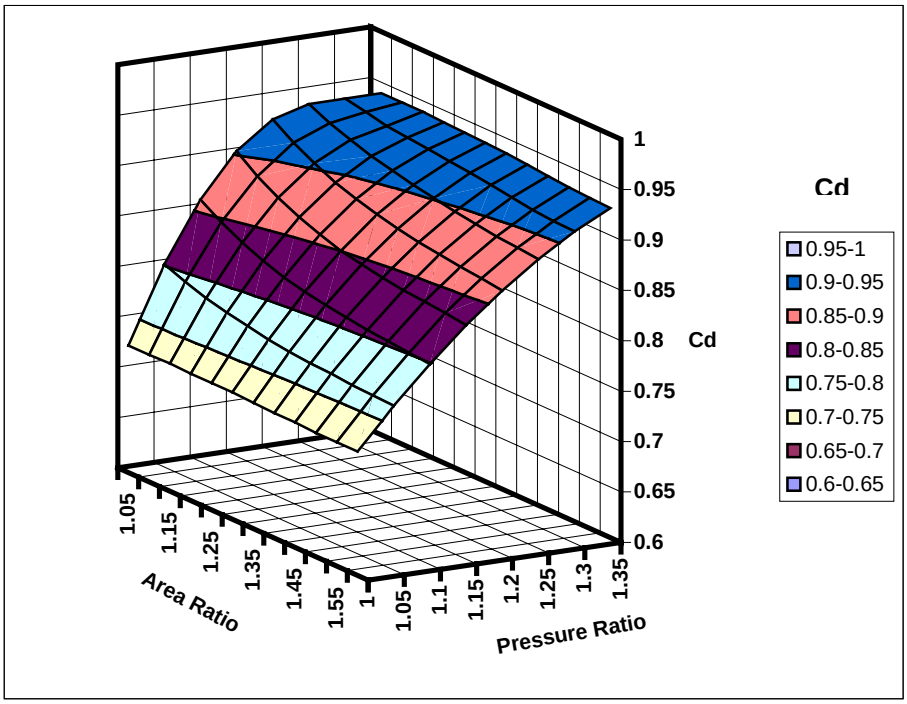

Figure 4.5: Cd-map for a 30 degree included angle reverse cone

In Figure 4.6 the results for the same 30 degree cone is shown but for four area ratios, 1.15, 1.30, 1.45 and 1.60 on the same two-dimensional graph. The effect of the area ratio on the Cd-value can be up to 5 percent between the smallest and largest area ratios.

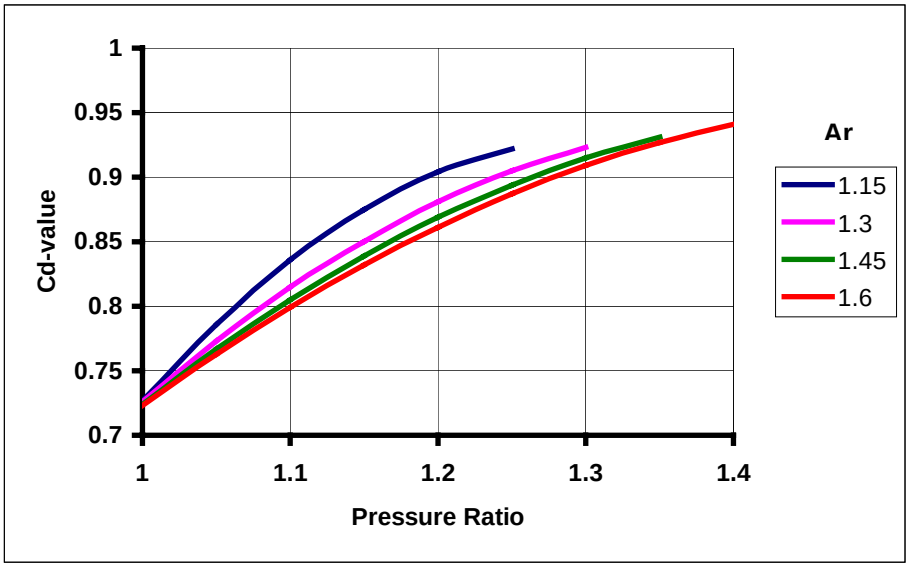

Figure 4.6: The effect of mesh length (area ratio) on Cd-values

4.5.2 The effect of reverse cone included angle.

The first four test pieces studied the effect of the reverse cone angle. The complete set of Cd-maps is included in Appendix F. For comparative purposes a graph was constructed by keeping the area ratio fixed at 1.2. This is shown in Figure 4.7.

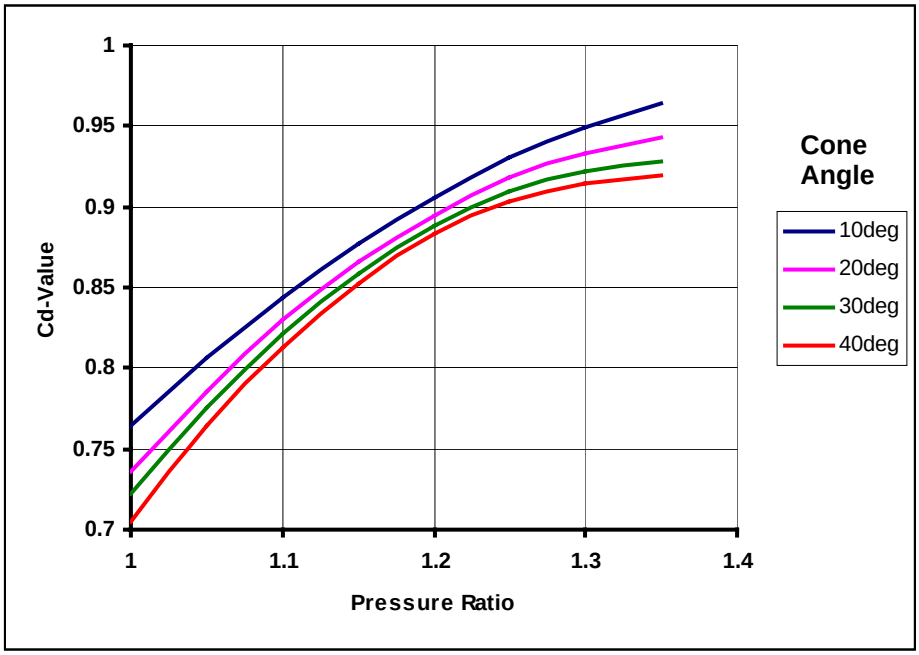

Figure 4.7: The effect of included cone angle on the Cd-values

The graph clearly shows that as the included angle decreases, thus approaching a straight pipe, the Cd-values increases and vice versa. This is in line with what is expected and the Cd-values should approach those of a plain open-ended pipe as the cone angle approaches 180 degrees.

4.5.3 The effect of the tail pipe diameter

The tailpipe diameter should not have an influence on the coefficient of discharge if the choice of non-dimensional dependant variables were correctly chosen. This is confirmed by the comparison in Figure 4.8. The original measured points are shown with the trend lines fitted using a least squares fit. The trend lines are very close together with a maximum deviation of 1.3% from the mean and inside the data scatter which has a maximum value of 2.8%.

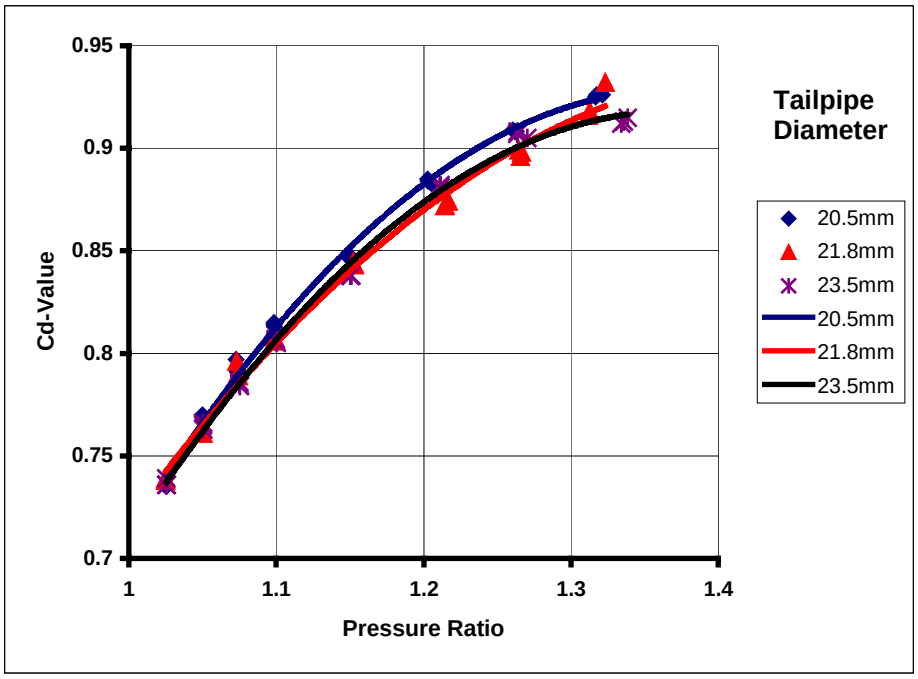

Figure 4.8: The effect of tailpipe diameter on the Cd-values

4.5.4 The effect of the Restrictor tail pipe geometry

This is one of the non-conventional tailpipe entry geometries under investigation. It is constructed by using a tailpipe that is larger than the end of the reverse cone. Two test pieces were investigated with the same size reverse cone end diameter of 20.5mm but with a 22.0mm and a 23.5mm tailpipe fitted respectively. The results are then compared to those of the conventional tailpipes of 20.5mm and 23.5mm. The mass flow results are shown in Figure 4.9 and the Cd-values in Figure 4.10.

From Figure 4.9 it is clear that the mass flow increases slightly with an increase in tailpipe diameter for the same restriction size but it follows the conventional 20.5mm tailpipe characteristic very closely, although with slightly more flow. Even with the 23.5mm tailpipe fitted the mass flow is close to that for the 20.5mm conventional tailpipe.

The coefficients of discharge increase with the size of the tailpipe. (Figure 4.10) Although it is the opposite to what is expected, it is indeed correct. The pressure ratio used is a function of the last reverse cone mesh pressure and the first tailpipe mesh pressure and while this is not incorrect, it would probably more correct to include the pressure in the vena contracta as well. This leads to additional complexity with the only advantage being a more consistent graph. The important fact is that the gasdynamic calculations would yield the correct mass flow results as long as the definition of the pressure ratio used for both the test results and its inclusion in the software is consistent.

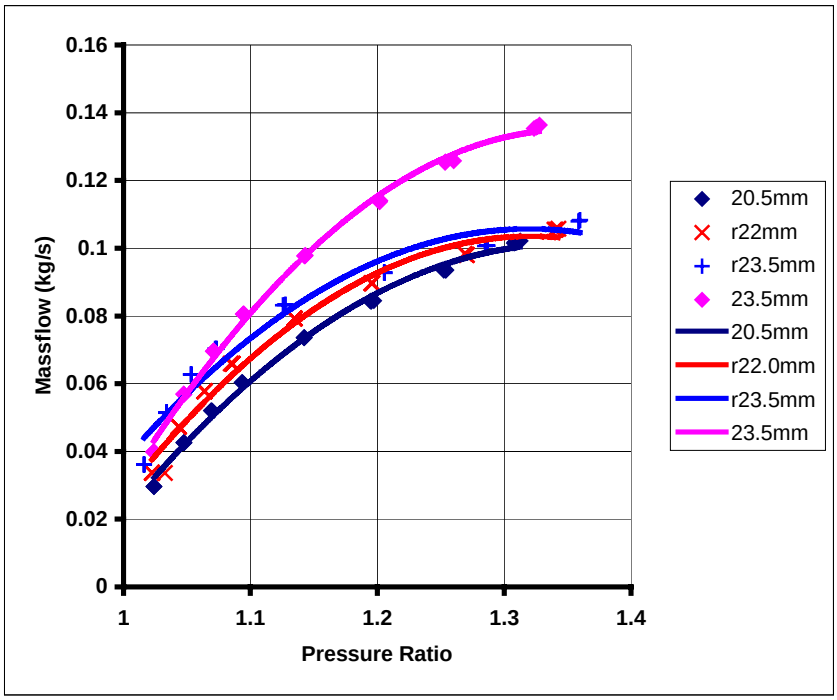

Figure 4.9: Mass flow values for restricted tailpipe entries

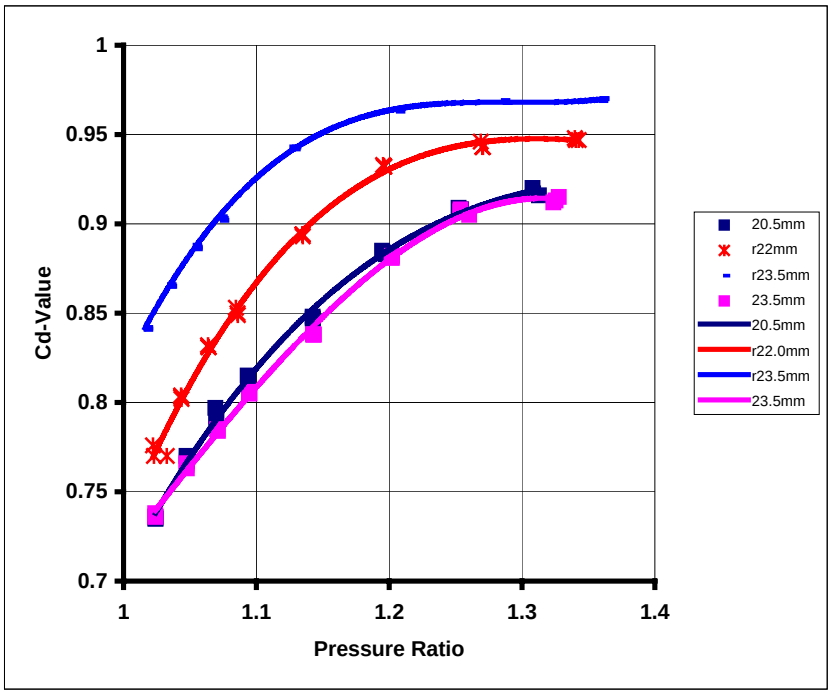

Figure 4.10: Cd-Values for the restricted tailpipe configuration

4.5.5 The effect of the gradual area change restriction (venturi)

The results for the venturi type tailpipe entry geometry test pieces are shown in Figures 4.11 and 4.12.

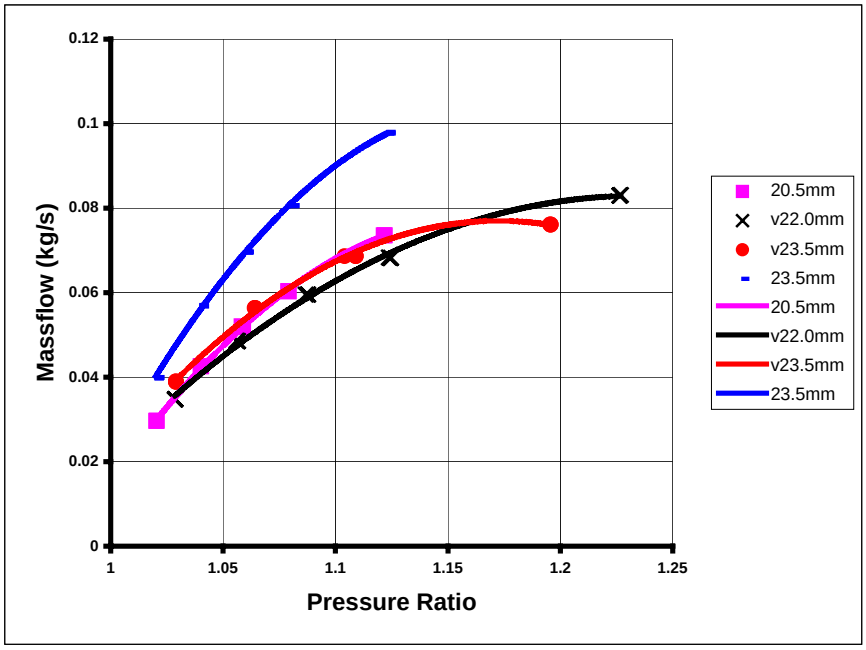

Figure 4.11: Mass flow results for the venturi type tailpipe entries

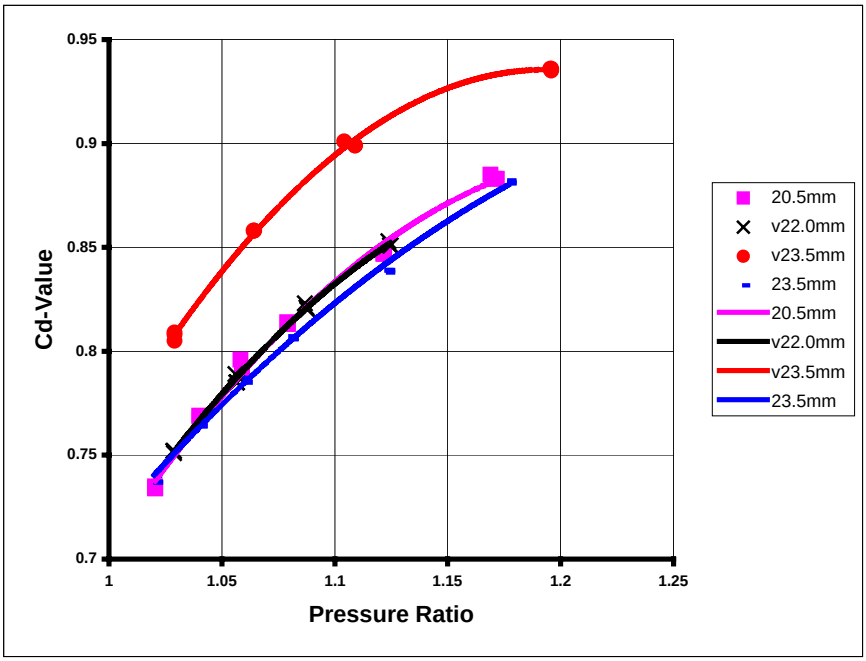

Figure 4.12: Cd-Values for the venturi type tailpipe entries

For comparative purposes the results for the conventional 20.5mm and 23.5mm conventional tailpipes are included on the graphs. Both the venturi with the 22.0mm tailpipe and the one with the 23.5mm tailpipe show virtually the same mass flow as the

conventional 20.5mm tailpipe. This is an unexpected result. The Cd-values does differ but that is because they are also a function of the mesh cross sectional diameters.

4.6 DISCUSSION OF RESULTS

The results showing the influence of the reverse cone angle on the Cd-values indicate clearly that the Cd-values are a function of the angle; it decreases with an increase in angle and vice versa. What is interesting is the small values (large losses) at small pressure ratios. This should have an effect on the simulation results and will be investigated in the next chapter. The effect of the tail pipe diameter was shown not to influence the Cd-values.

The restrictor tailpipe and the venturi tailpipe show unexpected results. The restrictor tail pipe mass flow follows the mass flow curve of the conventional tail pipe with the same diameter as the restrictor but with a small increase with an increase in tail pipe diameter. With the venturi tail pipe the mass flow follows the mass flow curve of the conventional tailpipe even closer.

A possible explanation for its usage on a racing motorcycle lies in the fact that the correct resistance of the tail pipe is important to its performance. On a racing motorcycle, because of its chassis and engine layout, it is not always possible to have the same length and diameter tail pipe and/or silencer on the exhaust pipe of each cylinder. Normally this would mean a large amount of testing and fine-tuning to match the resistances to the required value. Using a venturi of the correct size and a tail pipe and silencer of sufficient diameter will result in a pipe with the correct resistance. The resistor tail pipe will have the same trend but with a higher sensitivity to the tailpipe and silencer length and diameter.

This ties in with observations on the racetrack. The use of the restrictor tailpipe was first seen on the Aprillia RS250 racing motorcycle. It has one exhaust pipe fitted with a 75mm long tail pipe and a 180mm long silencer. The other pipe has a 100mm long tail pipe and a 250mm long silencer. The restrictor tail pipe probably supplies sufficient control over the resistances to match the two pipes.

The Honda NS250 racing motorcycle was the first motorcycle seen with the venturi tail pipes. It has the same length silencers on both pipes but the one exhaust has a 120mm long tail pipe and the other a 370mm long tail pipe. This motorcycle is also leased to various teams that use silencers from a range of suppliers. A venturi tail pipe will supply the needed control to maintain the required resistance.

4.7 CLOSING

In this chapter it was shown from experimental results that the Cd-values of the tail pipe entry are a function of pressure and reverse cone angle. The numerical method causes it to be a function of mesh length (area ratio) as well. The characteristics of the restrictor and venturi tailpipes were investigated and an explanation for its use was presented.

CHAPTER 5

SIMULATION STUDY

5.1 PRE-AMBLE

The effect of the experimentally determined coefficients of discharge on the performance prediction of two-stroke engines are determined by including the coefficient of discharge maps in the simulation software EngMod2T and conducting a range of simulations with and without the maps. The results are then compared to a dynamometer test of the same engine.

5.2 THE INCORPORATION OF THE CD-MAPS IN ENGMOD2T

During each simulation time step, a new value for the coefficient of discharge as a function of the pressure ratio, area ratio and the reverse cone angle is determined. This is done in the following manner:

i. During the start up of the main program a check is performed to determine between which two maps the reverse cone angle falls. These two maps are then read by the start up section of the program. (If it falls exactly on one of the maps the procedure is simplified.)

ii. During the gasdynamic calculation a bi-linear interpolation between the two area and the two pressure ratios that falls on either side of the point of interest on each map is performed. Thus a Cd-value is determined from each map.

iii. The final Cd-value is then determined by a linear interpolation between the two Cd-values.

iv. This value is then used for the next gasdynamic calculation.

v. For the next time step the procedure is repeated starting at point ii.

This process was coded into program EngMod2T and the four Cd-maps were prepared in the correct matrix format, similar to the Cd-maps for the engine ports and pipe ends, to allow the program to read them into memory during the start up process.

5.3 SIMULATED ENGINE PARAMETERS

The engine chosen for the simulation study is from a commercially available production motorcycle. Although it is meant for street use it is very popular as a racing motorcycle in modified form. The engine is twin cylinder engine in a 90degree V layout. The intake and exhaust systems of the two cylinders are completely independent and the engine can thus be simulated as a 125cc single cylinder.

Table 5.1: Major engine characteristics

Description of characteristic	Value
Engine type	90 deg V-2
Bore	54mm
Stroke	54mm
Capacity	125cc
Primary compression ratio	8.5:1
Secondary compression ratio	1.35:1
Type of exhaust port	Bridged
Number of transfer ports	5
Type of intake system	Reed valve

The complete set of input data used is listed in Appendix F. The exhaust pipe dimensions listed are for a pipe developed for this type of racing and used with success in racing application.

The physical data was obtained by measuring the engine. The values used in the combustion model were obtained from the experimental results of a similar engine (Blair, 1996).

5.4 VERIFICATION OF RESTRICT IN ENGMOD2T

To ensure that subroutine RESTRICT functions correctly and does not induce false results because of a numerical error a comparison was made between results obtained from the original version of EngMod2T and the updated version but with a Cd-value of 1.0. The new version but with a Cd-value of 1.0 should give the same results as the old version. The comparison of the power predicted by the two versions is shown in Figure 5.1. For all practical purposes the results are identical, proving that RESRICT gives the same results as CONTRACT for a Cd-value of 1.0. The small differences can be attributed to the numerical accuracy of the non-linear solution process. The influence of the coefficient of discharge can now be investigated.

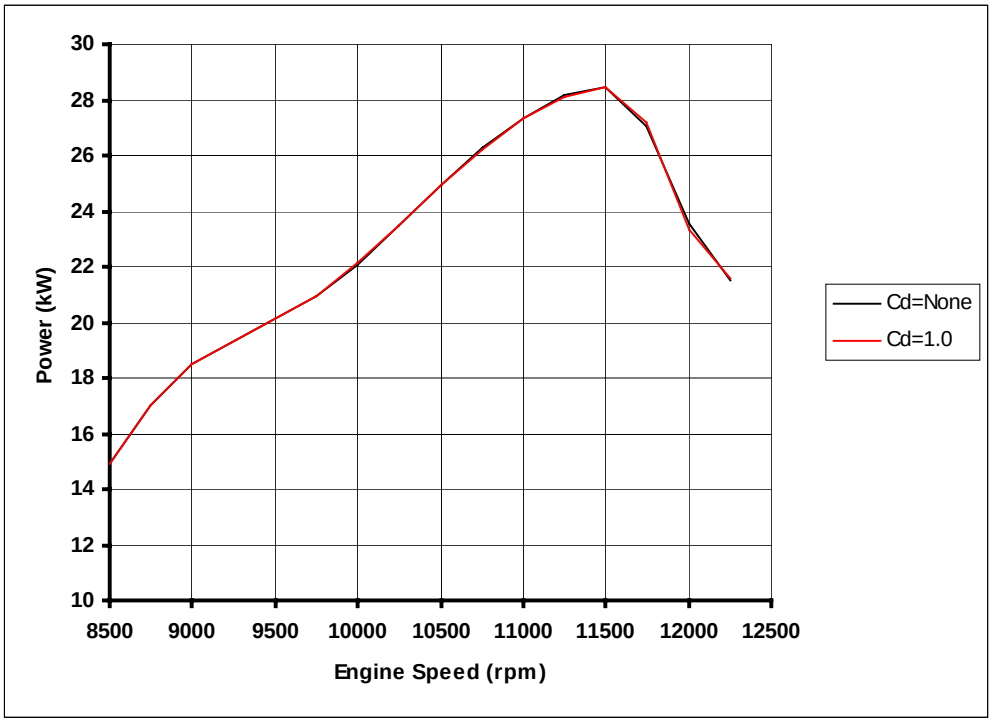

Figure 5.1: Comparison of the Power Predicted

5.5 THE EFFECT OF THE CD-MAPS ON THE SIMULATION RESULTS

To study the effect of the Cd-map on the simulation results the predicted power output, the delivery ratio and the maximum unburnt air temperature in the combustion chamber using the Cd-map are compared to those obtained with a Cd-value of 1.0. Figure 5.2 shows the predicted power output results.

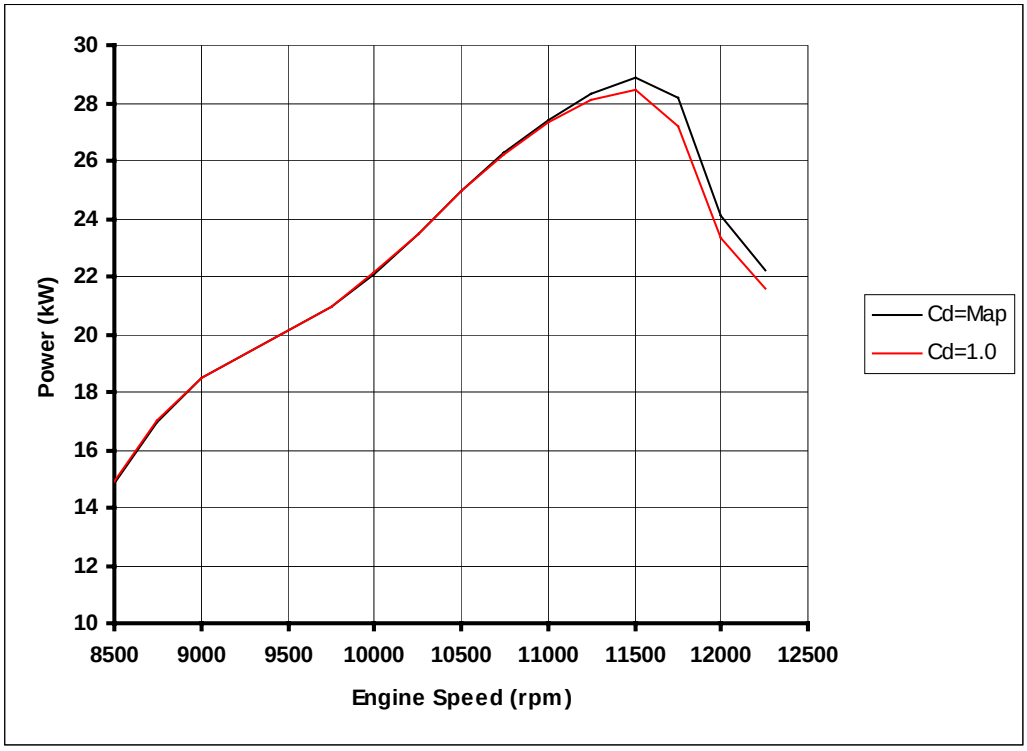

Figure 5.2: The Influence of the Cd-Map on the Power Predicted

The inclusion of the Cd-map increases the predicted power an increasing but small amount up to maximum power and has a large effect after maximum power. The portion of the power curve after maximum power is known as the “over run” of the engine and is very important on a racing engine because of the lengthening effect it has on the spread of useable power. (The so called “power band”) Accurately predicting the “over run” of an engine is an essential capability of a simulation program that is used for the development of competition engines.

The delivery ratio comparison (Figure 5.3) indicates that the increased resistance resulting from the Cd-map decreases the delivery ratio.

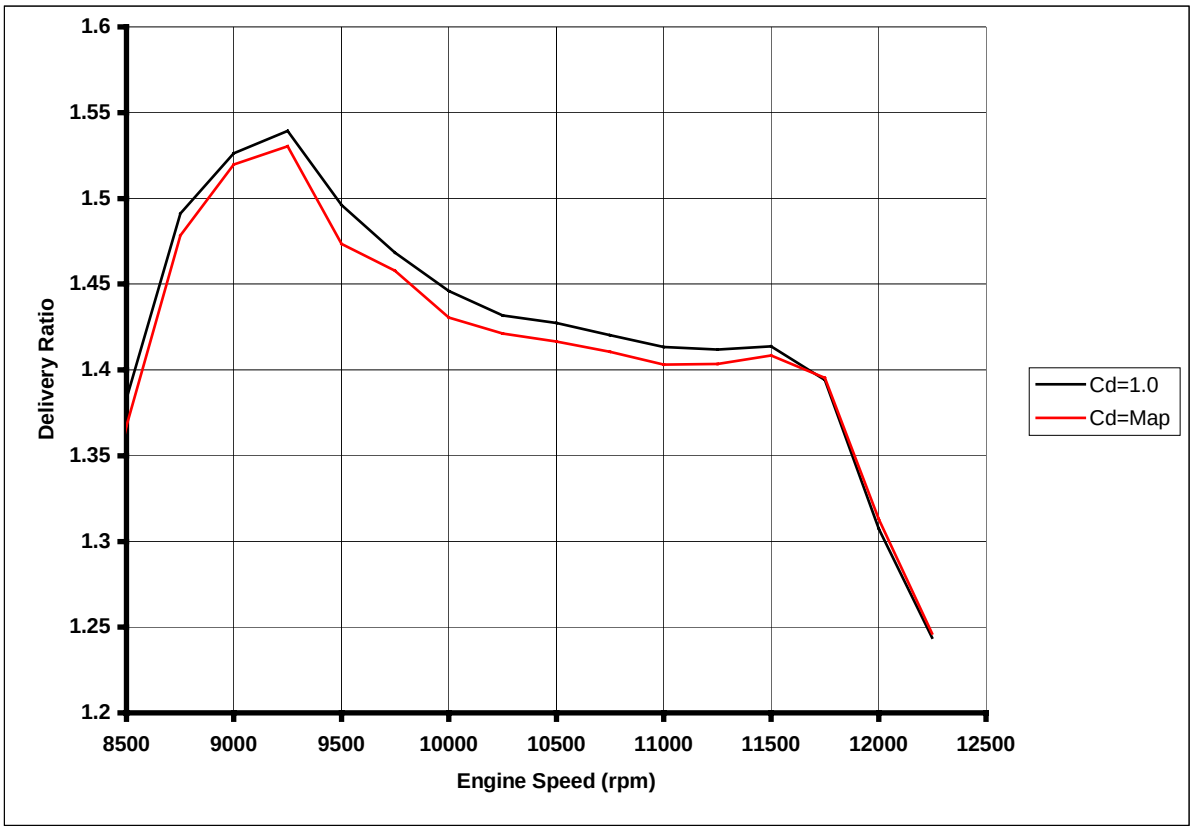

Figure 5.3: The Effect of the Cd-Map on the Delivery Ratio

The importance of this factor lays the effect the delivery ratio has on the temperature of the unburnt air during combustion. Two identical engines but with different delivery ratios and the same charging efficiency will produce the same power but the one with the lower delivery ratio will be more prone to detonation and pre-ignition. This is a direct result of less cool air flowing through the cylinder. The maximum temperature of the unburnt air before it becomes part of the combustion process indicates this. Figure 5.4 compares the maximum unburnt air temperatures for the two simulations.

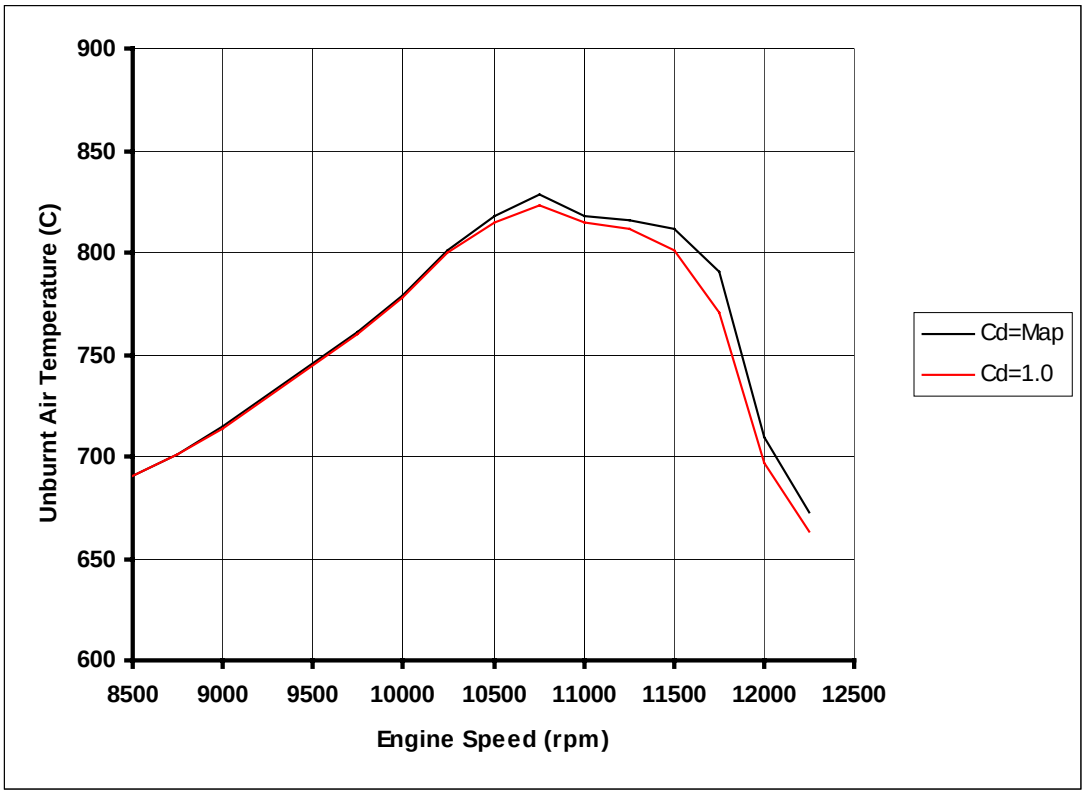

Figure 5.4: The Effect of the Cd-Map on the Maximum Unburnt Air Temperature

5.6 COMPARISON OF THE SIMULATED RESULTS WITH TEST RESULTS

To verify the improvement in the prediction of the power output of the software by the inclusion of the Cd-maps a comparison with measured results was made. The measured results are included as Appendix H. The tests were conducted on a Hyper Power dynamometer and a correction factor of 1.2 was used. Unfortunately this is not the correct factor but the tests had to fit in with other tests conducted on the motorcycle. The testing of a racing motorcycle is expensive (e.g. A set of pistons has a life of around 250 racing kilometres) and as many tests as possible must be conducted in the available time. This test was part of a test where different sets of exhaust pipes were compared.

The results in Appendix H show the power curves for the old and new version of the exhaust pipes. The results are in horsepower at the rear wheel. The results for the new pipe was converted to kilowatts and halved, as it is a two-cylinder engine. The results are compared with the predictions by the old and new version of EngMod2T in Figure 5.5. The absolute values are not the same because of losses through the drive train, water pump, ignition and the wheel to roller interface. For comparative purposes the measured results were “corrected” by multiplying it with a factor to have the same numerical maximum power as the new simulation. This comparison shows that the trend is correct for the new prediction. The inclusion of the Cd-maps improve the "over run" prediction to a similar curve shape as the measured result.

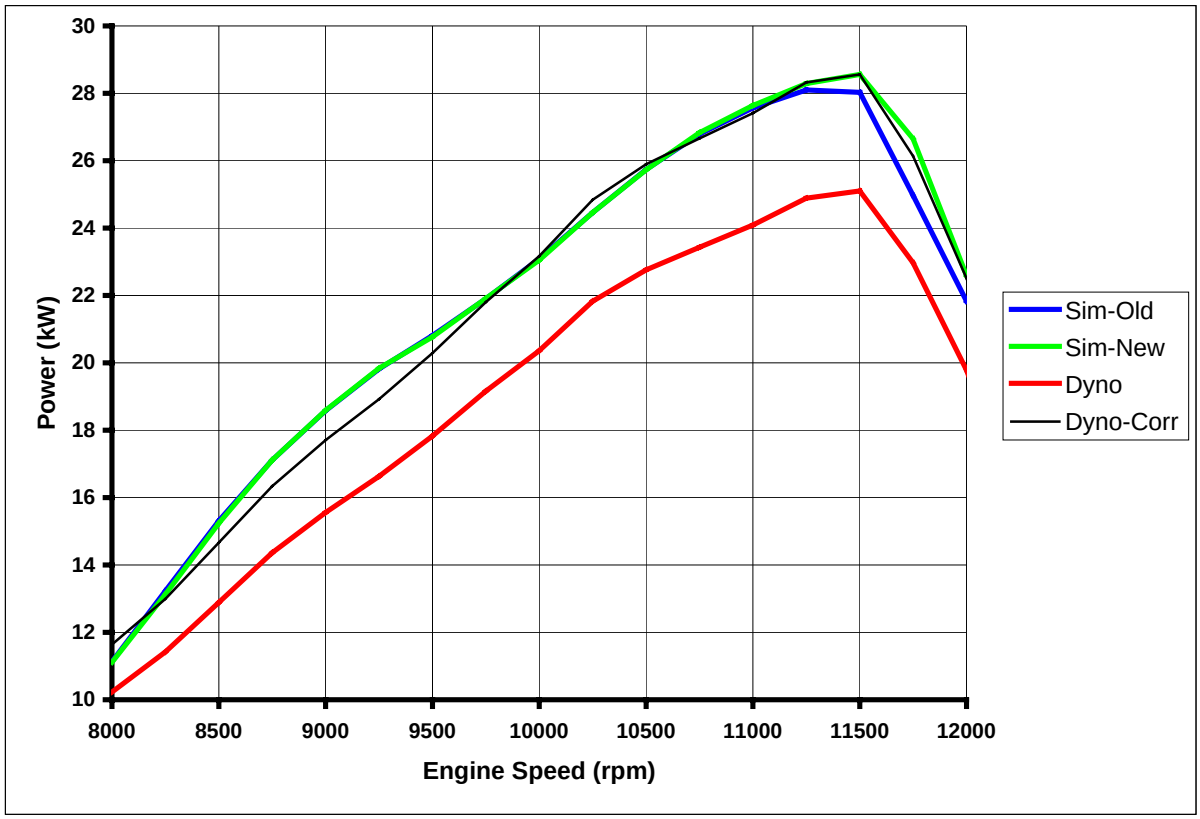

Figure 5.5: Comparisons of Predicted and Measured Power

5.7 CLOSING

The Cd-maps and subroutine RESTRICT were included in EngMod2T (version 2.3). It's influence on the predicted power and the other simulation results were investigated and compared to measured results. It was shown that the inclusion of the Cd-maps improves the accuracy of the simulation and is a necessary enhancement of the software.

CHAPTER 6

SUMMARY, CONCLUSION AND RECOMMENDATIONS

6.1 SUMMARY

The effect of a more accurate way of modelling the tail pipe entry geometry of the exhaust pipe of a high performance two-stroke engine in one-dimensional gasdynamic simulation software was investigated. Usually the entry to the tailpipe is modelled along similar lines as the rest of the reverse cone, as a normal area change. The effect of modelling the entry along the lines of a restriction with a coefficient of discharge was proposed for investigation.

A thermodynamically more sophisticated model that includes an increase in entropy on the expansion side was developed from the formulation by Blair, Kirkpatrick, Mackey and Fleck (1995) into a suitable format for the inclusion into simulation software. A Newton-Raphson method for solving a set of simultaneous non-linear equations was implemented to solve the equations for the restriction.

This implementation requires a coefficient of discharge value for the restriction. Apparatus for the experimental determination of the Cd-values for a range of reverse cone angles, pressure ratios and area ratios was constructed. A range of tests that cover the area and pressure ratios expected in an engine tailpipe was conducted and the results were presented in a format suitable for its inclusion in the simulation software.

The influence of the inclusion of this coding and Cd-maps in the software was investigated and the power predicted was compared with measured results. It turns out that using this approach improves the accuracy of the power output prediction at engine speeds higher than the speed at which maximum power occur.

At the same time the effect of special tailpipe entry geometry, the venturi inlet and the restriction inlet was investigated. It was concluded that their function is to control the exhaust outflow resistance to the required value and to remove its sensitivity to the geometry of the tail pipe and silencer that follows, as long as the tailpipe and silencer is of sufficient size not to cause an additional restriction.

6.2 CONCLUSION

A theoretical model taking the effect of a restriction at the tailpipe into consideration together with an increase in entropy on the expansion side was shown to change the performance predictions on a high specific power output two-stroke engine.

The size of the restriction was experimentally determined on a specially constructed test apparatus. The results were post processed into a series of Cd-maps. The maps showed that there is definitely a restriction (probably in the form of a vena contracta) present in the tail pipe entry.

Using the experimentally determined Cd-maps together with the newly developed restriction algorithm into the simulation model has a noticeable effect on the predicted performance results, mostly in the “over run” part of the power delivery. It also influences the predicted maximum unburned air temperature and the delivery ratio.

Comparing the old and the new predicted power curves with a measured one showed clearly that the new curve follows the measured curve much more closely on the part of the curve after maximum power and as good as the old one up to maximum power.

It is concluded that it is necessary to model the tailpipe entry geometry and flow conditions of a high performance two-stroke engine more accurately using a more sophisticated model combined with measured Cd-maps, especially if the area of interest is the “over run” portion of the power curve. Failing to do so can result in faulty deductions, insights and engine design compromises.

Additionally, the function of specially designed tail pipe entries was investigated. It was concluded that the main function of these special entries was to render the exhaust system insensitive to the geometry of the tail pipe and silencer provided they were not more restrictive than the tail pipe entry itself.

6.3 RECOMMENDATIONS AND FUTURE WORK

Comparing the predicted versus measured power characteristics the portion of the power curve up to maximum power shows distinct humps that is not there on the measured curve. This is probably resulting from the intake system resonant frequency. The shape of the delivery ratio curve, with humps corresponding to these in the power curve, highlights this. It is possible that a further improvement in the accuracy of the power prediction can be obtained by modelling the carburettor as a restriction similar to the tail pipe entry but with the cooling effect of the vaporising fuel taken into account. This should be an area of further study.

Appendix A

REFERENCES

ANNAND W.J.D. & ROE G.E. 1974. Gas Flow in the Internal Combustion Engine 1st Edition ISBN 0 85429 160 1 G T Foulis & Co Ltd

ANON. British Standard: BS1042: Section 1.1 and 1.4: 1984, Measurement of fluid flow in closed conduits.

BANNISTER F.K., Mucklow G.F. 1948. Wave Action Following Sudden Release Of Compressed Gas From A Cylinder. Proc. I. Mech. E., Vol. 159.

BANNISTER F.K. 1958. Pressure Waves In Gasses In Pipes. Acroyd Stuart Memorial Lectures, University Of Nottingham.

BENSON R.S. 1959. Experiments On Two Stroke Engine Exhaust Ports Under Steady And Unsteady Flow Conditions. Proc. Inst Mech. E, Vol 173, No 19.

BENSON R.S., Garg R.D. & Woollatt D. 1964. A Numerical Solution Of Unsteady Flow Problems. Int. J. Mech. Sci, Pergamon Press, Vol 6.

BENSON R.S. & Pool D.E. 1965a. Compressible Flow Through A Two-Dimensional Slit. Int. J. Mech Sci, Vol 7.

BENSON R.S. & Pool D.E. 1965b. The Compressible Flow Discharge Coefficients For A Two-Dimensional Slit. Int. J. Mech. Sci, Vol 7.

BLAIR A.J., Blair G.P. 1987. Gas Flow Modelling Of Valves And Manifolds In Car Engines. I. Mech. E. C11/87.

BLAIR G.P. 1976. Prediction Of Two-Cycle Engine Performance Characteristics. SAE 760645.

BLAIR G.P. 1990. The Basic Design Of Two-Stroke Engines. ISBN 1-56091-008-9, SAE R-104.

BLAIR G.P. 1991. An Alternative Method For The Prediction Of Unsteady Gas Flow Through The Internal Combustion Engine. SAE 911850.

BLAIR G.P. 1993. Correlation Of An Alternative Method For The Prediction Of Engine Performance Characteristics With Measured Data. SAE 930501.

BLAIR G.P. 1996. The Design And Simulation Of Two-Stroke Engines. ISBN 1-56091-685-0, SAE R-161.

BLAIR G.P. 1999. The Design And Simulation Of For-Stroke Engines. ISBN 0-7680-0440-3. SAE R-1861.

BLAIR G.P., Arbuckle J.A. 1970. Unsteady Flow In The Induction System Of A Reciprocating Internal Combustion Engine. SAE 700443.

BLAIR G.P., Ashe M.C. 1967. The Unsteady Gas Exchange Characteristics Of A Two-Cycle Engine. SAE 760644.

BLAIR G.P., Cahoon W.L. 1972. A More Complete Analysis Of Unsteady Gas Flow Through A High-Specific-Output Two-Cycle Engine. SAE 720156.

BLAIR G.P. & Drouin F.M.M. 1996. Relationship Between Discharge Coefficients And Accuracy Of Engine Simulations. SAE 962527.

BLAIR G.P., Goulburn J.R. 1967. The Pressure-Time History In The Exhaust System Of A High Speed Reciprocating Internal Combustion Engine. SAE 670477.

BLAIR G.P., Hinds E.T. & Fleck R. 1979. Predicting The Performance Characteristics Of Two-Cycle Engines Fitted With Reed Induction Valves. SAE 790842.

BLAIR G.P., Johnston M.B. 1968.Unsteady Flow Effects In Exhaust Systems Of Naturally Aspirated, Crankcase Compression Two Cycle Internal Combustion Engines. SAE 680594.

BLAIR G.P., Kirkpatrick S.J. & Fleck R. 1995. Experimental Validation Of A 1-D Modelling Code For A Pipe Containing Gas Of Varying Properties. SAE 950275**.**

BLAIR G.P., Kirkpatrick S.J., Mackey D.O. & Fleck R. 1995. Experimental Validation Of A 1-D Modelling Code For A Pipe System Containing Area Discontinuities. SAE 950276.

BLAIR G.P., Lau H.B., Cartwright A., Raghanathan B.D. & Mackey D.O. 1995. Coefficient Of Discharge At The Apertures Of Engines. SAE 952138.

BLAIR G.P., Magee S.J. 1993. Non-Isentropic Analysis of Varying Area Flow in Engine Ducting. SAE 932399.

BURDEN R.L. & Faires J.D. 2993. Numerical Analysis. 5th Ed, PWS Publishing Company.

CARTWRIGHT A & FLECK R. 1994. A Detailed Investigation of Exhaust System Design in High Performance Two-Stroke Engines, SAE 942515.

CHEN C., Veshagh A. & Wallace F.J. 1992. A Comparison Between Alternative Methods For Gas Flow And Performance Prediction Of Internal Combustion Engines. SAE 921734.

CORBERáN J.M., Royo R., Pérez A. & Santiago J. 1994. Optimisation of a 125 cc Racing 2-S Engine based on Modelling and Testing. SAE.

DECKER B.E.L. 1978. Compressible Flow Through Square Edge Rectangular Orifices. Proc. I. Mech. E., 1956, Vol 192.

DOUGLAS R., Mcginnity F.A. & Blair G.P. 1991. A Study Of Gas Temperature Effects On The Prediction Of Unsteady Flow. IMechE, C433/036.

EARNSHAW S. 1910. On The Mathematical Theory Of Sound, , Proc. Roy. Soc. 84.

FLECK R., Blair G.P. &, Houston R.A.R. 1987. An Improved Model For Predicting Reed Valve Behaviour In Two-Stroke Cycle Engines. SAE 871654.

FLECK R. & Cartwright A. 1996. Coefficients Of Discharge In High Performance Two Stroke Engines. SAE 962534.

FLECK R., Cartwright A. & Thornhill D. 1997. Mathematical Modelling Of Reed Valve Behaviour In High Speed Two-Stroke Engines. SAE 972738.

HINDS E.T., Blair G.P. 1978. Unsteady Gas Flow Through Reed Valve Induction Systems, SAE 780766.

IRVING P.E. 1969. Tuning for Speed, 5th edition. London : Newnes Books.

KIRKPATRICK S.J., Blair G.P., Fleck R. & McMullen R.K. 1994. Experimental Evaluation Of 1-D Computer Codes For The Simulation Of Unsteady Gas Flow Through Engines - A First Phase. SAE 941685.

LANEY C.B. 1998. Computational Gasdynamics. ISBN 0-521-57069-7. Cambridge University Press.

MACKEY D.O., Blair G.P. & Fleck R. 1996. Correlation Of Simulated And Measured Noise Emissions And Unsteady Gas Dynamic Flow From Engine Ducting. SAE 961806.

MCGINNITY F.A., Douglas R. & Blair G.P. 1990. Application Of An Entropy Analysis To Four-Cycle Engine Simulation. SAE 900681.

MUCKLOW G.F., Wilson A.J. 1955. Wave-Action In Gasses: The Attenuation And Reflection Of Compression Waves Propagated In Pipes. Proc. I. Mech. E. Vol 169.

ONORATI A., Winterbone D.E. & Pearson R.J. 1993. A Comparison Of The Lax-Wendroff Technique And The Method Of Characteristics For Engine Gas Dynamic Calculations Using Fast Fourier Transform Spectral Analysis. SAE 930428.

POLONI M., Winterbone D.E. & Nichols J.R. 1988. Flow With Variable Specific Heats In The Exhaust Pipe System Of The Internal Combustion Engine. SAE 885094.

VAN HOVE W. & Sierens R. 1991 Calculation of the unsteady flow in exhaust pipe systems: new algorithm to fulfil the conservation law in pipes with gradual area changes. Proc. I. Mech. E., Vol 205

WALLACE F.J., Boxer G. 1956. Wave Action In Diffusers For Exhaust-Pipe Systems, With Special Reference To The Scavenging Of Two-Stroke Engines. Proc. I. Mech. E.

WALLACE F.J., Nassif M.H. 1954. Air Flow In A Naturally Aspirated Two-Stroke Engine. Proc. I. Mech. E., Vol 168.

WALLACE F.J., Stuart-Mitchell R.W. 1953. Wave Action Following The Sudden Release Of Air Through An Engine Port System. Proc. I. Mech. E., Vol. 1b.

WINTERBONE D.E., Pearson R.J. 2000. Theory of Engine Manifold Design. 1st Edition. London. ISBN 1 86058 209 5 Professional Engineering Publishing Limited.

ZHANG H., Widener S.K. 1996. An Integrated Engine Cycle Simulation Model With Species Tracking In Piping System. SAE 960077.

Appendix B
Listing of subroutine RESTRICT.FOR

```
      SUBROUTINE RESTRICT(XI1,XI2,A01,G1,R,FA1,
     # FA2,PA,XR1,XR2,A02,T02,D02,FAT,CD,CT,XT,SING,T2)
C
C
C ****************************************************************
C This subroutine calculates the temperature, pressure, mass flow and
C entropy change through a restriction in a pipe. It was developed by
C CGJ van Niekerk based on the theoretical work of Professor GP Blair
C of the Queen's University of Belfast, Northern Ireland. The theory
C can be found in "Design and Simulation of Two-Stroke Engines", by
C GP Blair,SAE 1996.
C
C It solves the sets of non-linear equations using a Newton-Raphson
C scheme. The Jacobian is calculated numerically and the set of
C equations are solved using LU-factorization using two subroutines
C from from "NUMERICAL RECIPIES". LUDCMP does the decomposition and
C LUBKSB the back substitution.
C ****************************************************************
C
C FA1  = Left hand mesh sectional area
C FA2  = Right hand mesh sectional area
C FAT  = Throat area
C FEFF = Effective throat area
C CD   = Coefficient of discharge in throat
C XI1  = Left hand incidence wave pressure ratio
C XI2  = Right hand incidence wave pressure ratio
C XR1  = Left hand reflected wave pressure ratio
C XR2  = Right hand reflected wave pressure ratio
C
C
C
      IMPLICIT NONE
C
      CHARACTER SING*4

      REAL A(20,20),F(20)
      REAL D02,FA2,A02,XR2,XI2,G51,FA1,G71,A01,XI1,XR1,DELX,A02S,PA,T02
      REAL XMX,T2,AR,R,D,G1,G41,G61,A01S,FAT,XT,CT,CD,XTS,MST,MS1,MS2
      REAL FEFF,XR1S,XR2S,CTS

      INTEGER ITER,ITMAX,N,I,J,INDX(20)
C
C
       SING ='NONE'

       G71=2*G1/(G1-1)
       G51=2/(G1-1)
       G41=(3-G1)/(G1-1)
       G61=(G1+1)/(G1-1)

       FEFF =FAT*CD
```

```
C Parallel pipe positive flow for no restriction - do not use the restricted
subroutine

      IF(FA1.EQ.FA2.AND.FA1.EQ.FAT.AND.CD.GT.0.999)THEN

       CALL PARALLEL(XI1,XI2,A01,G1,G51,R,FA1,FA2,PA,XR1,
     # XR2,ITER,G41,G61,SING,T2,T02)

        IF(SING.EQ.'SING')THEN
         WRITE(6,*)'PIPE PARALLEL IN RESTRICT SINGULAR '
         STOP
        ENDIF

        A02=SQRT(G1*R*T02)
        GOTO 400
      ENDIF

! Initial starting values based on constant pressure

       AR  =FA2/FA1
       XR1S=((1-AR)*XI1+2*XI2*AR)/(1+AR)
       XR2S=(2*XI1-XI2*(1-AR))/(1+AR)
       XR1  =XR1S
       XR2  =XR2S

       IF(FA1.LE.FAT.AND.CD.GT.0.999)THEN
        XT  =XI1+XR1-1
        CT  =G51*A01*(XI1-XR1)
       ENDIF

! Results from previous cycle used as starting values

       CT   =ABS(CT)
       CTS  =CT
       XTS  =XT
       A02S =A02
       A01S =A01
C
C Subsonic restrictor flow
C
      A02=A02/100
      A01=A01/100
      CT =CT/100

      DELX = 0.001
      ITER = 0
      ITMAX= 15
      N    = 5
100   ITER=ITER+1

      DO I=1,N
       F(I)=0.0
       DO J=1,N
        A(I,J)=0.0
       ENDDO
      ENDDO

! Call subroutine with subsonic flow equations

      CALL SUBSONIC(DELX,XI1,XR1,XR2,XI2,FA1,FA2,FEFF,A01,A02,
     # G51,G71,XT,CT,F,A,G1)
```

```
      CALL LUDCMP(A,N,INDX,D,SING)

       IF(SING.EQ.'SING')THEN
        WRITE(6,*)'RESTRICT subsonic flow singularity'
         XR1=XR1S
         XR2=XR2S
         A02=A02S
         XT =XTS
         CT =CTS
        GOTO 400
       ENDIF

      CALL LUBKSB(A,N,INDX,F)

      XMX=-1.E5
      DO I=1,N
       XMX=AMAX1(ABS(F(I)),XMX)
      ENDDO

       XR1 =XR1 -F(1)
       A02 =A02 -F(2)
       XT  =XT  -F(3)
       XR2 =XR2 -F(4)
       CT  =ABS(CT-F(5))

! Test for sonic flow

      MST=ABS(CT/(A01*XT))

      IF(MST.GE.1.0)GOTO 300

      IF(XMX.LE.0.0001.OR.ITER.GT.ITMAX)GOTO 200
      GOTO 100

200   CONTINUE
      A02=A02*100
      A01=A01S
      CT =CT*100
      GOTO 400
C
C Sonic restrictor flow
C
300    CONTINUE

! Set initial values for sonic flow

         XR1=XI1-(G61-G51)/G51**2
         XR2=FA1*(XI1-XR1)/FA2+XI2
         A02=A01S/100
         XT=XI2+XR2-1
         A01=A01S/100

      DELX = 0.00002
      ITER = 0
      ITMAX= 45
      N    = 4

1200  ITER =ITER+1

      DO I=1,N
```

```
        F(I)=0.0
        DO J=1,N
         A(I,J)=0.0
        ENDDO
       ENDDO

! Call subroutine with sonic flow equations

       CALL SONIC(DELX,XI1,XR1,XR2,XI2,FA1,FA2,FEFF,A01,
      # A02,G51,G61,F,A,XT)

       CALL LUDCMP(A,N,INDX,D,SING)

        IF(SING.EQ.'SING')THEN
         WRITE(6,*)'RESTRICT sonic flow singularity'
         STOP
        ENDIF

       CALL LUBKSB(A,N,INDX,F)

       XMX=-1.E5
       DO I=1,N
        XMX=AMAX1(ABS(F(I)),XMX)
       ENDDO

        XR1 =XR1 -F(1)
        XT  =XT  -F(2)
        XR2 =abs(XR2 -F(3))
        A02 =abs(A02 -F(4))

       IF(XMX.LE.0.0001.OR.ITER.GT.ITMAX)GOTO 220
       GOTO 1200

220    CONTINUE

        A02=A02*100
        A01=A01S
        CT =XT*A01

400     T02=A02**2/(G1*R)
        T2 =T02*(XI2+XR2-1)**2
        D02=PA/(R*T02)

       RETURN
       END
C
C-----------------------------------------------------------------------
C
       SUBROUTINE SUBSONIC(DELX,XI1,XR1,XR2,XI2,FA1,FA2,FAT,A01,A02,
      # G51,G71,XT,CT,F,A,G1)
C
C This subroutine contains the equations for the subsonic flow conditions
C
       IMPLICIT NONE
C
       DIMENSION F(20),A(20,20)
       REAL FA2,A02,XR2,XI2,G51,FA1,G71,A01,XI1,XR1,F,A02S,A,G1
       REAL DELX,F1S,F2S,F3S,F4S,F5S,XR1S,XR2S,FAT,CT,CTS,XT,XTS
C
       F(1)=(XR1+XI1-1)**G51*A01*G51*(XI1-XR1)*FA1-FAT*XT**G51*CT
```

```
      F(2)=A02**2*FAT*XT**G51*CT-A01**2*(XR2+XI2-1)**G51*A02*G51*
     # (XR2-XI2)*FA2

      F(3)=G51*A01**2*(XR1+XI1-1)**2+(G51*A01*(XI1-XR1))**2-G51*A01**2*
     # XT**2-CT**2

      F(4)=G51*A01**2*XT**2+CT**2-G51*A02**2*(XR2+XI2-1)**2-(G51*A02*
     # (XR2-XI2))**2

      F(5)=A01**2*FA2*(XT**G71-(XR2+XI2-1)**G71)+G1*FA1*(XR1+XI1-1)**G51
     # *G51*A01*(XI1-XR1)*(CT-G51*A02*(XR2-XI2))

      F1S = F(1)
      F2S = F(2)
      F3S = F(3)
      F4S = F(4)
      F5S = F(5)

      XR1S  = XR1
      XR2S  = XR2
      XTS   = XT
      A02S  = A02
      CTS   = CT
C
      XR1 = XR1+DELX

      F(1)=(XR1+XI1-1)**G51*A01*G51*(XI1-XR1)*FA1-FAT*XT**G51*CT

      F(2)=A02**2*FAT*XT**G51*CT-A01**2*(XR2+XI2-1)**G51*A02*G51*
     # (XR2-XI2)*FA2

      F(3)=G51*A01**2*(XR1+XI1-1)**2+(G51*A01*(XI1-XR1))**2-G51*A01**2*
     # XT**2-CT**2

      F(4)=G51*A01**2*XT**2+CT**2-G51*A02**2*(XR2+XI2-1)**2-(G51*A02*
     # (XR2-XI2))**2

      F(5)=A01**2*FA2*(XT**G71-(XR2+XI2-1)**G71)+G1*FA1*(XR1+XI1-1)**G51
     # *G51*A01*(XI1-XR1)*(CT-G51*A02*(XR2-XI2))

      A(1,1) = (F(1)-F1S)/DELX
      A(2,1) = (F(2)-F2S)/DELX
      A(3,1) = (F(3)-F3S)/DELX
      A(4,1) = (F(4)-F4S)/DELX
      A(5,1) = (F(5)-F5S)/DELX

      XR1 = XR1S
C
      A02  = A02+DELX

      F(1)=(XR1+XI1-1)**G51*A01*G51*(XI1-XR1)*FA1-FAT*XT**G51*CT

      F(2)=A02**2*FAT*XT**G51*CT-A01**2*(XR2+XI2-1)**G51*A02*G51*
     # (XR2-XI2)*FA2

      F(3)=G51*A01**2*(XR1+XI1-1)**2+(G51*A01*(XI1-XR1))**2-G51*A01**2*
     # XT**2-CT**2

      F(4)=G51*A01**2*XT**2+CT**2-G51*A02**2*(XR2+XI2-1)**2-(G51*A02*
     # (XR2-XI2))**2
```

```
       F(5)=A01**2*FA2*(XT**G71-(XR2+XI2-1)**G71)+G1*FA1*(XR1+XI1-1)**G51
      # *G51*A01*(XI1-XR1)*(CT-G51*A02*(XR2-XI2))

       A(1,2) = (F(1)-F1S)/DELX
       A(2,2) = (F(2)-F2S)/DELX
       A(3,2) = (F(3)-F3S)/DELX
       A(4,2) = (F(4)-F4S)/DELX
       A(5,2) = (F(5)-F5S)/DELX

       A02  =  A02S
C
       XT   =  XT+DELX

       F(1)=(XR1+XI1-1)**G51*A01*G51*(XI1-XR1)*FA1-FAT*XT**G51*CT

       F(2)=A02**2*FAT*XT**G51*CT-A01**2*(XR2+XI2-1)**G51*A02*G51*
      # (XR2-XI2)*FA2

       F(3)=G51*A01**2*(XR1+XI1-1)**2+(G51*A01*(XI1-XR1))**2-G51*A01**2*
      # XT**2-CT**2

       F(4)=G51*A01**2*XT**2+CT**2-G51*A02**2*(XR2+XI2-1)**2-(G51*A02*
      # (XR2-XI2))**2

       F(5)=A01**2*FA2*(XT**G71-(XR2+XI2-1)**G71)+G1*FA1*(XR1+XI1-1)**G51
      # *G51*A01*(XI1-XR1)*(CT-G51*A02*(XR2-XI2))

       A(1,3) = (F(1)-F1S)/DELX
       A(2,3) = (F(2)-F2S)/DELX
       A(3,3) = (F(3)-F3S)/DELX
       A(4,3) = (F(4)-F4S)/DELX
       A(5,3) = (F(5)-F5S)/DELX

       XT   =  XTS
C
       XR2  =  XR2+DELX

       F(1)=(XR1+XI1-1)**G51*A01*G51*(XI1-XR1)*FA1-FAT*XT**G51*CT

       F(2)=A02**2*FAT*XT**G51*CT-A01**2*(XR2+XI2-1)**G51*A02*G51*
      # (XR2-XI2)*FA2

       F(3)=G51*A01**2*(XR1+XI1-1)**2+(G51*A01*(XI1-XR1))**2-G51*A01**2*
      # XT**2-CT**2

       F(4)=G51*A01**2*XT**2+CT**2-G51*A02**2*(XR2+XI2-1)**2-(G51*A02*
      # (XR2-XI2))**2

       F(5)=A01**2*FA2*(XT**G71-(XR2+XI2-1)**G71)+G1*FA1*(XR1+XI1-1)**G51
      # *G51*A01*(XI1-XR1)*(CT-G51*A02*(XR2-XI2))

       A(1,4) = (F(1)-F1S)/DELX
       A(2,4) = (F(2)-F2S)/DELX
       A(3,4) = (F(3)-F3S)/DELX
       A(4,4) = (F(4)-F4S)/DELX
       A(5,4) = (F(5)-F5S)/DELX

       XR2  =  XR2S
C
       CT   =  CT+DELX
```

```
       F(1)=(XR1+XI1-1)**G51*A01*G51*(XI1-XR1)*FA1-FAT*XT**G51*CT

       F(2)=A02**2*FAT*XT**G51*CT-A01**2*(XR2+XI2-1)**G51*A02*G51*
      # (XR2-XI2)*FA2

       F(3)=G51*A01**2*(XR1+XI1-1)**2+(G51*A01*(XI1-XR1))**2-G51*A01**2*
      # XT**2-CT**2

       F(4)=G51*A01**2*XT**2+CT**2-G51*A02**2*(XR2+XI2-1)**2-(G51*A02*
      # (XR2-XI2))**2

       F(5)=A01**2*FA2*(XT**G71-(XR2+XI2-1)**G71)+G1*FA1*(XR1+XI1-1)**G51
      # *G51*A01*(XI1-XR1)*(CT-G51*A02*(XR2-XI2))

       A(1,5) = (F(1)-F1S)/DELX
       A(2,5) = (F(2)-F2S)/DELX
       A(3,5) = (F(3)-F3S)/DELX
       A(4,5) = (F(4)-F4S)/DELX
       A(5,5) = (F(5)-F5S)/DELX

       CT   =  CTS
C
       F(1)=F1S
       F(2)=F2S
       F(3)=F3S
       F(4)=F4S
       F(5)=F5S

       RETURN
       END
C
C-------------------------------------------------------------------------
C
       SUBROUTINE SONIC(DELX,XI1,XR1,XR2,XI2,FA1,FA2,FAT,A01,
      # A02,G51,G61,F,A,XT)
C
C This subroutine contains the equations for the sonic flow conditions
C
       IMPLICIT NONE
C
       DIMENSION F(20),A(20,20)
       REAL FA2,A02,XR2,XI2,G51,FA1,A01,XI1,XR1,F,A02S,A,XT,XTS,G61
       REAL DELX,F1S,F2S,F3S,F4S,XR1S,XR2S,FAT
C
       F(1)=FA1*(XR1+XI1-1)**G51*G51*(XI1-XR1)-FAT*XT**G61

       F(2)=A02*FAT*XT**G61-FA2*A01*(XR2+XI2-1)**G51*
      # G51*(XR2-XI2)

       F(3)=G51*(XI1+XR1-1)**2+(G51*(XI1-XR1))**2-G61*XT**2

       F(4)=G61*A01**2*XT**2-G51*A02**2*(XR2+XI2-1)**2-(G51*A02*
      # (XR2-XI2))**2

       F1S = F(1)
       F2S = F(2)
       F3S = F(3)
       F4S = F(4)

       XR1S  = XR1
       XR2S  = XR2
```

```
      XTS   = XT
      A02S  = A02
C
      XR1 = XR1+DELX

      F(1)=FA1*(XR1+XI1-1)**G51*G51*(XI1-XR1)-FAT*XT**G61

      F(2)=A02*FAT*XT**G61-FA2*A01*(XR2+XI2-1)**G51*
     # G51*(XR2-XI2)

      F(3)=G51*(XI1+XR1-1)**2+(G51*(XI1-XR1))**2-G61*XT**2

      F(4)=G61*A01**2*XT**2-G51*A02**2*(XR2+XI2-1)**2-(G51*A02*
     # (XR2-XI2))**2

      A(1,1) = (F(1)-F1S)/DELX
      A(2,1) = (F(2)-F2S)/DELX
      A(3,1) = (F(3)-F3S)/DELX
      A(4,1) = (F(4)-F4S)/DELX

      XR1  =  XR1S
C
      XT   =  XT+DELX

      F(1)=FA1*(XR1+XI1-1)**G51*G51*(XI1-XR1)-FAT*XT**G61

      F(2)=A02*FAT*XT**G61-FA2*A01*(XR2+XI2-1)**G51*
     # G51*(XR2-XI2)

      F(3)=G51*(XI1+XR1-1)**2+(G51*(XI1-XR1))**2-G61*XT**2

      F(4)=G61*A01**2*XT**2-G51*A02**2*(XR2+XI2-1)**2-(G51*A02*
     # (XR2-XI2))**2

      A(1,2) = (F(1)-F1S)/DELX
      A(2,2) = (F(2)-F2S)/DELX
      A(3,2) = (F(3)-F3S)/DELX
      A(4,2) = (F(4)-F4S)/DELX

      XT   =  XTS
C
      XR2  =  XR2+DELX

      F(1)=FA1*(XR1+XI1-1)**G51*G51*(XI1-XR1)-FAT*XT**G61

      F(2)=A02*FAT*XT**G61-FA2*A01*(XR2+XI2-1)**G51*
     # G51*(XR2-XI2)

      F(3)=G51*(XI1+XR1-1)**2+(G51*(XI1-XR1))**2-G61*XT**2

      F(4)=G61*A01**2*XT**2-G51*A02**2*(XR2+XI2-1)**2-(G51*A02*
     # (XR2-XI2))**2

      A(1,3) = (F(1)-F1S)/DELX
      A(2,3) = (F(2)-F2S)/DELX
      A(3,3) = (F(3)-F3S)/DELX
      A(4,3) = (F(4)-F4S)/DELX

      XR2  =  XR2S
C
      A02  =  A02+DELX
```

```
      F(1)=FA1*(XR1+XI1-1)**G51*G51*(XI1-XR1)-FAT*XT**G61

      F(2)=A02*FAT*XT**G61-FA2*A01*(XR2+XI2-1)**G51*
     # G51*(XR2-XI2)

      F(3)=G51*(XI1+XR1-1)**2+(G51*(XI1-XR1))**2-G61*XT**2

      F(4)=G61*A01**2*XT**2-G51*A02**2*(XR2+XI2-1)**2-(G51*A02*
     # (XR2-XI2))**2

      A(1,4) = (F(1)-F1S)/DELX
      A(2,4) = (F(2)-F2S)/DELX
      A(3,4) = (F(3)-F3S)/DELX
      A(4,4) = (F(4)-F4S)/DELX

      A02  =  A02S
C
      F(1)=F1S
      F(2)=F2S
      F(3)=F3S
      F(4)=F4S

      RETURN
      END
```

Appendix C

Test Instrumentation

Table C.1 List of Test Instrumentation

Instrument	Manufacturer	Range
Personal Computer with Transcap 32bit Acquisition System	TLC Software Eagle PC 30 F card	N/A
Pressure Transducers (3)	Wika Type 891.13.500	0 to 100 kPa
Thermocouples	K-type	0 to 1200 ^{o}C
Barometer	Longacre	60 to 110 kPa
Thermometer	Rueger	-15 to 60 ^{o}C
Pressure Master Gauge	Wika	0 to 160 kPa
Pressure Transducer Calibrator	Budenburg	N/A
Thermocouple display	ERO Electronic 90.44.450 E	N/A
Orifice Plate	Boart Longyear Seco	32.02mm

Figure C.1 Pressure Transducer Calibration Layout.

Calibration of Pressure Transducers

Figure C.1 shows the personal computer with the sampling software and instrumentation. Next to it is the Budenburg calibrator with a pressure transducer fitted to the one port and the Wika master gauge fitted to the other port.

Each pressure transducer connected to its cable and junction box was calibrated in turn. This connection chain was not disturbed or swapped with other components during the testing phase in an effort to improve the accuracy of the results.

The transducers were calibrated against the master gauge at a range of pressures starting at 0.0 kPa gauge pressure and finishing at 100 kPa gauge pressure. A polynomial function was fitted to these values and used to correct the measured results after testing.

Master Gauge Calibration Certificate

WIKA

WIKA INSTRUMENTS (PTY) LTD

calibration protocol:

Inspections certificate

BOART SECO

WS/69291 — 29/08/2000

commission:

1 — 312.20.160.Q — 160mm

0.30 % — 0...160 kPa — A259

WIKA Präzisions-DMU (0..2.500 bar) — 08000221

pressure: Pressure:	signal up: Signal up:	failure up: error up:	signal down: Signal down:	failure down: error down:
000.00	000.00	00.00%	000.00	00.00%
020.00	019.85	-00.09%	019.90	-00.06%
040.00	040.20	00.13%	039.80	-00.13%
060.00	060.17	00.11%	059.97	-00.02%
080.00	079.97	-00.02%	079.97	-00.02%
100.00	100.20	00.12%	100.18	00.11%
120.00	120.18	00.11%	120.15	00.09%
140.00	140.30	00.19%	140.13	00.08%
160.00	160.00	00.00%	160.00	00.00%

1. The measuring standard used for the purpose of this certificate was calibrated by or is traceable to an approved laboratory: Messrs. Denel (Pty) Ltd., Eskom or PTB (Germany).
2. **Validity of Calibration**
   The values in this certificate are correct at the time of calibration/certification. Subsequently the accuracy will depend on such factors as operating temperature, the care exercised in handling, frequency of use and its use under conditions other than specified by the manufacturer and/or conditions of calibration/certification. Recertification should be performed after a period that has been chosen to ensure that the equipment's accuracy remains within the desired limits.
3. In the event of a mistake being made by WIKA INSTRUMENTS in calibration/certification work performed for the applicant, any legal liability arising therefrom shall be limited to the cost of recalibration and/or certification, but the applicant indemnifies WIKA INSTRUMENTS against any consequential or other loss.

cal. temp. / Testing temp.: 19.2 °C

accuracy of the reference system or: The above readings are subject to an error of: 0.1 %

the max. failure equals: The max. error is: 0.19%

the max. hysteresis equals: The max. hysteresis is: 0.26%

cal. dep.: Z. SLLC

testperson: D DAVIDS

29.08.2000

Least Squares fit of Master Gauge to Calibration Certificate Values

```
Coefficients in least-squares approximation:

Order of polynomial: 5
   Coefficient  0: -8.2919782151691E-0016
   Coefficient  1:  1.0157834572045E+0000
   Coefficient  2: -4.7953476951502E-0004
   Coefficient  3: -2.7639025259987E-0006
   Coefficient  4:  1.6499562728280E-0007
   Coefficient  5: -1.0701338001727E-0009

Variance           :  6.5701984E-0028
Standard deviation :  0.0000000E+0000
```

	x	y obs	y calc	y obs - calc
1	0.0000000E+0000	0.0000000E+0000	-8.2919782E-0016	-8.2919782E-0016
2	1.9875000E+0001	2.0000000E+0001	2.0000000E+0001	0.0000000E+0000
3	4.0000000E+0001	4.0000000E+0001	4.0000000E+0001	7.1054274E-0015
4	6.0070000E+0001	6.0000000E+0001	6.0000000E+0001	1.4210855E-0014
5	7.9970000E+0001	8.0000000E+0001	8.0000000E+0001	-1.4210855E-0014
6	1.0019000E+0002	1.0000000E+0002	1.0000000E+0002	1.4210855E-0014

```
Least-squares polynomial curve fit

Order of polynomial: 5
```

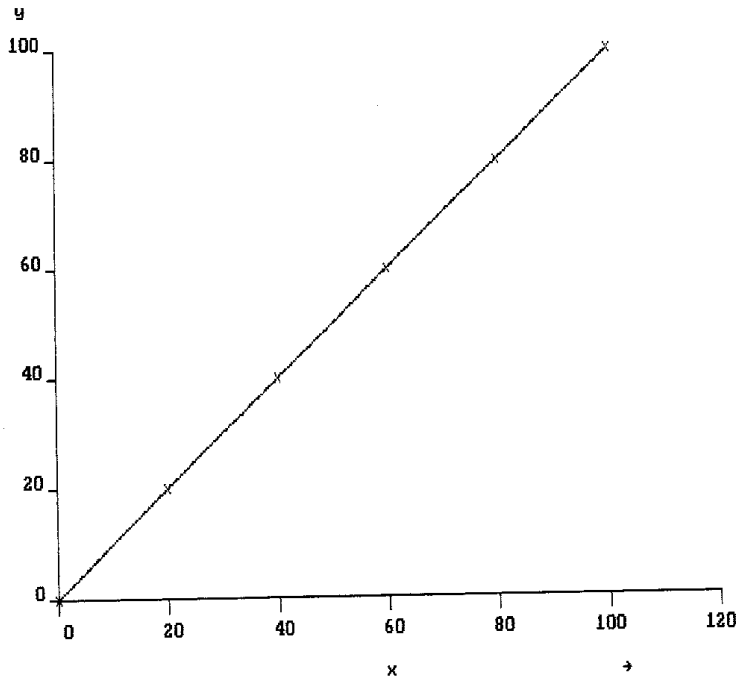

BS1042 Orifice Dimensions

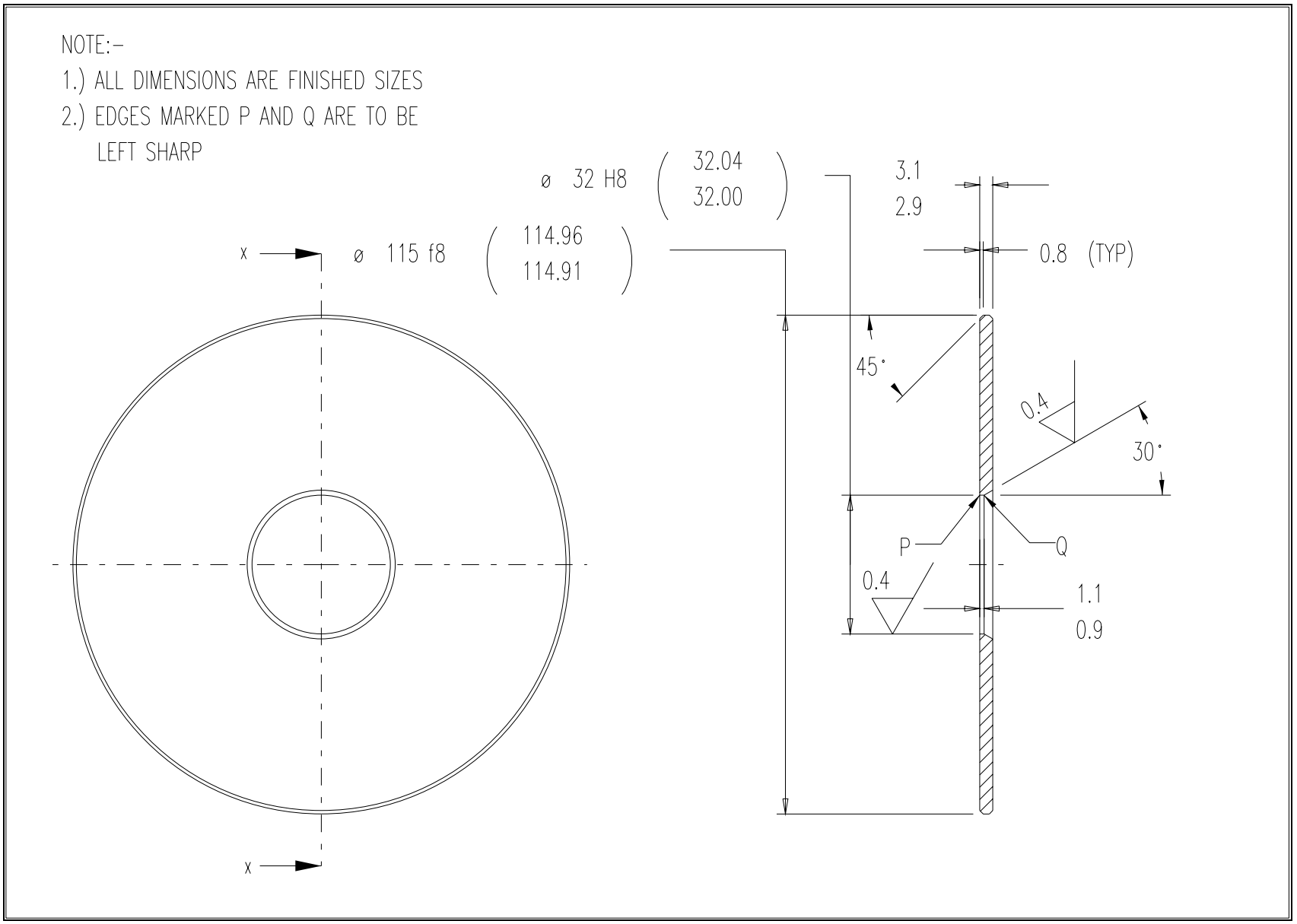

Appendix D

Simulated Tailpipe Mass Flow and Pressure Ratio

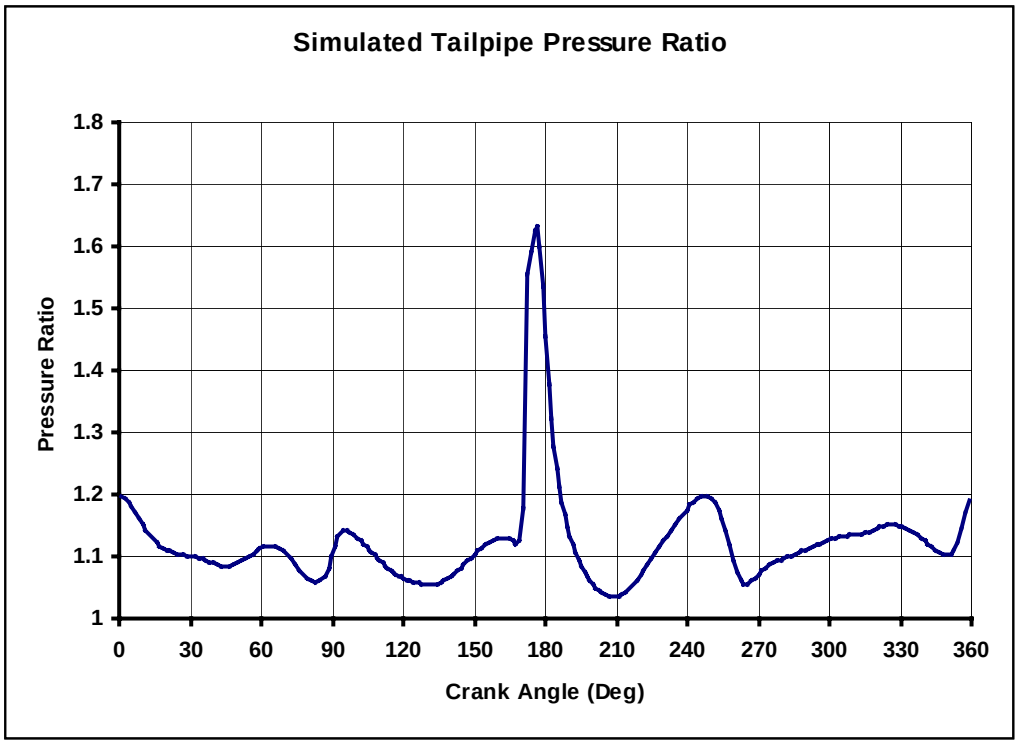

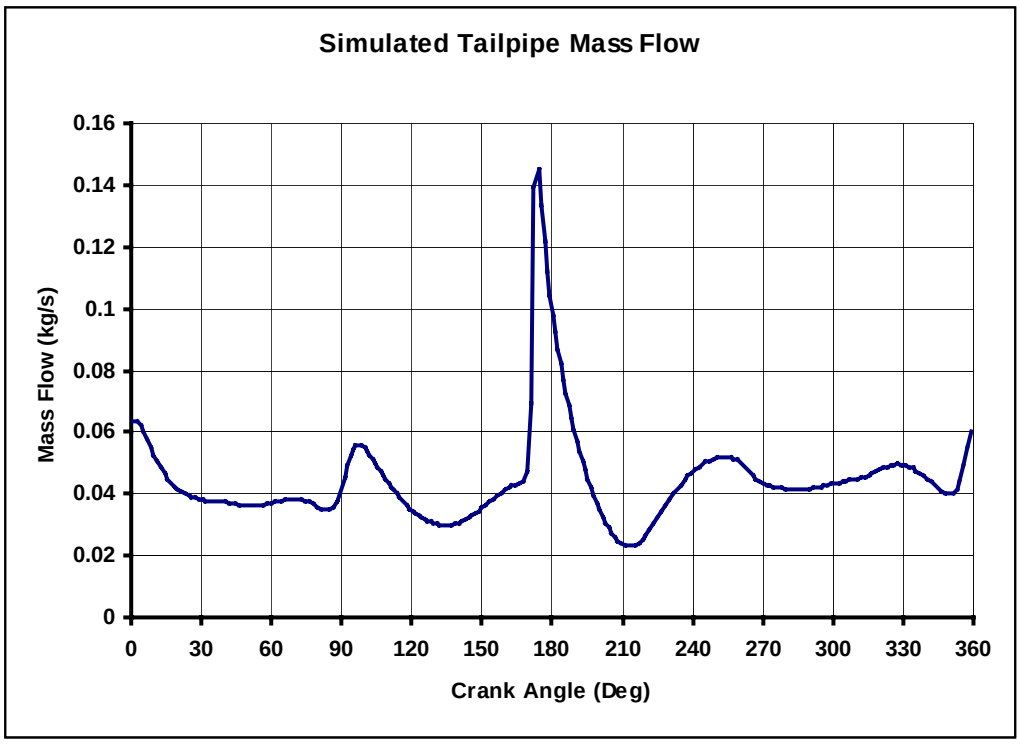

Appendix E

Mass Flow Test Results

This Appendix contains the measured orifice test results, the corrected values for the measured pressures and the calculated mass flow results for the 10 test pieces. Each test piece was tested at 8 different reservoir pressures and three sets of measurements were taken at each pressure. This resulted in 24 sets of results for each test piece and a total number of 240 sets of test results.

The measured pressures were firstly corrected according to the pressure transducer calibration curves against the master gauge and then corrected according to the master gauge calibration certificate. The calibrations are given in Appendix C.

The atmospheric conditions are given in Table E.1 and the test and mass flow results according to BS1042 in Table E.2 to Table E.11.

Table E.1 Atmospheric Conditions

Test piece Number	Pressure (kPa)	Temperature (^{o}C)
1	87.7	18.5
2	87.3	18.2
3	87.1	19.0
4	87.1	19.3
5	86.8	20.0
6	86.8	20.0
7	86.8	20.0
8	86.8	20.0
9	86.8	19.8
10	86.8	19.0

TABLE E.2 TEST PIECE 1, 10 DEGREE CONE, 21.8MM TAILPIPE, PLAIN TAILPIPE ENTRY

Test result file name	Pum	Pdm	Prm	Puc	Pdc	Prc	Tu	Tr	$\dot{m}$
ngd_10_051.ASC	8.2051	5.8399	5.1352	8.2805	6.0084	5.3468	21.3000	19.1000	0.03571
ngd_10_052.ASC	8.1603	5.8028	5.1035	8.2351	5.9704	5.3140	21.3800	19.2000	0.03572
ngd_10_053.ASC	8.1313	5.7796	5.0799	8.2057	5.9466	5.2895	21.4500	19.3000	0.03568
ngd_10_101.ASC	15.5541	11.3168	10.0504	15.6975	11.5741	10.3593	20.9000	18.9000	0.05001
ngd_10_102.ASC	15.5339	11.3037	10.0349	15.6772	11.5609	10.3437	21.0500	19.0000	0.04995
ngd_10_103.ASC	15.5322	11.2945	10.0175	15.6755	11.5517	10.3262	21.2000	19.1000	0.04998
ngd_10_151.ASC	22.1575	16.3739	14.6301	22.3149	16.6460	14.9320	20.0500	18.5000	0.06030
ngd_10_152.ASC	22.0342	16.2829	14.5426	22.1917	16.5551	14.8452	20.3000	18.6500	0.06008
ngd_10_153.ASC	22.0518	16.3005	14.5554	22.2093	16.5727	14.8579	20.5500	18.8000	0.06006
ngd_10_201.ASC	29.9683	22.5614	20.2447	30.0968	22.8002	20.4665	19.5000	17.8000	0.07059
ngd_10_202.ASC	29.9189	22.5035	20.1970	30.0477	22.7427	20.4197	19.7500	18.0000	0.07058
ngd_10_203.ASC	29.8800	22.4637	20.1702	30.0091	22.7033	20.3934	20.0000	18.2000	0.07055
ngd_10_301.ASC	42.9137	33.0355	29.8882	42.9372	33.1717	29.9219	18.4000	17.1000	0.08577
ngd_10_302.ASC	42.7528	32.9034	29.7862	42.7778	33.0409	29.8218	18.9000	17.4000	0.08553
ngd_10_303.ASC	42.6369	32.8086	29.6962	42.6629	32.9471	29.7334	19.4000	17.7000	0.08533
ngd_10_401.ASC	55.4965	43.5552	39.7580	55.4267	43.6054	39.6568	16.9000	16.3000	0.09877
ngd_10_402.ASC	55.0820	43.2588	39.4605	55.0144	43.3108	39.3618	17.4500	16.6300	0.09806
ngd_10_403.ASC	54.8381	43.0620	39.2727	54.7718	43.1153	39.1757	18.0000	16.9500	0.09769
ngd_10_501.ASC	67.4975	53.9069	49.5381	67.4017	53.9189	49.4059	15.2000	15.8000	0.10996
ngd_10_502.ASC	67.0516	53.5550	49.2031	66.9555	53.5676	49.0704	15.8500	15.9300	0.10931
ngd_10_503.ASC	66.7845	53.2883	48.9356	66.6882	53.3013	48.8026	16.5000	16.0500	0.10908
ngd_10_601.ASC	80.3947	65.2991	60.3731	80.3327	65.3058	60.2891	14.5000	16.0000	0.12087
ngd_10_602.ASC	80.4263	65.3135	60.4072	80.3644	65.3202	60.3234	14.7000	15.8500	0.12091
ngd_10_603.ASC	80.5492	65.4364	60.5087	80.4877	65.4431	60.4255	14.9500	15.7000	0.12090

Pum = Upstream measured pressure
Pdm = Downstream measured pressure
Prm = Measured reservoir pressure
Puc = Upstream corrected pressure
Pdc = Downstream corrected pressure
Prc = Corrected reservoir pressure
Tu = Upstream temperature
Tr = Reservoir temperature
$\dot{m}$ = Calculated mass flow

TABLE E.3 TEST PIECE 2, 20 DEGREE CONE, 21.8MM TAILPIPE, PLAIN TAILPIPE ENTRY

Test result file name	Pum	Pdm	Prm	Puc	Pdc	Prc	Tu	Tr	$\dot{m}$
ngd_20_051.ASC	7.5116	5.3621	4.7390	7.5775	5.5181	4.9363	32.2000	27.8000	0.03357
ngd_20_052.ASC	7.4639	5.3214	4.7020	7.5291	5.4763	4.8979	32.1000	27.7000	0.03352
ngd_20_053.ASC	7.4311	5.3018	4.6828	7.4959	5.4561	4.8780	32.0000	27.6000	0.03341
ngd_20_101.ASC	15.6940	11.4295	10.1488	15.8382	11.6878	10.4584	32.5000	28.1000	0.04925
ngd_20_102.ASC	15.6347	11.3882	10.1210	15.7786	11.6461	10.4304	32.4500	28.1500	0.04914
ngd_20_103.ASC	15.6158	11.3708	10.1065	15.7596	11.6286	10.4158	32.4500	28.2000	0.04913
ngd_20_151.ASC	22.8601	16.9226	15.1055	23.0167	17.1935	15.4029	32.5000	28.1000	0.06004
ngd_20_152.ASC	22.8077	16.8920	15.0782	22.9644	17.1630	15.3759	32.5000	28.1500	0.05992
ngd_20_153.ASC	22.8027	16.8609	15.0660	22.9594	17.1320	15.3638	32.5000	28.2000	0.06005
ngd_20_201.ASC	30.0012	22.5522	20.2408	30.1295	22.7910	20.4627	32.5000	28.0000	0.06929
ngd_20_202.ASC	29.8791	22.4567	20.1465	30.0082	22.6963	20.3701	32.5000	28.1000	0.06913
ngd_20_203.ASC	29.8293	22.4005	20.0899	29.9587	22.6406	20.3145	32.5000	28.2000	0.06914
ngd_20_301.ASC	42.3869	32.5772	29.4587	42.4151	32.7180	29.5003	32.0000	27.4000	0.08340
ngd_20_302.ASC	42.3382	32.5322	29.4174	42.3668	32.6734	29.4598	32.2000	27.6000	0.08334
ngd_20_303.ASC	42.3315	32.5283	29.4153	42.3602	32.6696	29.4577	32.4000	27.8000	0.08330
ngd_20_401.ASC	55.5241	43.5582	39.7290	55.4542	43.6084	39.6280	31.9000	26.4000	0.09643
ngd_20_402.ASC	55.3570	43.4064	39.5519	55.2880	43.4575	39.4524	31.9000	26.8000	0.09631
ngd_20_403.ASC	55.2928	43.3442	39.5030	55.2241	43.3957	39.4040	31.9000	27.2000	0.09628
ngd_20_501.ASC	67.8123	54.1025	49.6842	67.7168	54.1141	49.5522	28.4000	24.1000	0.10811
ngd_20_502.ASC	67.6059	53.9442	49.5123	67.5102	53.9561	49.3800	29.2500	24.9500	0.10770
ngd_20_503.ASC	67.5891	53.9208	49.4884	67.4934	53.9327	49.3561	30.1000	25.8000	0.10757
ngd_20_601.ASC	81.2044	65.8645	60.8829	81.1447	65.8712	60.8019	26.3000	23.1000	0.11970
ngd_20_602.ASC	81.5396	66.1940	61.1937	81.4808	66.2007	61.1145	26.9000	23.5500	0.11973
ngd_20_603.ASC	81.3794	66.0615	61.0521	81.3202	66.0682	60.9721	27.5000	24.0000	0.11944

Pum = Upstream measured pressure
Pdm = Downstream measured pressure
Prm = Measured reservoir pressure
Puc = Upstream corrected pressure
Pdc = Downstream corrected pressure
Prc = Corrected reservoir pressure
Tu = Upstream temperature
Tr = Reservoir temperature
$\dot{m}$ = Calculated mass flow

TABLE E.4 TEST PIECE 3, 30 DEGREE CONE, 21.8MM TAILPIPE, PLAIN TAILPIPE ENTRY

Test result file name	Pum	Pdm	Prm	Puc	Pdc	Prc	Tu	Tr	$\dot{m}$
ngd_30_051.ASC	7.7631	5.5631	4.9211	7.8325	5.7245	5.1251	33.8000	28.4000	0.03392
ngd_30_052.ASC	7.7358	5.5422	4.8992	7.8048	5.7030	5.1024	33.6500	28.3000	0.03387
ngd_30_053.ASC	7.7223	5.5334	4.8934	7.7911	5.6940	5.0964	33.5000	28.2000	0.03384
ngd_30_101.ASC	15.3742	11.2178	9.9705	15.5167	11.4743	10.2788	34.0000	28.6000	0.04843
ngd_30_102.ASC	15.3160	11.1663	9.9244	15.4582	11.4224	10.2324	34.0000	28.6000	0.04838
ngd_30_103.ASC	15.2811	11.1403	9.9066	15.4231	11.3961	10.2145	34.0000	28.6000	0.04832
ngd_30_151.ASC	22.5429	16.6494	14.8624	22.6999	16.9209	15.1622	33.5000	28.6000	0.05964
ngd_30_152.ASC	22.5533	16.6828	14.9043	22.7103	16.9543	15.2037	33.7000	28.6500	0.05951
ngd_30_153.ASC	22.6215	16.7414	14.9424	22.7784	17.0127	15.2414	33.9000	28.7000	0.05955
ngd_30_201.ASC	29.4750	22.1338	19.8359	29.6065	22.3760	20.0651	32.8000	28.3000	0.06861
ngd_30_202.ASC	29.5972	22.2286	19.9459	29.7280	22.4701	20.1731	33.1500	28.4500	0.06873
ngd_30_203.ASC	29.5766	22.2109	19.9298	29.7075	22.4525	20.1573	33.5000	28.6000	0.06867
ngd_30_301.ASC	43.6607	33.7066	30.2357	43.6777	33.8362	30.2631	31.3000	27.9000	0.08451
ngd_30_302.ASC	43.6083	33.6425	30.1651	43.6257	33.7728	30.1938	31.8500	28.0500	0.08447
ngd_30_303.ASC	43.5836	33.6019	30.1936	43.6012	33.7326	30.2218	32.4000	28.2000	0.08445
ngd_30_401.ASC	57.0357	45.0645	40.5495	56.9586	45.1062	40.4420	29.5000	27.4000	0.09637
ngd_30_402.ASC	56.4839	44.5625	40.1510	56.4093	44.6069	40.0466	30.2500	27.5500	0.09586
ngd_30_403.ASC	56.4415	44.5032	40.0997	56.3671	44.5480	39.9957	31.0000	27.7000	0.09579
ngd_30_501.ASC	66.8781	53.5635	48.7492	66.7819	53.5760	48.6160	27.3000	27.1000	0.10547
ngd_30_502.ASC	66.9557	53.6327	48.5545	66.8595	53.6451	48.4212	28.1500	27.1000	0.10538
ngd_30_503.ASC	66.9413	53.6848	48.4802	66.8451	53.6971	48.3469	29.0000	27.1000	0.10497
ngd_30_601.ASC	79.7927	64.5533	59.5846	79.7289	64.5600	59.4959	30.8000	28.2000	0.11790
ngd_30_602.ASC	75.6779	61.2908	56.4588	75.6006	61.2975	56.3523	28.9000	27.6500	0.11354
ngd_30_603.ASC	76.1472	61.7319	56.7135	76.0714	61.7385	56.6084	27.0000	27.1000	0.11418

Pum = Upstream measured pressure
Pdm = Downstream measured pressure
Prm = Measured reservoir pressure
Puc = Upstream corrected pressure
Pdc = Downstream corrected pressure
Prc = Corrected reservoir pressure
Tu = Upstream temperature
Tr = Reservoir temperature
$\dot{m}$ = Calculated mass flow

TABLE E.5 TEST PIECE 4, 40 DEGREE CONE, 21.8MM TAILPIPE, PLAIN TAILPIPE ENTRY

Test result file name	Pum	Pdm	Prm	Puc	Pdc	Prc	Tu	Tr	$\dot{m}$
ngd_40_051.ASC	8.0752	5.7978	5.0983	8.1489	5.9653	5.3086	34.0000	27.7000	0.03435
ngd_40_052.ASC	8.0883	5.8047	5.1105	8.1621	5.9723	5.3212	33.9500	27.7000	0.03440
ngd_40_053.ASC	8.0682	5.7883	5.1005	8.1418	5.9555	5.3109	33.9000	27.7000	0.03438
ngd_40_101.ASC	15.6337	11.3904	10.1023	15.7776	11.6483	10.4116	34.6000	28.2000	0.04857
ngd_40_102.ASC	15.6817	11.4248	10.1395	15.8258	11.6830	10.4490	34.6000	28.2500	0.04866
ngd_40_103.ASC	15.7054	11.4538	10.1476	15.8496	11.7123	10.4572	34.6000	28.3000	0.04864
ngd_40_151.ASC	22.9367	16.9620	15.0916	23.0932	17.2328	15.3892	34.6000	28.2000	0.05964
ngd_40_152.ASC	22.9940	17.0005	15.1358	23.1504	17.2712	15.4329	34.7500	28.2500	0.05974
ngd_40_153.ASC	22.9508	16.9735	15.1053	23.1073	17.2443	15.4027	34.9000	28.3000	0.05963
ngd_40_201.ASC	29.6228	22.2504	19.8285	29.7534	22.4917	20.0578	34.1000	27.7000	0.06815
ngd_40_202.ASC	29.5897	22.2060	19.7878	29.7205	22.4476	20.0178	34.3500	27.8500	0.06816
ngd_40_203.ASC	29.5053	22.1268	19.7414	29.6366	22.3691	19.9723	34.6000	28.0000	0.06808
ngd_40_301.ASC	43.4793	33.5293	30.0397	43.4978	33.6607	30.0707	32.0000	26.8000	0.08364
ngd_40_302.ASC	43.3694	33.3741	29.9361	43.3889	33.5070	29.9689	32.7500	27.2000	0.08368
ngd_40_303.ASC	43.4286	33.4629	29.9839	43.4476	33.5949	30.0159	33.5000	27.6000	0.08358
ngd_40_401.ASC	56.2241	44.3756	39.9786	56.1507	44.4211	39.8756	29.2000	26.1000	0.09565
ngd_40_402.ASC	56.2255	44.3225	39.9608	56.1521	44.3683	39.8579	30.2000	26.3500	0.09571
ngd_40_403.ASC	56.2518	44.3240	39.9536	56.1783	44.3698	39.8508	31.2000	26.6000	0.09565
ngd_40_501.ASC	68.9758	55.5441	50.2164	68.8816	55.5538	50.0854	27.5000	25.4000	0.10766
ngd_40_502.ASC	68.3579	55.0280	49.7026	68.2629	55.0383	49.5706	28.2500	25.6000	0.10691
ngd_40_503.ASC	68.3722	54.9498	49.7846	68.2772	54.9602	49.6528	29.0000	25.8000	0.10713
ngd_40_601.ASC	81.0432	66.4060	60.2365	80.9831	66.4127	60.1517	25.2000	25.6000	0.11723
ngd_40_602.ASC	80.8029	66.1972	60.1951	80.7421	66.2039	60.1100	26.2000	25.5000	0.11682
ngd_40_603.ASC	80.7185	66.1653	60.1711	80.6575	66.1720	60.0859	27.2000	25.4000	0.11640

Pum = Upstream measured pressure
Pdm = Downstream measured pressure
Prm = Measured reservoir pressure
Puc = Upstream corrected pressure
Pdc = Downstream corrected pressure
Prc = Corrected reservoir pressure
Tu = Upstream temperature
Tr = Reservoir temperature
$\dot{m}$ = Calculated mass flow

TABLE E.6TEST PIECE 5, 30 DEGREE CONE, 20.5MM TAILPIPE, PLAIN TAILPIPE ENTRY

Test result file name	Pum	Pdm	Prm	Puc	Pdc	Prc	Tu	Tr	$\dot{m}$
ngt_205_051.ASC	7.2230	5.5098	4.9980	7.2848	5.6698	5.2048	35.0000	29.2000	0.02962
ngt_205_052.ASC	7.2383	5.5206	5.0126	7.3003	5.6809	5.2199	34.9500	29.1000	0.02967
ngt_205_053.ASC	7.2443	5.5249	5.0112	7.3064	5.6853	5.2184	34.9000	29.0000	0.02969
ngt_205_101.ASC	14.3781	11.1130	10.1432	14.5146	11.3686	10.4528	35.5000	29.6000	0.04256
ngt_205_102.ASC	14.3985	11.1331	10.1578	14.5351	11.3889	10.4675	35.3500	29.6000	0.04258
ngt_205_103.ASC	14.3764	11.1098	10.1306	14.5129	11.3654	10.4401	35.2000	29.6000	0.04259
ngt_205_151.ASC	20.9755	16.3940	15.0173	21.1334	16.6660	15.3156	36.0000	29.7000	0.05207
ngt_205_152.ASC	20.9198	16.3741	14.9966	21.0776	16.6462	15.2951	35.9000	29.7000	0.05186
ngt_205_153.ASC	20.9556	16.4033	15.0179	21.1135	16.6753	15.3162	35.8000	29.7000	0.05192
ngt_205_201.ASC	27.7733	21.9831	20.2187	27.9139	22.2265	20.4410	36.0000	29.6000	0.06037
ngt_205_202.ASC	27.7562	21.9752	20.2201	27.8969	22.2186	20.4424	36.0000	29.6500	0.06032
ngt_205_203.ASC	27.7821	22.0015	20.2287	27.9227	22.2447	20.4508	36.0000	29.7000	0.06032
ngt_205_301.ASC	40.3769	32.6040	30.1719	40.4230	32.7445	30.2005	35.6000	29.1000	0.07359
ngt_205_302.ASC	40.3125	32.5396	30.1219	40.3592	32.6808	30.1514	35.8500	29.3500	0.07354
ngt_205_303.ASC	40.3612	32.5773	30.1797	40.4074	32.7181	30.2081	36.1000	29.6000	0.07358
ngt_205_401.ASC	52.4486	43.0833	40.0798	52.3966	43.1364	39.9759	34.5000	28.2000	0.08447
ngt_205_402.ASC	52.2814	42.9016	39.8898	52.2305	42.9559	39.7875	34.8000	28.5500	0.08444
ngt_205_403.ASC	52.2534	42.9007	39.8977	52.2027	42.9550	39.7953	35.1000	28.9000	0.08427
ngt_205_501.ASC	63.6674	53.0652	49.5539	63.5720	53.0787	49.4217	33.2000	26.9000	0.09352
ngt_205_502.ASC	63.4777	52.8624	49.3820	63.3825	52.8763	49.2496	33.8000	27.3500	0.09343
ngt_205_503.ASC	63.5912	52.9486	49.4885	63.4959	52.9623	49.3562	34.4000	26.9000	0.09349
ngt_205_601.ASC	74.9695	63.4207	59.3744	74.8899	63.4274	59.2845	28.2000	27.3000	0.10212
ngt_205_602.ASC	74.3327	62.7379	58.7750	74.2511	62.7445	58.6816	30.3500	27.0500	0.10174
ngt_205_603.ASC	74.1451	62.5118	58.5808	74.0629	62.5184	58.4863	32.5000	27.3000	0.10148

Pum = Upstream measured pressure
Pdm = Downstream measured pressure
Prm = Measured reservoir pressure
Puc = Upstream corrected pressure
Pdc = Downstream corrected pressure
Prc = Corrected reservoir pressure
Tu = Upstream temperature
Tr = Reservoir temperature
$\dot{m}$ = Calculated mass flow

TABLE E.7 TEST PIECE 6, 30 DEGREE CONE, 23.5MM TAILPIPE, PLAIN TAILPIPE ENTRY

Test result file name	Pum	Pdm	Prm	Puc	Pdc	Prc	Tu	Tr	$\dot{m}$
ngt_235_051.ASC	8.9227	5.9023	4.9898	9.0074	6.0724	5.1963	36.1000	29.1000	0.03996
ngt_235_052.ASC	8.8595	5.8570	4.9431	8.9434	6.0260	5.1479	36.0000	29.0500	0.03984
ngt_235_053.ASC	8.8206	5.8307	4.9342	8.9040	5.9990	5.1387	35.9000	29.0000	0.03975
ngt_235_101.ASC	17.4241	11.7613	9.9847	17.5757	12.0221	10.2932	36.5000	29.3000	0.05681
ngt_235_102.ASC	17.4528	11.7717	10.0015	17.6045	12.0326	10.3101	36.4000	29.3000	0.05692
ngt_235_103.ASC	17.4750	11.7782	10.0179	17.6268	12.0391	10.3266	36.4000	29.3000	0.05700
ngt_235_151.ASC	25.5092	17.5445	14.9808	25.6593	17.8136	15.2794	36.6000	28.9000	0.06964
ngt_235_152.ASC	25.4498	17.4957	14.9421	25.6001	17.7650	15.2411	36.6000	29.0500	0.06958
ngt_235_153.ASC	25.4796	17.5113	14.9673	25.6298	17.7805	15.2661	36.6000	29.2000	0.06965
ngt_235_201.ASC	33.2814	23.2530	19.9681	33.3872	23.4859	20.1949	36.2000	28.3000	0.08055
ngt_235_202.ASC	33.3765	23.3310	20.0382	33.4816	23.5633	20.2638	36.3500	28.5000	0.08063
ngt_235_203.ASC	33.3138	23.2700	19.9842	33.4193	23.5028	20.2107	36.5000	28.7000	0.08058
ngt_235_301.ASC	47.5287	34.1858	29.6451	47.5128	34.3108	29.6833	35.0000	27.2000	0.09795
ngt_235_302.ASC	47.3863	34.0690	29.5257	47.3716	34.1951	29.5660	35.5000	27.5500	0.09773
ngt_235_303.ASC	47.4617	34.1212	29.5895	47.4464	34.2468	29.6287	36.0000	27.7000	0.09776
ngt_235_401.ASC	62.2014	46.0276	40.3349	62.1081	46.0645	40.2290	30.6000	25.5000	0.11410
ngt_235_402.ASC	62.1100	45.9212	40.2313	62.0169	45.9586	40.1262	32.2000	25.9500	0.11382
ngt_235_403.ASC	62.1368	45.9008	40.2281	62.0436	45.9383	40.1231	33.8000	26.4000	0.11369
ngt_235_501.ASC	74.1609	56.1964	49.7293	74.0788	56.2054	49.5974	27.0000	25.1000	0.12575
ngt_235_502.ASC	73.6332	55.5962	49.1127	73.5495	55.6058	48.9799	28.1000	25.3500	0.12553
ngt_235_503.ASC	73.5620	55.5099	48.9991	73.4781	55.5196	48.8662	29.2000	25.6000	0.12532
ngt_235_601.ASC	86.8294	67.2460	59.8879	86.7768	67.2526	59.8010	27.1000	26.1000	0.13640
ngt_235_602.ASC	86.2691	66.8123	59.3452	86.2168	66.8189	59.2551	27.1500	25.8000	0.13575
ngt_235_603.ASC	85.9102	66.5395	58.9911	85.8580	66.5462	58.8989	27.2000	25.5000	0.13531

Pum = Upstream measured pressure
Pdm = Downstream measured pressure
Prm = Measured reservoir pressure
Puc = Upstream corrected pressure
Pdc = Downstream corrected pressure
Prc = Corrected reservoir pressure
Tu = Upstream temperature
Tr = Reservoir temperature
$\dot{m}$ = Calculated mass flow

TABLE E.8 TEST PIECE 7, 30 DEGREE CONE, 22.0MM TAILPIPE, 20.5MM RESTRICTED TAILPIPE ENTRY

Test result file name	Pum	Pdm	Prm	Puc	Pdc	Prc	Tu	Tr	$\dot{m}$
ngr_220_051.ASC	8.0256	5.8508	5.2077	8.0986	6.0196	5.4218	35.7000	30.8000	0.03363
ngr_220_052.ASC	8.0595	5.8753	5.2348	8.1329	6.0447	5.4498	35.6000	30.7500	0.03372
ngr_220_053.ASC	8.0683	5.8895	5.2435	8.1419	6.0593	5.4588	35.5000	30.7000	0.03368
ngr_220_101.ASC	15.5265	11.5225	10.3126	15.6698	11.7815	10.6232	36.4000	31.5000	0.04738
ngr_220_102.ASC	15.5175	11.5165	10.3003	15.6608	11.7755	10.6108	36.2000	31.4000	0.04738
ngr_220_103.ASC	15.5291	11.5352	10.3170	15.6724	11.7943	10.6276	36.7000	31.8000	0.04730
ngr_220_151.ASC	22.6430	17.0550	15.3465	22.7999	17.3256	15.6415	36.9000	31.8000	0.05781
ngr_220_152.ASC	22.5758	16.9944	15.2752	22.7328	17.2651	15.5709	36.8000	31.8000	0.05777
ngr_220_153.ASC	22.6087	17.0306	15.3200	22.7656	17.3012	15.6152	36.7000	31.8000	0.05777
ngr_220_201.ASC	29.1438	22.2792	20.1420	29.2772	22.5202	20.3657	37.1000	31.8000	0.06586
ngr_220_202.ASC	29.1315	22.2661	20.1374	29.2650	22.5073	20.3612	37.0500	31.9000	0.06587
ngr_220_203.ASC	29.0964	22.2058	20.0726	29.2301	22.4474	20.2975	37.0000	32.0000	0.06598
ngr_220_301.ASC	41.7554	32.7405	29.8845	41.7892	32.8797	29.9183	37.1000	31.8000	0.07926
ngr_220_302.ASC	41.7454	32.7264	29.8817	41.7793	32.8657	29.9155	37.1500	31.9000	0.07926
ngr_220_303.ASC	41.6899	32.6923	29.8334	41.7243	32.8319	29.8681	37.2000	32.0000	0.07915
ngr_220_401.ASC	53.7598	43.1741	39.8017	53.6997	43.2267	39.7001	37.0000	31.6000	0.08964
ngr_220_402.ASC	53.7028	43.1137	39.7518	53.6430	43.1666	39.6506	37.0500	31.7000	0.08963
ngr_220_403.ASC	53.7187	43.1276	39.7575	53.6588	43.1804	39.6563	37.1000	31.8000	0.08964
ngr_220_501.ASC	65.5006	53.7335	50.0310	65.4041	53.7458	49.8996	36.5000	31.0000	0.09842
ngr_220_502.ASC	65.3469	53.6522	49.9550	65.2505	53.6646	49.8235	36.7500	31.2500	0.09804
ngr_220_503.ASC	65.3930	53.6980	49.9962	65.2965	53.7103	49.8648	37.0000	31.5000	0.09801
ngr_220_601.ASC	76.3447	63.7478	59.7434	76.2696	63.7545	59.6557	35.0000	29.6000	0.10577
ngr_220_602.ASC	76.0320	63.4490	59.4812	75.9558	63.4557	59.3919	35.5500	30.1000	0.10551
ngr_220_603.ASC	76.0034	63.3941	59.4548	75.9272	63.4008	59.3654	36.1000	30.6000	0.10551

Pum = Upstream measured pressure
Pdm = Downstream measured pressure
Prm = Measured reservoir pressure
Puc = Upstream corrected pressure
Pdc = Downstream corrected pressure
Prc = Corrected reservoir pressure
Tu = Upstream temperature
Tr = Reservoir temperature
$\dot{m}$ = Calculated mass flow

TABLE E.9 TEST PIECE 8, 30 DEGREE CONE, 23.5MM TAILPIPE, 20.5MM RESTRICTED TAILPIPE ENTRY

Test result file name	Pum	Pdm	Prm	Puc	Pdc	Prc	Tu	Tr	$\dot{m}$
ngr_235_051.ASC	8.1824	5.6793	4.9370	8.2575	5.8437	5.1416	36.6000	32.0000	0.03616
ngr_235_052.ASC	8.1443	5.6550	4.9092	8.2189	5.8188	5.1128	36.4500	31.9000	0.03606
ngr_235_053.ASC	8.1677	5.6735	4.9239	8.2426	5.8378	5.1280	36.3000	31.8000	0.03611
ngr_235_101.ASC	16.2459	11.5513	10.1031	16.3928	11.8105	10.4124	37.2000	32.6000	0.05142
ngr_235_102.ASC	16.2475	11.5480	10.1083	16.3944	11.8072	10.4176	37.1000	32.5000	0.05146
ngr_235_103.ASC	16.3209	11.6098	10.1626	16.4681	11.8695	10.4723	37.0000	32.4000	0.05155
ngr_235_151.ASC	23.8995	17.3823	15.3392	24.0542	17.6519	15.6342	37.6000	32.9000	0.06263
ngr_235_152.ASC	23.8927	17.3581	15.3165	24.0474	17.6278	15.6118	37.5500	32.9000	0.06271
ngr_235_153.ASC	23.9805	17.4419	15.3864	24.1350	17.7113	15.6809	37.5000	32.9000	0.06276
ngr_235_201.ASC	30.1369	22.3211	19.8299	30.2644	22.5618	20.0592	37.9000	33.0000	0.07034
ngr_235_202.ASC	30.0472	22.2330	19.7490	30.1752	22.4744	19.9797	37.8500	33.0500	0.07031
ngr_235_203.ASC	30.0938	22.2866	19.8001	30.2216	22.5276	20.0299	37.8000	33.1000	0.07030
ngr_235_301.ASC	42.8806	32.9328	29.7246	42.9044	33.0701	29.7613	37.8000	32.9000	0.08335
ngr_235_302.ASC	42.7629	32.8297	29.6218	42.7878	32.9680	29.6604	38.0000	33.0500	0.08322
ngr_235_303.ASC	42.6459	32.7160	29.5033	42.6718	32.8554	29.5441	38.0000	33.2000	0.08317
ngr_235_401.ASC	55.2009	43.9371	40.2580	55.1327	43.9851	40.1527	37.5000	32.8000	0.09275
ngr_235_402.ASC	55.2475	43.9536	40.2952	55.1790	44.0015	40.1896	37.6000	32.9000	0.09287
ngr_235_403.ASC	55.2054	43.9164	40.2554	55.1372	43.9645	40.1502	37.7000	33.0000	0.09282
ngr_235_501.ASC	66.6399	54.3671	50.4083	66.5436	54.3783	50.2777	36.7000	32.2000	0.10078
ngr_235_502.ASC	66.6034	54.3376	50.3754	66.5071	54.3489	50.2447	36.9500	32.3500	0.10070
ngr_235_503.ASC	66.4918	54.2122	50.2583	66.3954	54.2237	50.1274	37.2000	32.5000	0.10068
ngr_235_601.ASC	77.1695	64.0140	59.7918	77.0971	64.0207	59.7044	35.1000	31.3000	0.10826
ngr_235_602.ASC	77.0941	63.9357	59.7110	77.0215	63.9424	59.6231	35.7000	31.5500	0.10814
ngr_235_603.ASC	76.9227	63.7852	59.5590	76.8495	63.7919	59.4702	36.3000	31.8000	0.10789

Pum = Upstream measured pressure
Pdm = Downstream measured pressure
Prm = Measured reservoir pressure
Puc = Upstream corrected pressure
Pdc = Downstream corrected pressure
Prc = Corrected reservoir pressure
Tu = Upstream temperature
Tr = Reservoir temperature
$\dot{m}$ = Calculated mass flow

TABLE E.10 TEST PIECE 9, 30 DEGREE CONE, 22.0MM TAILPIPE, 20.5MM VENTURI TAILPIPE ENTRY

Test result file name	Pum	Pdm	Prm	Puc	Pdc	Prc	Tu	Tr	$\dot{m}$
ngv_220_051.ASC	8.2181	5.9072	5.2140	8.2937	6.0774	5.4283	36.0000	31.0000	0.03472
ngv_220_052.ASC	8.2448	5.9283	5.2349	8.3207	6.0991	5.4499	35.8000	30.8000	0.03478
ngv_220_053.ASC	8.2634	5.9381	5.2477	8.3396	6.1091	5.4631	35.6000	30.6000	0.03486
ngv_220_101.ASC	15.6250	11.4236	10.1306	15.7688	11.6818	10.4401	36.5000	31.5000	0.04856
ngv_220_102.ASC	15.6041	11.3894	10.0934	15.7478	11.6473	10.4026	36.4000	31.4000	0.04864
ngv_220_103.ASC	15.5755	11.3828	10.0936	15.7191	11.6407	10.4028	36.3000	31.0000	0.04851
ngv_220_151.ASC	22.9209	17.0007	15.1486	23.0774	17.2714	15.4456	37.0000	31.7000	0.05954
ngv_220_152.ASC	22.9060	16.9790	15.1342	23.0625	17.2498	15.4313	37.0000	31.7000	0.05957
ngv_220_153.ASC	22.8276	16.9062	15.0665	22.9843	17.1772	15.3643	37.0000	31.7000	0.05952
ngv_220_201.ASC	29.5871	22.2180	19.8965	29.7179	22.4595	20.1246	37.0000	31.7000	0.06830
ngv_220_202.ASC	29.6158	22.2705	19.9331	29.7465	22.5116	20.1605	37.0000	31.7500	0.06821
ngv_220_203.ASC	29.6285	22.2813	19.9537	29.7591	22.5223	20.1808	37.0000	31.8000	0.06822
ngv_220_301.ASC	43.0193	33.1857	30.0081	43.0419	33.3204	30.0396	36.6000	31.3000	0.08310
ngv_220_302.ASC	42.9573	33.1247	29.9679	42.9804	33.2601	30.0002	36.8000	31.5000	0.08304
ngv_220_303.ASC	42.9472	33.1211	29.9646	42.9704	33.2565	29.9969	37.0000	31.7000	0.08299
ngv_220_401.ASC	54.3755	43.4708	39.9419	54.3118	43.5215	39.8392	35.0000	30.4000	0.09142
ngv_220_402.ASC	54.3006	43.4023	39.8699	54.2373	43.4535	39.7678	35.6000	29.6500	0.09128
ngv_220_403.ASC	54.2766	43.3497	39.8433	54.2135	43.4012	39.7414	35.6000	30.9000	0.09139
ngv_220_501.ASC	65.5254	53.7436	49.9340	65.4289	53.7558	49.8024	32.4000	29.3000	0.09914
ngv_220_502.ASC	65.4294	53.6354	49.8348	65.3329	53.6478	49.7031	33.3000	29.0000	0.09901
ngv_220_503.ASC	65.5519	53.7274	49.9223	65.4554	53.7397	49.7907	34.2000	30.0000	0.09903
ngv_220_601.ASC	76.8598	64.2513	60.1565	76.7864	64.2580	60.0712	28.5000	28.4000	0.10713
ngv_220_602.ASC	76.9190	64.2441	60.1580	76.8458	64.2508	60.0727	29.0000	28.5000	0.10733
ngv_220_603.ASC	76.8634	64.1973	60.1006	76.7900	64.2040	60.0150	29.5000	28.6000	0.10719

Pum = Upstream measured pressure
Pdm = Downstream measured pressure
Prm = Measured reservoir pressure
Puc = Upstream corrected pressure
Pdc = Downstream corrected pressure
Prc = Corrected reservoir pressure
Tu = Upstream temperature
Tr = Reservoir temperature
$\dot{m}$ = Calculated mass flow

TABLE E.11 TEST PIECE 10, 30 DEGREE CONE, 23.5MM TAILPIPE, 20.5MM VENTURI TAILPIPE ENTRY

Test result file name	Pum	Pdm	Prm	Puc	Pdc	Prc	Tu	Tr	$\dot{m}$
ngv_235_051.ASC	8.7412	5.8521	4.9717	8.8236	6.0210	5.1775	36.1000	31.5000	0.03904
ngv_235_052.ASC	8.6854	5.8105	4.9424	8.7671	5.9783	5.1472	36.3500	31.3500	0.03892
ngv_235_053.ASC	8.6852	5.8154	4.9473	8.7669	5.9833	5.1522	36.6000	31.2000	0.03886
ngv_235_101.ASC	17.5578	11.9859	10.2339	17.7099	12.2483	10.5440	36.6000	32.0000	0.05638
ngv_235_102.ASC	17.5621	11.9929	10.2478	17.7142	12.2553	10.5580	36.5500	31.9500	0.05638
ngv_235_103.ASC	17.5447	11.9769	10.2285	17.6967	12.2392	10.5386	36.5000	31.9000	0.05637
ngv_235_151.ASC	25.5866	17.8479	15.3406	25.7364	18.1159	15.6356	36.9000	32.1000	0.06867
ngv_235_152.ASC	25.5802	17.8555	15.3412	25.7301	18.1235	15.6362	36.9000	32.1500	0.06861
ngv_235_153.ASC	25.5359	17.7941	15.2884	25.6859	18.0623	15.5840	36.9000	32.2000	0.06867
ngv_235_201.ASC	31.9698	22.9354	19.9947	32.0851	23.1711	20.2210	36.8000	32.0000	0.07614
ngv_235_202.ASC	31.9753	22.9528	19.9966	32.0906	23.1883	20.2229	36.9000	32.1000	0.07608
ngv_235_203.ASC	31.9501	22.9166	19.9757	32.0656	23.1524	20.2024	37.0000	32.2000	0.07611
ngv_235_301.ASC	43.3577	33.3270	30.0643	43.3773	33.4604	30.0948	36.2000	31.8000	0.08405
ngv_235_302.ASC	43.3598	33.3355	30.0778	43.3794	33.4688	30.1081	36.4000	31.9500	0.08400
ngv_235_303.ASC	43.4334	33.4235	30.1510	43.4524	33.5559	30.1799	36.6000	32.1000	0.08394
ngv_235_401.ASC	54.2550	43.3763	39.8441	54.1920	43.4276	39.7422	35.0000	31.2000	0.09127
ngv_235_402.ASC	53.9865	43.1165	39.5847	53.9250	43.1694	39.4850	35.5000	31.3500	0.09107
ngv_235_403.ASC	53.9302	43.0866	39.5483	53.8691	43.1397	39.4489	36.0000	31.5000	0.09088
ngv_235_501.ASC	65.5752	53.8089	50.0037	65.4787	53.8210	49.8723	33.8000	30.8000	0.09887
ngv_235_502.ASC	65.4238	53.6633	49.8536	65.3273	53.6757	49.7219	34.3000	30.9500	0.09871
ngv_235_503.ASC	65.5476	53.7476	49.9538	65.4511	53.7598	49.8223	34.8000	31.1000	0.09884
ngv_235_601.ASC	77.0565	64.3279	60.2122	76.9838	64.3346	60.1272	34.8000	31.1000	0.10658
ngv_235_602.ASC	77.3522	64.6187	60.5033	77.2804	64.6254	60.4201	36.0500	31.0500	0.10649
ngv_235_603.ASC	77.5739	64.8438	60.7464	77.5029	64.8505	60.6646	37.3000	31.0000	0.10635

Pum = Upstream measured pressure
Pdm = Downstream measured pressure
Prm = Measured reservoir pressure
Puc = Upstream corrected pressure
Pdc = Downstream corrected pressure
Prc = Corrected reservoir pressure
Tu = Upstream temperature
Tr = Reservoir temperature
$\dot{m}$ = Calculated mass flow

Appendix F

Cd Calculations and Maps

Creation of Cd-Maps

The Cd-Values for the 24 test points for each test piece was calculated for 4 area ratios spanning the mesh lengths from 5mm to 25 mm using program FLOWPROG.

For each area ratio a second order polynomial was fitted using a least squares fit. These four polynomials represented four sections through the Cd-map at constant area ratios and as a function of pressure ratio. The R^2-values is given in Table F.1. A third order polynomial was fitted to each of the three coefficients of the four polynomials. This allows the construction of a polynomial for each area ratio required to create the Cd-map.

These polynomials were programmed into FORTRAN programs and the Cd-maps for the first four test pieces were an output in a text file in matrix format for each. It was not necessary to create Cd-maps for the rest of the test pieces because the required information could be obtained from graphs at a fixed area ratio. (Refer to the discussions in paragraph 4.5.3 to paragraph 4.6)

The second order polynomial for the Cd-value is in the following format:

$$Cd = a_0 + a_1 x + a_2 x^2$$

And the third order polynomials for the coefficients:

$$a_i = b_{i0} + b_{i1} y + b_{i2} y^2 + b_{i3} y^3$$

The b coefficient values are given in Table F.2.

Table F.1: R^2-Values for a_i- coefficients

10 Deg		20 Deg		30 Deg		40 Deg	
Ar	R^2	Ar	R^2	Ar	R^2	Ar	R^2
1.05	0.9950	1.10	0.9960	1.15	0.9900	1.20	0.9944
1.10	0.9944	1.20	0.9981	1.30	0.9933	1.45	0.9966
1.15	0.9941	1.30	0.9973	1.45	0.9944	1.70	0.9968
1.20	0.9933	1.40	0.9973	1.60	0.9952	1.95	0.9966

Table F.2 Coefficient b_{ij} values

Test Piece		b_{i0}	b_{i1}	b_{i2}	b_{i3}
1 10deg	a_0	-1052.3515	2651.5077	-2232.7000	627.7333
	a_1	2261.9171	-5684.1343	4775.7200	-1339.8667
	a_2	-1212.9117	3043.6833	-2552.9000	715.0667
2 20deg	a_0	-208.7952	460.8358	-341.7900	84.8167
	a_1	466.4534	-1025.8242	759.4500	-188.1833
	a_2	-255.2668	561.0048	-424.4700	102.5167
3 30deg	a_0	-84.4488	167.0196	-111.7022	25.0074
	a_1	194.2309	-382.3848	255.4837	-57.1605
	a_2	-109.241	215.7780	-144.0881	32.2272
4 40deg	a_0	-26.7475	42.8133	-23.6664	4.3787
	a_1	62.7314	-99.1487	54.6626	-10.0896
	a_2	-35.4456	56.6835	-31.2317	5.7621

Map and Data for 10 Degree Cone

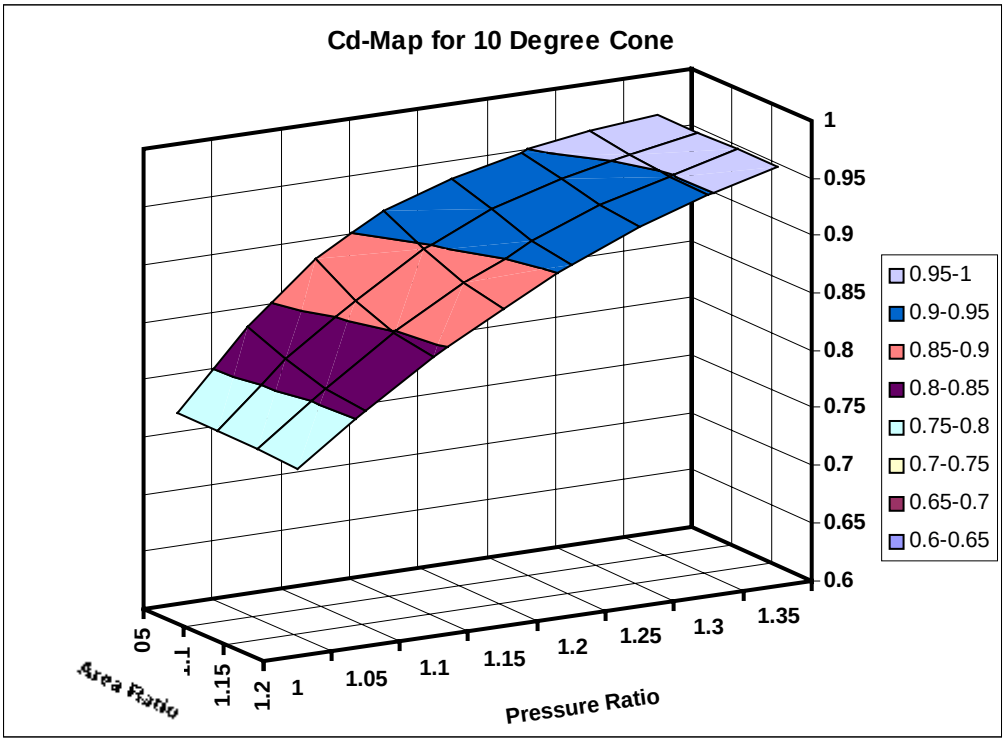

Pressure Ratio	Area Ratio			
	1.05	1.1	1.15	1.2
1	0.767	0.766	0.765	0.764
1.05	0.832	0.819	0.81	0.806
1.1	0.882	0.862	0.849	0.844
1.15	0.916	0.897	0.883	0.877
1.2	0.934	0.923	0.911	0.906
1.25	0.949	0.941	0.933	0.93
1.3	0.959	0.953	0.949	0.949
1.35	0.964	0.964	0.964	0.964

Map and Data for 20 Degree Cone

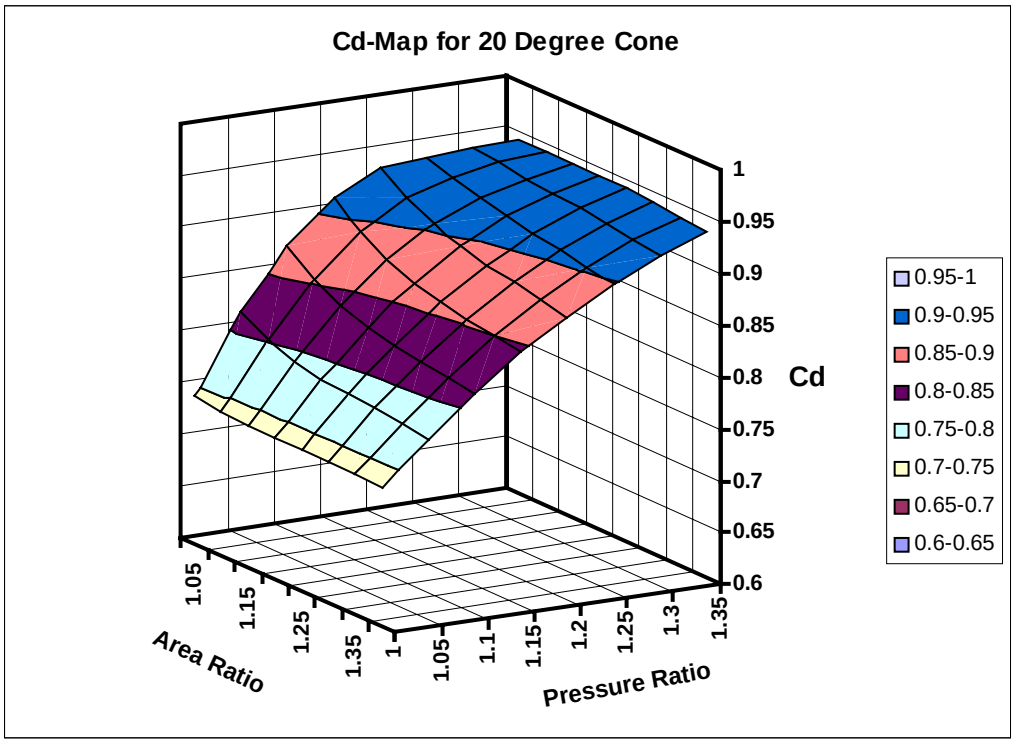

Pressure Ratio	Area Ratio							
	1.05	1.1	1.15	1.2	1.25	1.3	1.35	1.4
1	0.742	0.738	0.736	0.736	0.736	0.737	0.736	0.735
1.05	0.817	0.802	0.792	0.786	0.783	0.781	0.779	0.775
1.1	0.874	0.853	0.839	0.83	0.824	0.82	0.816	0.812
1.15	0.913	0.892	0.877	0.866	0.859	0.854	0.85	0.845
1.2	0.935	0.918	0.905	0.895	0.888	0.883	0.878	0.873
1.25	0.938	0.931	0.924	0.918	0.912	0.907	0.903	0.898
1.3	0.942	0.939	0.935	0.933	0.93	0.927	0.922	0.919
1.35	0.943	0.943	0.943	0.943	0.943	0.941	0.938	0.936

Map and Data for 30 Degree Cone

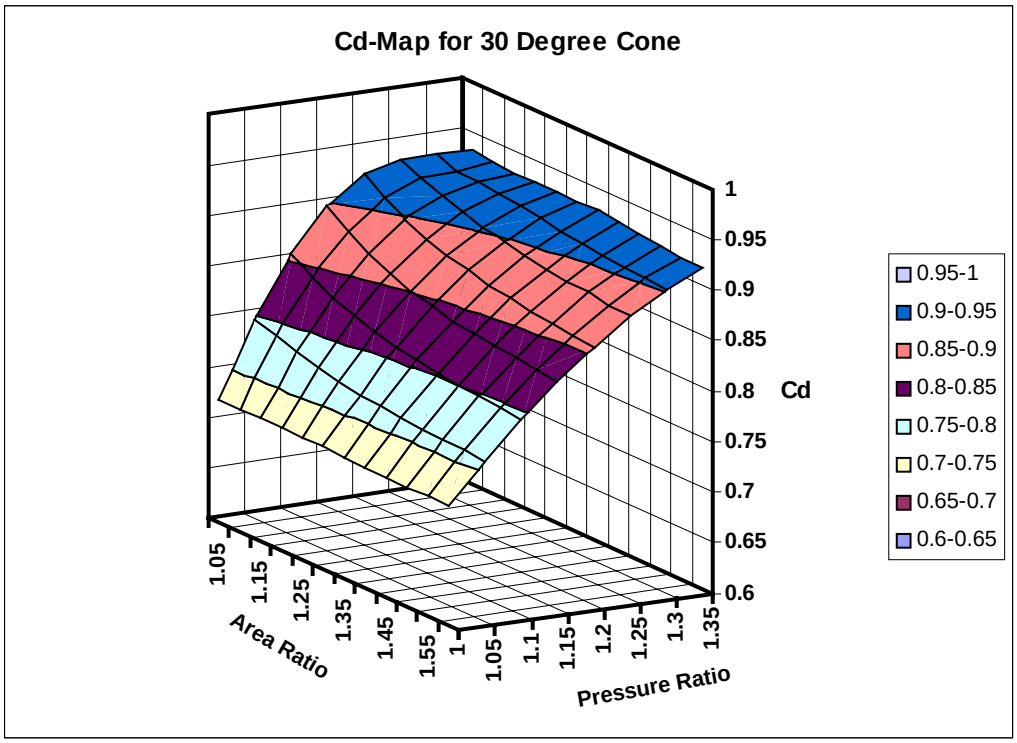

Pressure Ratio	Area Ratio											
	1.05	1.1	1.15	1.2	1.25	1.3	1.35	1.4	1.45	1.5	1.55	1.6
1	0.722	0.722	0.722	0.722	0.722	0.722	0.721	0.72	0.72	0.719	0.719	0.719
1.05	0.797	0.789	0.782	0.776	0.772	0.768	0.766	0.764	0.762	0.761	0.76	0.758
1.1	0.856	0.842	0.831	0.822	0.815	0.81	0.806	0.802	0.8	0.798	0.796	0.794
1.15	0.898	0.882	0.87	0.859	0.851	0.845	0.84	0.836	0.834	0.831	0.829	0.826
1.2	0.924	0.91	0.898	0.888	0.881	0.875	0.87	0.866	0.863	0.86	0.857	0.855
1.25	0.933	0.924	0.916	0.909	0.903	0.898	0.894	0.89	0.887	0.885	0.882	0.88
1.3	0.933	0.925	0.924	0.922	0.919	0.916	0.913	0.91	0.907	0.905	0.903	0.901
1.35	0.933	0.929	0.928	0.928	0.928	0.928	0.928	0.926	0.923	0.921	0.919	0.918

Map and Data for 40 Degree Cone

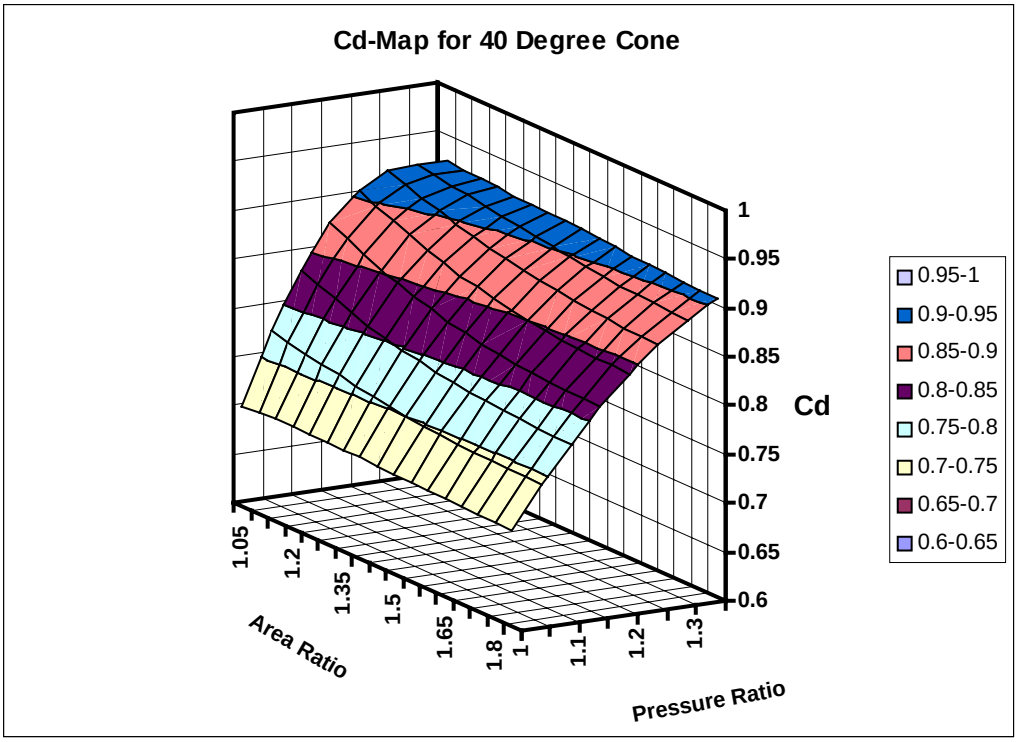

Pressure Ratio	Area Ratio																
	1.05	1.1	1.15	1.2	1.25	1.3	1.35	1.4	1.45	1.5	1.55	1.6	1.65	1.7	1.75	1.8	1.85
1	0.703	0.704	0.705	0.705	0.705	0.705	0.705	0.705	0.704	0.703	0.703	0.702	0.702	0.701	0.701	0.7	0.7
1.05	0.775	0.771	0.767	0.764	0.761	0.758	0.755	0.752	0.75	0.748	0.747	0.745	0.744	0.743	0.743	0.742	0.742
1.1	0.833	0.826	0.819	0.813	0.807	0.802	0.798	0.794	0.791	0.788	0.786	0.784	0.782	0.781	0.78	0.78	0.779
1.15	0.877	0.868	0.86	0.852	0.846	0.84	0.835	0.83	0.827	0.823	0.82	0.818	0.816	0.815	0.814	0.813	0.813
1.2	0.906	0.898	0.89	0.883	0.876	0.87	0.865	0.861	0.857	0.853	0.85	0.848	0.846	0.844	0.843	0.843	0.842
1.25	0.922	0.915	0.909	0.903	0.898	0.893	0.889	0.885	0.881	0.878	0.876	0.873	0.871	0.87	0.869	0.868	0.867
1.3	0.923	0.92	0.917	0.915	0.912	0.909	0.906	0.903	0.901	0.898	0.896	0.894	0.892	0.891	0.89	0.889	0.888
1.35	0.923	0.921	0.92	0.919	0.918	0.917	0.917	0.916	0.915	0.913	0.912	0.91	0.909	0.908	0.906	0.906	0.906

Appendix G

Engine data for Simulation

```
*****************************************************


   This file lists the input data as set up for the:

              suvj23 engine

   for use by the ENGMOD2T engine simulation program.

    This data file was constructed on:  6-10-2000
                                  at: 15h:20min

 *****************************************************

 General engine data:
 --------------------

 Number of cylinders                                 1
 Bore                                        54.00000     mm
 Stroke                                      54.50000     mm
 Conrod length                               110.0000     mm
 Rpm for max power                           11500.00
 Trapped compression ratio                   8.500000
 Crankcase compression ratio                 1.350000
 Number of cycles                               18
 Exhaust wall temperature                    250.0000     C

  The exhaust port data:
  ----------------------

   This engine has a BRIDGED type main exhaust port

 Exhaust port opens at (ATDC)                82.50000     deg
 Exhaust port fully open at (ATDC)           180.0000     deg
 Overall width of bridged exhaust port       48.00000     mm
 Radius of top corner of port window         8.000000     mm
 Radius of bottom corner of port window      8.000000     mm
 Radius of top corner of bridge              3.000000     mm
 Radius of bottom corner of bridge           3.000000     mm
 Width of bridge                             4.500000     mm
 Overall width of bottom of port             30.00000     mm
 Radius of top edge of port (0=straight)    0.0000000E+00 mm
 Radius of bot edge of port (0=straight)    0.0000000E+00 mm
 Length of exhaust port passage              70.00000     mm
 Diameter of exhaust port at manifold end    37.00000     mm

   This engine has AUXILLARY exhaust ports

 Auxiliary port opens at (ATDC)              85.00000     mm
 Auxiliary port fully open at (ATDC)         110.0000     mm
 Number of auxiliary exhaust ports              2
 Width of one port window                    12.00000     mm
 Radius of top corner of port window         3.000000     mm
 Radius of bottom corner of port window      3.000000     mm
 Height of auxiliary port passage            12.00000     mm
 Width of auxiliary port passage             12.00000     mm
 Radius of passage corners                   3.000000     mm
```

Transfer port data:

Transfer port opens at (ATDC)	114.0000	deg
Transfer port is fully open at (ATDC)	180.0000	deg
Number of transfer ports	5	
Width of one port	19.00000	mm
Radius of top corner of port window	2.000000	mm
Radius of bottom corner of port window	2.000000	mm
Type of scavenging model	YAM12	

Intake port type and data:

This engine has a REED VALVE type intake port

The reed petal material is GLASSFIBRE

Number of reed valve petals	6	
Thickness of petals	0.420000	mm
Width of petals	22.70000	mm
Free length of petals	37.00000	mm
Young's modulus	21.50000	MPa
Density of petal material	1850.000	Kg/m^3
Damping factor for mode 1	0.2500000	
Damping factor for mode 2	0.1500000	
Included angle of reed valve block	47.00000	deg
Diameter of port in reed valve block	34.00000	mm
Maximum tip displacement	13.00000	mm
Width of port in reed valve block	19.00000	mm
Length of port in reed valve block	32.00000	mm
Corner radius of port in reed valve block	2.000000	mm

There is no curved stop plate

The EXHAUST system has the following characteristics:

The exhaust system layout has:

An individual pipe per cylinder and,
a tuned pipe collector.

The data for pipe no 1
The length of pipe section 1 = 200.0 mm
The length of pipe section 2 = 235.0 mm
The length of pipe section 3 = 60.0 mm
The length of pipe section 4 = 90.0 mm
The length of pipe section 5 = 205.0 mm
The length of pipe section 6 = 200.0 mm

The data for pipe no 1
The diameter of pipe section 0 = 37.0 mm
The diameter of pipe section 1 = 48.0 mm
The diameter of pipe section 2 = 95.0 mm
The diameter of pipe section 3 = 118.0 mm
The diameter of pipe section 4 = 118.0 mm
The diameter of pipe section 5 = 22.2 mm
The diameter of pipe section 6 = 22.2 mm

```
 The TRANSFER port passage data:
 -------------------------------

Transfer port passage length                80.00000     mm
Crankcase to cylinder port area ratio       1.400000

The INTAKE system has the following characteristics:
 ----------------------------------------------------


The intake system layout has:

    An individual pipe per cylinder and,
    an open pipe collector.

The data for pipe no  1
The length of pipe section    1 =   30.0 mm
The length of pipe section    2 =   35.0 mm
The length of pipe section    3 =   80.0 mm

The data for pipe no  1
The diameter of pipe section  0 =   38.0 mm
The diameter of pipe section  1 =   30.0 mm
The diameter of pipe section  2 =   30.0 mm
The diameter of pipe section  3 =   34.0 mm

 The ignition model data:
 ------------------------

Wiebe index "A"                              6.000000
Wiebe index "M"                              1.100000
Combustion efficiency                       0.8250000
Combustion period                            50.00000     deg
Ignition delay period                        6.000000     deg
Type of fuel                              UNLEADED
```

Appendix H

Dynamometer Results

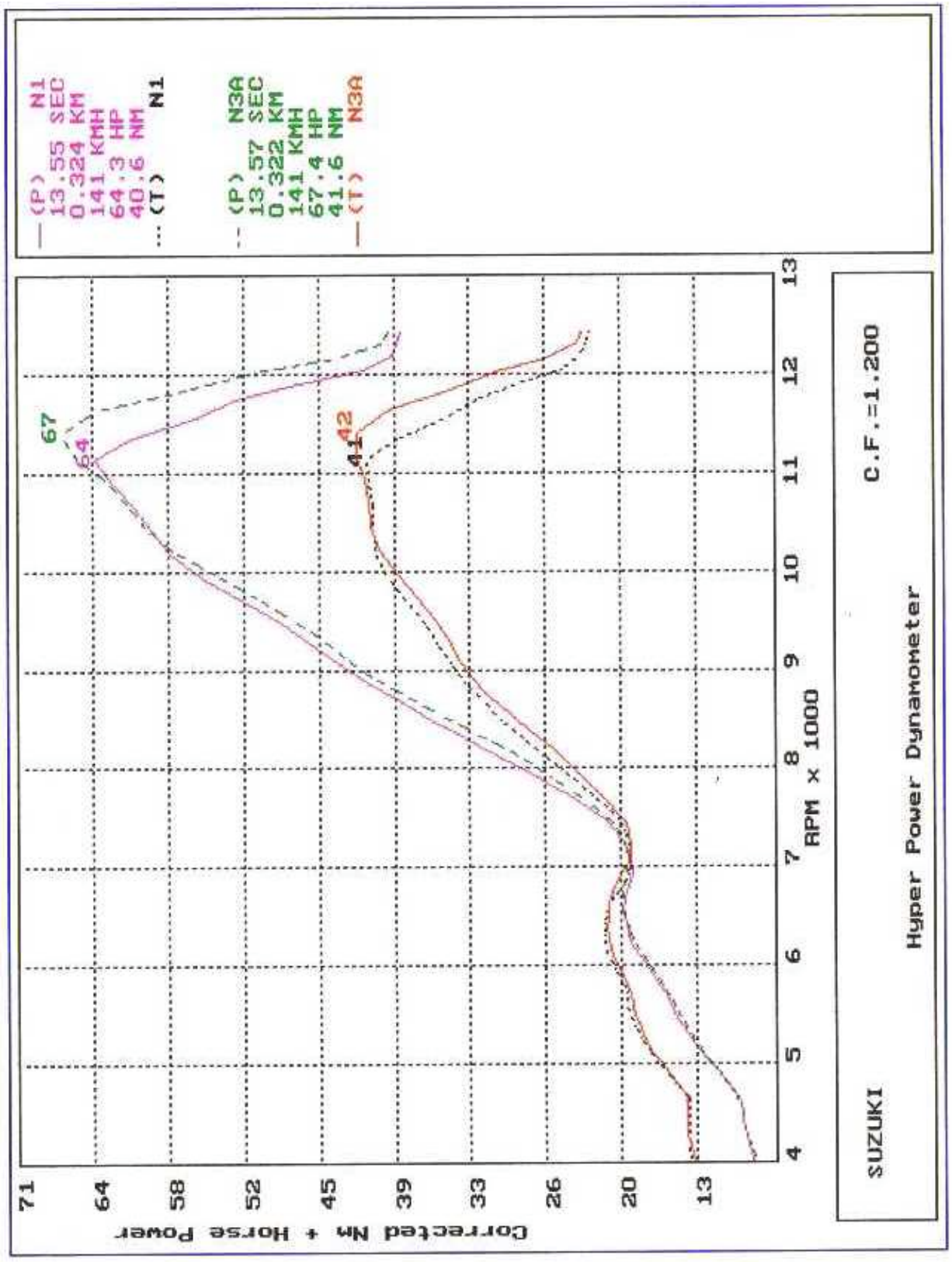

Appendix I

Description of Program EngMod2T

I.1 INTRODUCTION

Program EngMod2T is a one-dimensional gasdynamics based program that simulates the flow, combustion and scavenging in a two stroke engine to predict its power output. It was created as an alternative to dynamometer testing of high performance (motorcycle grand prix level) engines. Testing of these engines is a costly and expensive affair. Engine components seldom have a life of more than 500 kilometres or 2 hours. Stabilizing the engine on the dynamometer at the correct exhaust pipe temperatures is a complex operation that uses a large portion of the actual testing time. Testing at the correct temperature is crucial because the resonant frequency of the exhaust system is dependant on the temperature.

As input it uses the engine physical characteristics for all the ducts, ports and plenums. It further uses model parameters based on test results for the combustion and scavenging models. The duct and plenum wall temperatures are also an input. From these inputs the pressures and temperatures in al the ducts and plenums are calculated as a function of time.

I.2 HISTORY

EngMod2T started as a simple Method of Characteristics based program in 1985. It could simulate a single cylinder piston port engine using a simple heat release rate combustion model and an empirical scavenging model. By 1990 a sophisticated reed valve based intake system was added as an option and the port subroutines were updated to accommodate most of the typical geometries used in modern engines. At this stage one of the biggest drawbacks was the fact that the exhaust pipe temperature was a user defined input.

Various newer methods like the Lax-Wendroff Two Step with Flux Correction and others were investigated to get around this problem. In 1991 a new method was published by Professor Gordon P Blair of the Queen's University of Belfast (Blair, 1991) that not only calculated the temperature at each point in a duct but also its chemical composition as an inherent part of the method. (Professor Blair was the leader of a research group at that university that specialized in two-stroke engine gasdynamics and simulation starting in the mid 1960's) EngMod2T was updated to use this new method, known as the GPB-method and has continually been updated since then as more sophisticated combustion, scavenging and boundary condition models were developed.

In 1998 it was further expanded to allow the simulation of engines with up to four cylinders and complex branch type intake and exhaust systems.

I.3 DESCRIPTION OF ENGMOD2T

To aid in the preparation of the input data a pre-processing program was developed. For a new project it prompts the user for the input data and it allows editing of the data for an existing project. The data in Appendix G is a printout from this program.

Each pipe or duct in the intake or exhaust system can be divided into 20 segments of which each can be area expanding, contracting or constant. This allows the construction of multi-stage diffusers and reverse cones.

I.3.1 Exhaust System

Three configurations of exhaust manifold systems can be analysed:

- Individual pipes on each cylinder.
- Branch manifold type. This is a manifold where all the header pipes join in a common junction followed by a common collector pipe.
- Log manifold type. This type has common collector pipe with each header joining it independently.

From the manifold outlet (or in the case of the individual pipe configuration from the exhaust port outlet) a further three options exists:

- Tuned pipes. This is the so called “expansion box” type of exhaust pipe as used on the high performance engines. It automatically applies the restriction subroutine to the tail pipe entrance. (**This is the enhancement developed in this dissertation)**
- Open pipe. This is a plain type outlet pipe although it can be configured to be the same as the tuned pipe but with an important difference. It does not apply the restriction subroutine to the tail pipe entry.
- Box type. The collector pipe exits into a plenum or “box” with an additional pipe exiting from the plenum. This is a typical system as used on industrial and outboard engines.

I.3.2 Intake System

The intake system is largely a mirror image of the exhaust system that also allows the same three manifold systems. Each of these systems can be open to the atmosphere or pass through a plenum. This plenum can be an air box or an air filter box.

I.3.3 Transfer Ducts

The transfer ducts join the cylinder with the crankcase volume. They can be of constant area or a continuous taper. The current version of EngMod2T lumps all the transfer ducts together and treats it as one duct.

I.3.4 Exhaust Port Window

The exhaust port can be of two main configurations:

- Single Main Port. This is the more common layout and uses a oval shaped port window.
- Bridged Main Port. To gain extra width in a port window without the rings snagging on the top or bottom edge a bridge is added to divide the window into two.

To gain additional flow area extra little exhaust ports are added above the transfer port windows, known as sub-exhausts. This can be added to either configuration of main exhaust port.

I.3.5 Transfer Port Windows

The current version of EngMod2T allows for square shaped transfer port windows with radiused corners only. They all have to open and close at the same time as well.

I.3.6 Intake Port Control

The intake port can be of one of three configurations:

- Piston Port. This is the original configuration where the intake port window opening and closing is controlled by the bottom edge of the piston skirt.
- Rotary Valve. This configuration usually consists of a thin steel disc with a cut out mounted to the one end of the crankshaft. The size of the cut out controls the intake opening, closing and duration.
- Reed Valve. The reed valve motion is controlled by the pressure differential between the intake port and the crankcase. It is modelled as a cantilever beam using the first three vibratory mode shapes and a forcing function.

I.3.7 Scavenging Model (Cylinder Open Cycle)

The scavenging model is based on the scavenging ratio test results as a function of scavenging ratio as determined in a constant volume test rig, (Blair 1993, 1996). The mass flow into and out of the cylinder is calculated for each time step and the scavenging ratio and scavenging efficiency as a function of mass flow is determined using the purity values of the transfer port inflow gas and the exhaust port outflow gas. Using the thermodynamic conditions in the cylinder this is converted to volume

based values and from this the purity value at the exhaust port is determined from the curve fitted to the test results for the next time step. The new cylinder temperature, pressure and state variables are calculated from volume and thermodynamic values.

I.3.8 Combustion Model (Cylinder Closed Cycle)

During the compression phase the effect of cooling by the vaporisation of the fuel droplets are included in the energy equation. This is necessary because the cooling effect plays a large role in high performance two-stroke engines.

The combustion model itself is a two zone model with one zone containing unburnt mixture and the other the combustion products. A Wiebe function is fitted to the experimentally determined mass fraction burnt as a function of crank angle. This function is used to transfer mass from the unburnt to the burnt zone in each time step until combustion is complete (Blair, 1996).

The program uses the spark timing, delay period, the combustion duration, the Wiebe function constants and combustion efficiency as input values.

I.3.9 Cd-Values and Cd-Maps

Cd-functions or Cd-maps are supplied for all the ports, pipe ends and pipe joints based on the work at The Queen's University of Belfast. [34,35,46] The exception is the tail pipe entry Cd-map as that was determined in this dissertation. These values are for the standard types of port and pipe configurations.

I.3.10 Chemical Equilibrium and Purity Values

As part of the GPB-method the purity in each mesh volume is calculated at each time step. The same is true for each plenum. From this the chemical specie concentration is determined and using the gas composition, temperature and pressure the values for C_p, C_v, R and γ for each control volume and plenum is calculated.

I.3.11 Typical Outputs

Currently the outputs are: Power, BMEP, IMEP, FMEP, PMEP, Delivery ratio, Scavenging efficiency, Trapping efficiency, Charging efficiency, Maximum cylinder pressure and temperature, Maximum unburnt air temperature and the Exhaust centre section temperature, all of which are written to a project file. The pressure and temperature traces at selected points in the ducts and for the cylinders and plenums are written to a separate file. During the analysis the user can also select to have certain pressure traces displayed on the screen. Figure I.1 shows a typical screen output from the program.

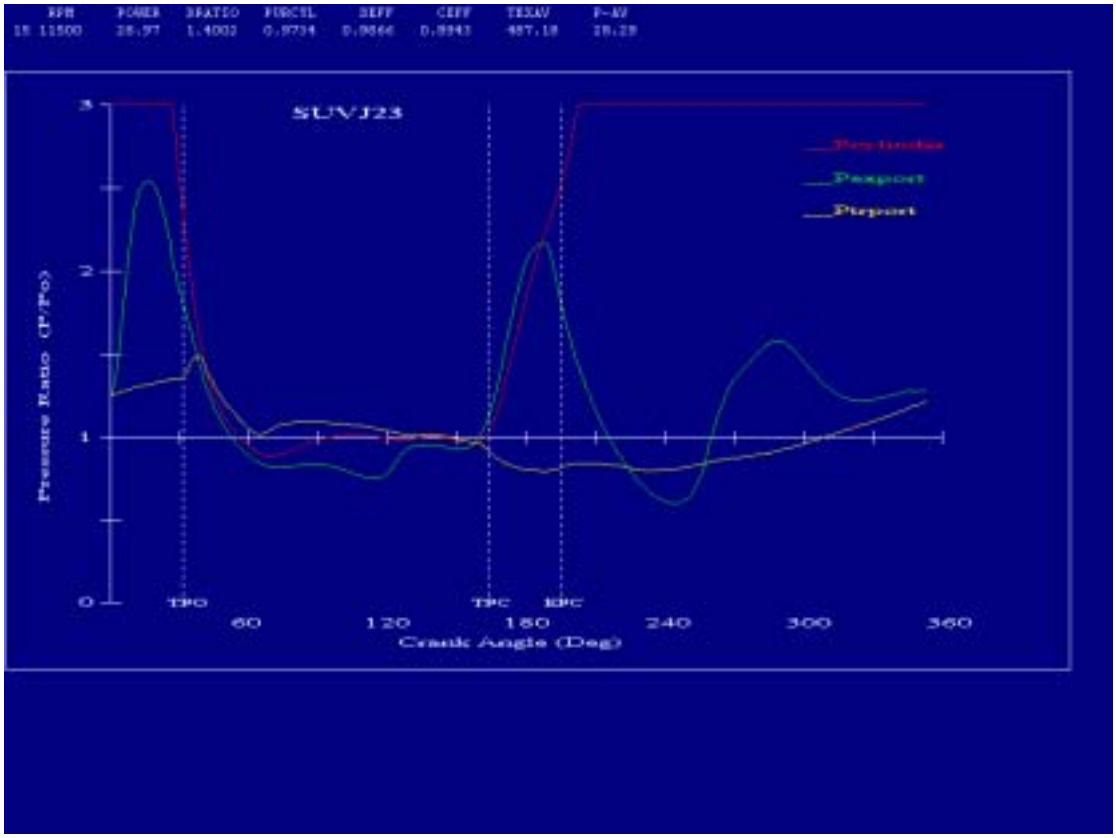

Figure I.1: A typical output screen of EngMod2T

The screen plot shows the pressure ratio traces for the cylinder (limited to 3 in the graphical output), the transfer port at the port window and the exhaust port at the port window. The crank angle is zero at the exhaust port opening. The exhaust blow down pulse from exhaust open to transfer open (TPO), the suction pulse from transfer open (TPO) to transfer closing (TPC) and the plugging pulse from transfer closing (TPC) to exhaust closing (EPC) is clearly identifiable on the exhaust pressure trace.

I.4 VERFICATION

The verification of EngMod2T was done by comparing the results from the sub models with published results and by comparing the simulation results with measured results.

I.4.1 Sub Models

The sub models (port in and out flow, expanding and contracting duct flow, multiple pipe junctions, 2-zone combustion and scavenging) were based on the work of Blair (1996) and were compared to the results as published by Blair (1996, 1999).

I.4.2 Simulation Results

The second part of the verification consisted (and consists as refining it is an ongoing process) of comparing the predicted results with measured results. Firstly,

the predicted duct pressure traces, in cylinder pressure traces and reed valve lift profiles were compared with measured results. Next the predicted engine performance characteristics were compared to measured results. The publication by Cartwright and Fleck (1994) in which they measured the pressure traces in the exhaust as well as the engine performance of a high performance grand prix motorcycle was used extensively to validate the software. Two samples from this publication will be used here as examples.

I.4.2.1 Pressure Trace Comparison

The pressure traces from a high performance engine with a tuned pipe poses the biggest problem to 1-dimensional gas dynamic simulation. Of utmost importance is to accurately predict the phasing of the pressure pulses as that determines the positioning of maximum torque and the shape of the power curve. Figures I.2 and I.3 compares the measured and simulated results at 9600rpm and at 12000rpm respectively.

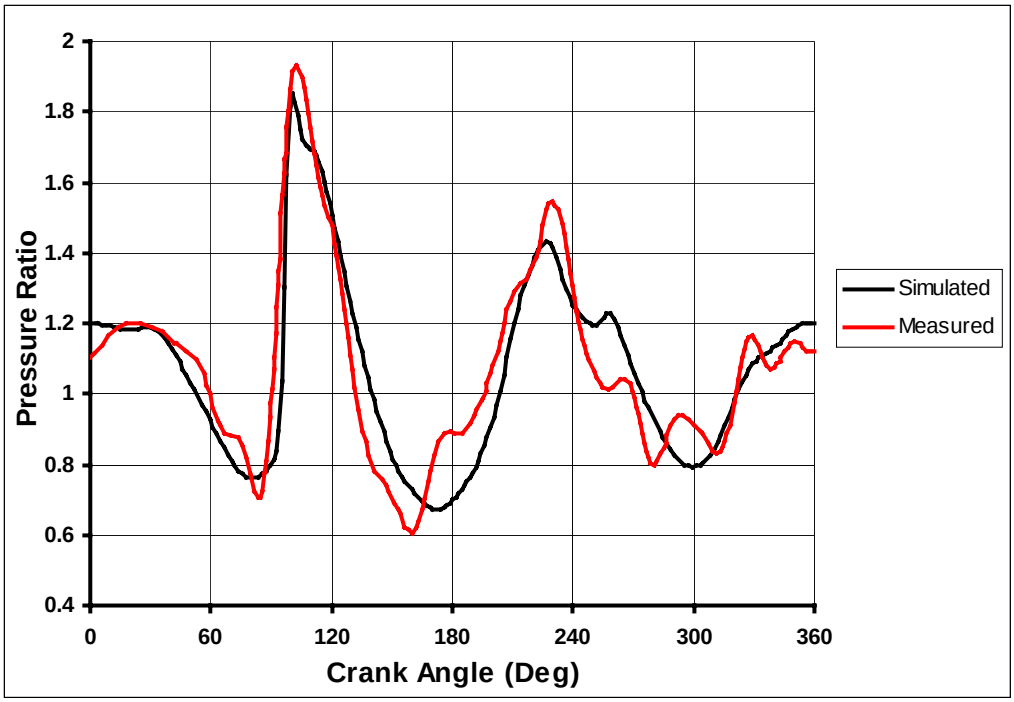

Figure I.2 Exhaust Pressure Trace at 9600rpm

The results show very good correspondence in phasing and good correspondence in amplitude. The simulation misses some of the high frequency content of the measured traces, probably as a result of the finite length of the meshes and some numerical smearing.

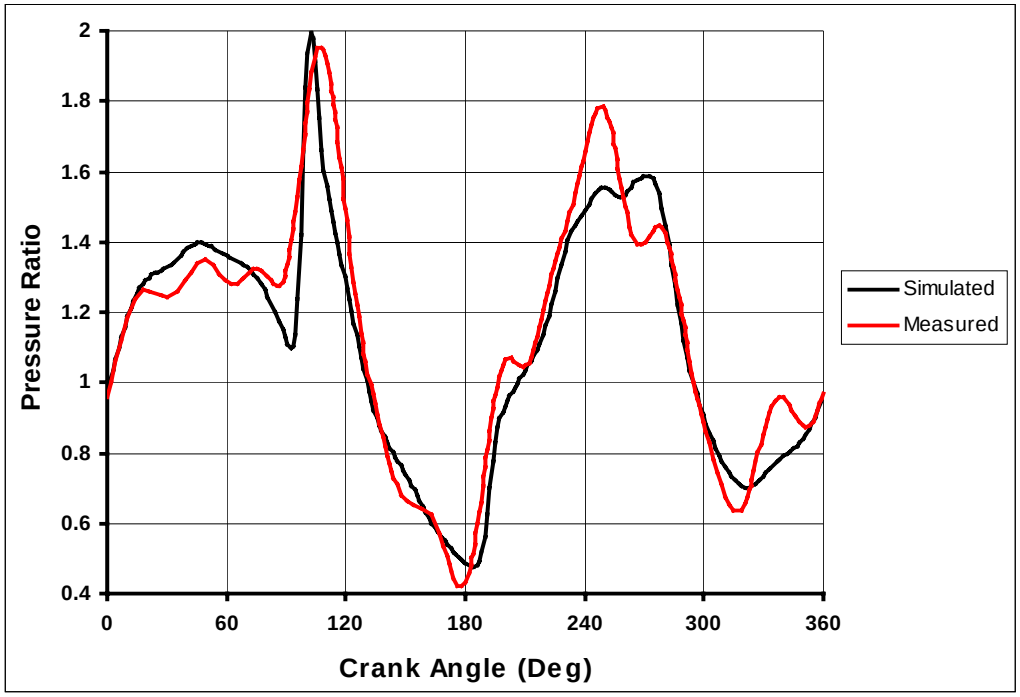

Figure I.3 Exhaust Pressure Trace at 12000rpm

I.4.2.2 Performance Prediction Validation

Cartwright and Fleck (1994) also measured the performance of this engine. Figure I.4 shows the comparison between the measured and predicted brake mean effective pressure and Figure I.5 the comparison for the exhaust system centre section mean temperature.

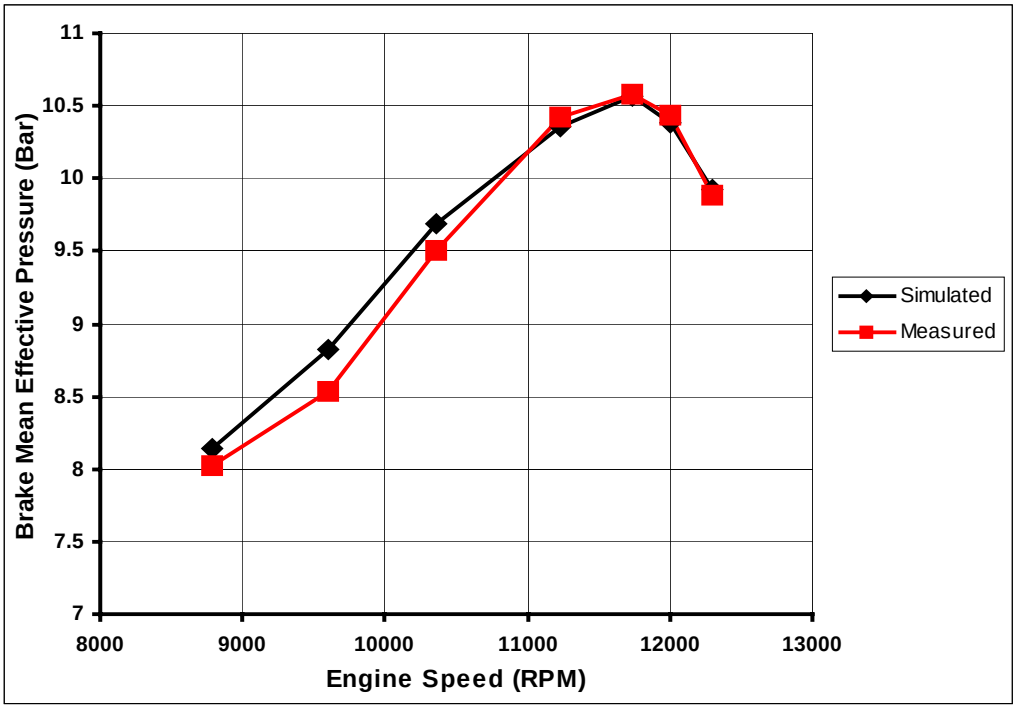

Figure I.4 Brake Mean Effective pressure

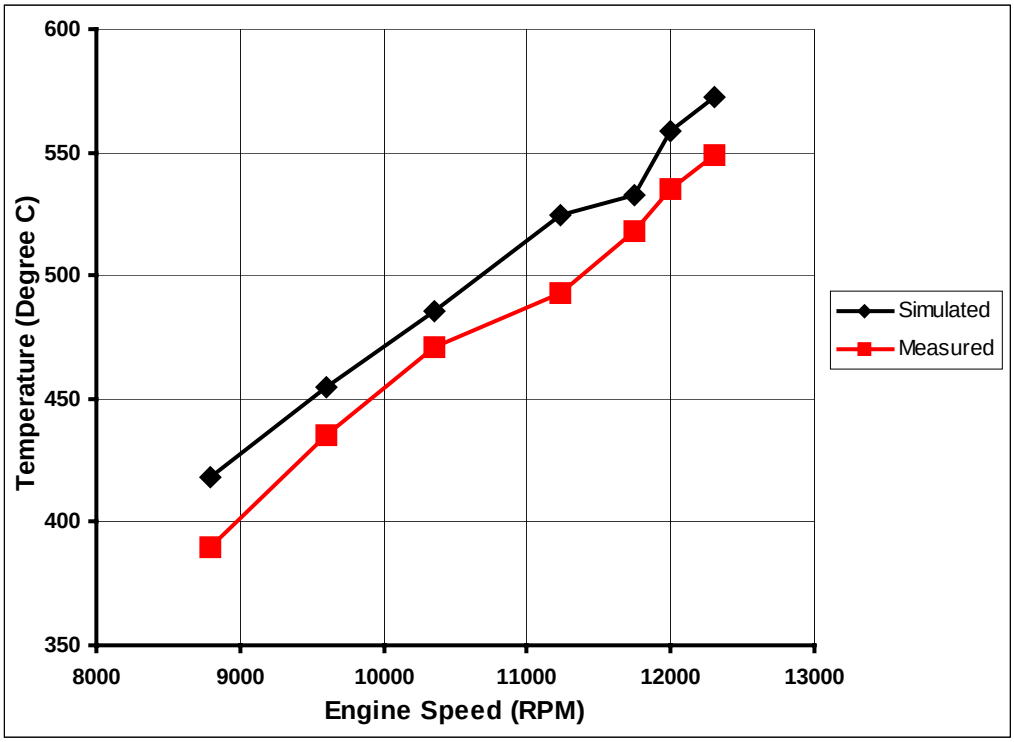

Figure I.5 Exhaust Centre Section Temperature

Both show good correlation. The simulation predicts slightly higher power at lower revolutions and slightly higher exhaust temperatures through the range.

I.4.2.3 Further Validation

The software (and its four-stroke counterpart) has been further validated for engines fitted with box type exhaust pipes versus the tuned pipe results shown here, multi cylinder engines with branch manifolds and with log manifolds.

I.5 CLOSING

EngMod2T simulates the processes in a two-stroke engine with a large degree of detail and with further development will be able to predict emissions and noise emitted from the exhaust and intake systems.